Distribution Agreement

In presenting this thesis or dissertation as a partial fulfillment of the requirements for an advanced degree from Emory University, I hereby grant to Emory University and its agents the non-exclusive license to archive, make accessible, and display my thesis or dissertation in whole or in part in all forms of media, now or hereafter known, including display on the world wide web. I understand that I may select some access restrictions as part of the online submission of this thesis or dissertation. I retain all ownership rights to the copyright of the thesis or dissertation. I also retain the right to use in future works (such as articles or books) all or part of this thesis or dissertation.

Signature:

_____ _____

In Ki Cho Date

MagA as a genetic MRI reporter for longitudinal *in vivo* stem cell monitoring

By
In Ki Cho

Doctor of Philosophy

Graduate Division of Biological and Biomedical Science
Genetics and Molecular Biology

_____
Anthony W.S. Chan, DVM, Ph.D.
Co-Advisor

_____
Hui Mao, Ph.D.
Co-Advisor

_____
Guy M. Benian, M.D.
Committee Member

_____
Tamara Caspary, Ph.D.
Committee Member

_____
H. Criss Hartzell Jr., Ph.D.
Committee Member

_____
Victor Faundez., M.D., Ph.D.
Committee Member

Accepted:

_____
Lisa A. Tedesco, Ph.D.
Dean of the James T. Laney School of Graduate Studies

_____
Date

MagA as a genetic MRI reporter for longitudinal *in vivo* stem cell monitoring

By

In Ki Cho
B.S., Troy University, 2006
M.S., Troy University, 2009

Advisor: Anthony W.S. Chan, D.V.M., Ph.D.

Hui Mao, Ph.D.

An abstract of
A dissertation submitted to the Faculty of the
James T. Laney School of Graduate Studies of Emory University
in partial fulfillment of the requirements for the degree of

Doctor of Philosophy
Graduate Division of Biological and Biomedical Science
Genetics and Molecular Biology

2014

Abstract

MagA as a genetic MRI reporter for longitudinal *in vivo* stem cell monitoring

By

In Ki Cho

The ability to longitudinally monitor cell grafts and assess their condition is critical for the clinical translation of stem cell therapy in regenerative medicine. Here, we investigate feasibility of using MagA as a genetic MRI reporter for longitudinal stem cell graft *in vivo*. MagA is a bacterial gene involved in forming iron oxide nanocrystals. MagA expression was regulated by the Tet-On switch, hence reducing cytotoxicity and allowing inducible monitoring by supplementing doxycycline (Dox). We established a mouse embryonic stem cell-line carrying Tet-MagA (mESC-MagA) by lentivirus transduction. Expression of MagA in mESCs resulted in significant changes in transverse relaxation rate (R_2 or $1/T_2$) *in vitro*. mESC with and without MagA (mESC-MagA and mESC-WT) were grafted to striatum of mice brains and longitudinally monitored *in vivo* using MRI with "ON" (Dox^+) and "OFF" (Dox^-) conditions. Intracranial mESC-MagA grafts generated sufficient T_2 and susceptibility weighted contrast at 7T, allowing for visualization of the graft by MRI longitudinally in controlled "ON" and "OFF" fashion upon induced expression of MagA by administrating Dox in diet. Our results suggest MagA can be used to monitor cell grafts noninvasively and longitudinally by repeated induction, enabling the assessment of cell graft conditions.

MagA as a genetic MRI reporter for longitudinal *in vivo* stem cell monitoring

By

In Ki Cho
B.S., Troy University, 2006
M.S., Troy University, 2009

Advisor: Anthony W.S. Chan, D.V.M., Ph.D.,

Hui Mao, Ph.D.

A dissertation submitted to the Faculty of the
James T. Laney School of Graduate Studies of Emory University
in partial fulfillment of the requirements for the degree of

Doctor of Philosophy
Graduate Division of Biological and Biomedical Science
Genetics and Molecular Biology

2014

Acknowledgements

First and foremost, I would like to give thanks and all the glory to God. I cannot even begin to describe blessings He has bestowed upon me. He has truly been in every steps of my life, and He has surely guided me through this part of my life.

I would like to thank my truly awesome advisor Dr. Anthony Chan for his guidance and support throughout my graduate school career. From my bumpy start to immigration crisis, he was always there to support me and believed in me. His work ethic and focus on details set the standard that I have to strive for. Also, I believe his guidance and training made me a better scientist. I also would like to thank my co-advisor Dr. Hui Mao. He always provided a solution when I run into a trouble. I would also like to thank my committee members, who provided time and valuable comments throughout my graduate career: Drs. Guy Benian, Tamara Caspary, Victor Faundez, and Criss Hartzell.

I would also like to thank all the past and current members of the Chan Lab for their support and friendship. I would like to thank Jin Yang for being the lab mom. I especially want to acknowledge Sean Moran for helping me with the mouse surgery. I would also like to thank people in MRI Core facility: Drs. Xiaodong Zhang, Ramesh Paudyal, Ruth Connelly, Doty Kempf, and Silun Wang. I would also like to Susan Jenkins for Nissl staining. I also would like to thank my classmate and lab mate Dr. Richard Carter for his friendship and support. I also would like to thank former members Karolina Piotrowska-Nitsche and Pei-Hsun Cheng for vector construct and cell-line establishment.

I also have to express my deepest gratitude to my family members for their support throughout my graduate school career. I would like to thank my father, Sie Gearl Cho, for his financial support and advice. I thank my mother, Woon Sun Park, for her emotional support as well as all the food she had cooked and baked for me and my friends. I would like to thank my big sister, Wendy Yoon Jee Cho, for crazy karaoke nights and making graphs for the thesis. I would like to thank my little big sister, Yoon Young Cho, for all the pocket money she has given me and emotional support when I was down. I would also like to thank all my wonderful friends whom I met in Atlanta and all the friends I have in my adopted hometown, Luverne, AL. Without anyone of them, I would not be able to complete this study.

Table of Contents

Index of figures and tables

List of abbreviations

293FT –	human embryonic kidney cell 293 FT
7-AAD -	7-aminoactinomcin D
ANOVA -	analysis of variance
ASC –	adult stem cell
β-Mer -	β-mercaptothanol
BLI –	bioluminescence imaging
CT –	computed tomography
DAB -	3.3'-diaminobenzidine
DMEM -	Dulbecco's modified Eagle's medium
Dox -	doxycycline
EB -	embryo bodies
ESC –	embryonic stem cell
FBS -	fetal bovine serum
FC -	ferric citrate
FLASH -	fast low angle shot
FLI –	fluorescence light imaging
FOV -	field of view
FTH –	ferritin heavy chain
FTL –	ferritin light chain
GRE -	gradient echo
H&E -	hematoxylin and eosin
HA –	hemagglutinin
hLIF -	human recombinant leukemia inhibiting factor
ICC -	immunocytochemistry
IHC -	immunohistochemistry
iPS –	induced pluripotent stem cell
L-glutamine -	L-Glu
MEF -	mouse embryonic fibroblasts
mESC –	mouse ESC
mESC-MagA -	MagA transduced mouse emborynic stem cell
mESC-WT -	wild-type mouse embryonic stem cell
MRI –	magnetic resonance imaging
NEAA -	Non-essential Amino Acid
NPC –	neural progenitor cells
p.o. -	post-operation
P/S -	penicillin and streptomycin
PET –	positron emission tomography
PFA -	paraformaldehyde
qPCR -	quantitative polymerase chain reaction
ROI -	region of interest
rTA –	reverse tetracycline transactivator
RT-PCR -	real-time polymerase chain reaction
SCID -	severe combined immune deficient

SE -	spin-echo
SEM -	standard error of the mean
SPECT –	single photon emission CT
SPIO –	superparamagnetic iron oxide
TE -	echo time
Tet –	tetracycline
TR -	time of repetition
TRE -	tetracycline response element

Chapter 1

Introduction

Whole or part of this chapter will be published in an invited review.

1.1 General introduction

In recent years, with the rapid development of stem cell technology, the clinical translation of cell replacement therapy is within reach. In this chapter, a brief introduction about the development of recent stem cell technology will be provided followed by the descriptions of imaging modalities utilized in *in vivo* monitoring of cell grafts. In order to facilitate the understanding of advantages and disadvantages of each imaging technique, the basic background on how images are created by each imaging modality will be provided with some recent developments. A special emphasis will be given to magnetic resonance imaging (MRI) which is the main focus of this dissertation. The MRI contrast agents and reporters will be described in detail, and the possible utility of magnetosome as a MRI reporter gene will be provided at the end with the proposal of utilizing MagA as a genetic MRI reporter for longitudinal stem cell graft monitoring.

The term "stem cell" broadly describes a population of cells that are able to both self-renew and give rise to multiple cell types. The term was first used by a German biologist, Ernst Haeckel, in 1868 when he described the fertilized egg that gives rise to an organism (Haeckel 1868). The first experimental evidence of the existence of blood stem cells was demonstrated by Canadian scientists Ernest McCulloch and James Till (Till and McCulloch 1963). In 1981, Martin Evans and Gail Martin independently demonstrated the isolation of pluripotent stem cells from mouse embryos (Evans and Kaufman 1981, Martin 1981). Since then, stem cell technology has revolutionized the field of biology. With the success of isolating pluripotent stem cells and maintaining them *in vitro*, stem cell research

has advanced exponentially over the past three decades. Various stem cell technologies including isolation of human embryonic stem cells (Thomson et al. 1998), directed stem cell differentiation (Brustle et al. 1999, Reubinoff et al. 2000, Schuldiner et al. 2000), transdifferentiation (Selman and Kafatos 1974, Davis, Weintraub, and Lassar 1987), iPSC (Takahashi and Yamanaka 2006), and successful derivation of patient-specific pluripotent stem cells by somatic cell nuclear transfer (Chung et al. 2014) demonstrates that the stem cell technology is advancing in a tremendous pace. Stem cells have potential to be employed in, but not limited to, developmental biology, cancer biology, genetics, drug discovery, and cell replacement therapy.

In general, stem cells can be divided into three categories: embryonic, adult, and induced pluripotent. Embryonic stem cells (ESC) are isolated from the inner cell mass (ICM) of blastocysts. ESCs are referred to as being “pluripotent” because they can give rise to all the cells in the body, are capable of self-renewal, and are immortal. Adult stem cells (ASCs) can only give rise to specific cell types and have limited proliferation capacity. ASCs are considered to be multipotent. Many tissues contain of stem cells that can be isolated and expanded in culture. The last type of stem cell is the induced pluripotent stem cells (iPSCs). iPSCs are derived from somatic or progenitor cells by ectopic expression of reprogramming factors Oct4, Sox2, cMyc, and Klf4 collectively called Yamanaka Factors (Takahashi and Yamanaka 2006). Like ESCs, iPSCs are pluripotent and immortal. However, whether iPSCs are the same as ESCs is still being debated

(Narsinh, Plews, and Wu 2011) while ESCs remain as the gold standard in stem cell research.

Pluripotency and unlimited proliferation capacity are two key characteristics of ESCs that made them a perfect tool for regenerative medicine. One of the advantages of using ESCs over adult stem cells is the pluripotency of ESCs. Although transplanting undifferentiated ESCs results in the formation of teratomas, with the development of more sophisticated methods to derive homogeneous differentiated cell populations from ESC, differentiated cells can be utilized in treating multiple diseases. Moreover, the established ESCs can be maintained indefinitely for future treatment. Indeed, after the first approval of an embryonic stem cell clinical trial by FDA in 2009, numerous clinical trials have taken place using ESCs or ESC-derived progenitor cells. One other advantage of using ESCs is the possibility of employing gene therapy or genetic engineering (Chen et al. 2014). When the ESC is established, using genetic engineering, diseased genes can be replaced with healthier genes. These engineered cells can later be used to replenish the depleted cell type or even deliver therapeutic genes (Chen et al. 2014). Conventional gene therapy of transducing host cells with viral vectors can be used, and genetically modified stem cell transplantation can provide a continuous supply of the therapeutic gene *in vivo*. Gene editing of endogenous genes by the newly invented CRISPR (clustered regularly interspaced short palindromic repeats) technology holds the tremendous promise of correcting mutations in ESCs. There are many advantages of using gene editing

– lack of insertion of a viral vectors, lack of restriction about how large the gene can be used, and an ease of use.

Stem cell replacement therapy holds great potential in curing diseases such as diabetes, bone degenerative diseases, autoimmune diseases, and neurodegenerative diseases (Bachoud-Levi et al. 2000, Arenas 2002, Park et al. 2003, Lee et al. 2006, Wernig et al. 2008, Schwarz and Schwarz 2010, Chen et al. 2014, Carter and Chan 2012). The primary goal of cell replacement therapy is to replenish damaged or degenerated cell populations. Besides immune rejection and functionality of cell grafts, one of the major obstacles for clinical translation is the lack of understanding of the fate of implanted cells and their correlation with clinical outcomes. Thus, there is an urgent need for a reporting system that allows noninvasive and longitudinal evaluation of cell grafts. The interest in *in vivo* cell imaging has increased exponentially in the past decade (Figure 1-1a). The current methods of evaluating cell grafts rely on indirect markers or soluble markers after initial treatment (Jha et al. 2010). In order to develop and evaluate efficacy of cell replacement therapies, it is essential to effectively determine or assess cell survival, proliferation, migration, lineage differentiation, and functional integration at the graft site longitudinally (Vande Velde, Himmelreich, and Neeman 2013, Vandsburger et al. 2013, Kircher, Gambhir, and Grimm 2011).

In vivo monitoring of grafted cells was first reported in 1976 (Segal et al. 1976). In this inaugural study, leukocytes were extracted from patients, labelled with indium-111, reintroduced to patients and followed for two days (Segal et al. 1976). With the development of *lacZ* (β-galactosidase) in 1980 (Casadaban, Chou,

and Cohen 1980) and green fluorescent protein (GFP) in 1994 (Chalfie et al. 1994), colorimetric and fluorescent reporter genes have been used in basic biomedical research extensively. There are many imaging modalities available, and multiple reporters have been examined to study various aspects such as basic cell biology, developmental biology, and molecular biology. For *in vivo* cell graft tracking, several imaging modalities have been investigated, which include positron emission topography (PET) (Qin, Cheng, et al. 2013, Terrovitis et al. 2008), computed tomography (CT) (Terrovitis et al. 2008), single photon emission CT (SPECT) (Auricchio et al. 2003), ultrasound (US) (Cui et al. 2013, Klibanov et al. 2004), bioluminescence imaging (BLI) (Welsh and Kay 2005, Bernau et al. 2014), fluorescence light imaging (FLI) (Sevick-Muraca, Houston, and Gurfinkel 2002, Frangioni 2003, Ntziachristos, Bremer, and Weissleder 2003), magnetic resonance imaging (MRI) (Koretsky et al. 1996, Cohen et al. 2005, Liu et al. 2009, Gilad et al. 2008, Zurkiya, Chan, and Hu 2008, Vande Velde, Himmelreich, and Neeman 2013, Rohani et al. 2014, Bar-Shir et al. 2014, Qin, Cheng, et al. 2013), and more recently chemical exchange saturation transfer (CEST) (Ward, Aletras, and Balaban 2000). Among these available imaging modalities, MRI and PET are most frequently used for cell monitoring and tracking *in vivo* (Figure 1-1b). More recently, various combinations of imaging methods have been investigated for *in vivo* cell imaging (Figure 1-1c).

1.2 Criteria for an ideal imaging reporter

While different imaging methods have been developed for tracking cell grafts *in vivo*, an ideal imaging reporter should be comprised of specific characteristics as

summarized in Table 1-1. The first criterion is nontoxicity (Frangioni and Hajjar 2004). An ideal imaging reporter should be biodegradable and safe for biological systems. Also, the labeled cells should have the same viability as the non-labeled cells. Although most solid-state reporters such as nanoparticles have shown promising results in tracking cell grafts, long-term safety and biocompatibility are still under investigation. The second criterion is neutral impact on stem cell function. Another important aspect to consider in tracking stem cell graft is the potential impact on stem cell function. Whether the reporter is used for tracking pluripotent stem cell or lineage specific stem cell (i.e. neural stem cell), a reporter should have little or no impact on differentiation potential of the stem cell (Au et al. 2009). There are reports showing no impact on differentiation potential (Au et al. 2009, Wang et al. 2012, Blaber et al. 2013, Rosenberg et al. 2013) while others showing preference to a certain lineage specific cell types (Chen et al. 2010, Julke et al. 2013, Chung, Hsiao, et al. 2011, Choi et al. 2013). The third criterion is the sensitivity. An ideal imaging reporter will be sensitive enough to detect a single cell, which will enable quantification of exact cell numbers and providing high resolution. The resolution is particularly important for stem cell therapy due to the migration of stem cells from the graft site, which will be one of the critical evaluation points as successful integration and functionality of the stem cells. Despite several imaging modalities having potential to visualize single-cells *in vivo*, only few imaging modalities have actually demonstrated such capacity. Superparamagnetic iron oxide (SPIO) particles have demonstrated the single-cell resolution with MRI (Shapiro et al. 2007, Heyn et al. 2006). The fourth criterion is signal persistency. An ideal imaging reporter should not be diluted with cell

division. Although single-cell resolution has been achieved with SPIO, precise quantification remained challenging because of the continued dilution of SPIO as cells divide and proliferate. The fifth criterion is specificity. The contrast should come specifically from the grafted cells and not from other cells (i.e. specificity). When cells undergo cell division, apoptosis, or cell death, nanoparticles can be released or lost from the cells. These particles can be picked up by adjacent cells or persist in the extracellular matrix and give false positive signals. Therefore, it is important that the contrast signal is retained in the grafted cells or daughter cells. The sixth criterion is noninvasiveness. An ideal imaging reporter should permit noninvasive imaging. The imaging modalities listed in the previous section, PET, CT, SPECT, US, BLI, FLI, MRI, and CEST, allow noninvasive imaging. However, each imaging modality has its own advantages and disadvantages, which will be discussed in section 1.3. The seventh criterion is longitudinal imaging. An ideal imaging probe should allow longitudinal monitoring of the cell grafts. An ideal imaging reporter should be able to generate contrast for months to years for long term monitoring and assessment for clinical evaluation (Frangioni and Hajjar 2004). The final criterion is no injectable contrast agent. Injectable contrast agents add complexity due to their pharmacokinetics, specificity, and half-lives. Therefore, injectable contrast agents should be avoided (Frangioni and Hajjar 2004).

1.3 Introduction to available imaging modalities

For each imaging modality, accumulation and amplification of a specific signal make it possible to visualize cells and create contrast for quantification and

localization purposes. How to create the signal and the methods used to visualize the signal differ from one imaging modality to the other. A brief summary of the characteristics of imaging modalities is presented in Table 1-2. With the rapid advancement of imaging methods and imaging probes, the parameters presented here are only applicable for the current state (focused on the past five years) of each technology. Among these imaging modalities, a special emphasis will be given to MRI, and more detail will be discussed about MRI. At present, there is no imaging modality that can satisfy all 8 criteria, though some come close to satisfying all or most criteria.

1.3.1 Single-photon emission computed tomography (SPECT)

Nuclear medicine has been utilized extensively for tracking grafted cells *in vivo*. For SPECT, the signal emitted as γ-rays from radioactive isotopes with long half-lives ($t_{1/2}$), such as ^{99m}Tc, ^{111}In, and ^{123}I, is detected by a rotating collimated gamma camera. The collected signal is later reconstructed as a 3-dimensional image. One of the advantages of SPECT is that it allows multi-spectral imaging using multiple radionuclides, (e.g. ^{111}In and ^{99m}TC (Zhou et al. 2005)). Moreover, SPECT combined with CT has shown improved resolution of labeled cells in an anatomical context like MRI, yet SPECT is not as sensitive as PET (Blackwood et al. 2008) with the ability to visualize only up to 1 x 10^4 labeled cells with 16 minutes of temporal resolution (Jin et al. 2005). While most studies reported no detrimental impact of isotopes used in SPECT imaging, one study demonstrated low labeling efficiency (32%), reduced viability, and complete impairment of proliferation and differentiation in $CD34^+$ hematopoietic progenitor cells

(Brenner et al. 2004). Another study involving human mesenchymal stem cells (hMSC) demonstrated ^{111}In-oxiquinolon affecting cell migration (Gildehaus et al. 2011). Also, SPECT radioisotopes exhibited substantial efflux within 24 hours (Zhou et al. 2005). Finally, the emitted γ-rays are potentially mutagenic and carcinogenic.

In recent years, SPECT reporter gene methods, such as enzymatic conversion/retention and receptor-mediated targeting, have been reported. Sodium iodide symporter (NIS) can be imaged with ^{123}I or ^{99m}Tc for SPECT and ^{124}I for PET (Huang et al. 2001). Norepinephrine transporter (NET) that can be labeled with ^{124}I-MIBG (Moroz et al. 2007) as well as dopamine receptor and transporter has also been used as SPECT reporter (Auricchio et al. 2003). These methods have been applied in monitoring neural stem cell (Kim et al. 2005) and cardiac stem cell (Terrovitis et al. 2008) grafts as well as in monitoring of neuronal differentiation (Hwang do et al. 2008).

1.3.2 Positron emission tomography (PET)

Due to an extraordinary sensitivity ranging in the picomolar (10^{-11} – 10^{-12} mol/l) (Zhou, Acton, and Ferrari 2006), PET is promising in tracking relatively scarce neural stem cells (Couillard-Despres et al. 2011). However, PET does not have as high a spatial resolution as MRI (Couillard-Despres et al. 2011) and cannot distinguish between different radionuclides like SPECT (Blackwood et al. 2008). The signal for PET is produced from positron emitting radionuclides such as ^{11}C, ^{13}N, or ^{18}F (Blackwood et al. 2008). Upon annihilation of a positron, the emission of two anti-parallel γ photons with energy of 511-keV is detected by a sensitive

photodetector. The signal is later computed for spatial position with intensity of the emission sources. Direct labeling and genetic reporter systems have both been used with PET. In a recent study, noninvasive *in vivo* monitoring of neural stem cell migration has been reported with 3'-deoxy-3'-[^{18}F]fluoro-L-thymidine (Rueger et al. 2010). In another recent study, mouse embryonic stem cells were labeled with fludeoxyglucose ([^{18}F]-FDG) to monitor retention of grafted cells *in vivo* (Lang et al. 2013). Again, the possible mutagenic and carcinogenic effect of high energy γ photons cannot be underestimated.

The reporter gene and reporter probe paradigm have also been developed for PET. Herpes simplex virus type 1 thymidine kinase (HSV-tk) and reporter probe (2'-fluoro-2'-deoxy-l-)3-D-arabinofuranosyl-5-iodouracil (FIAU) have been evaluated for myocardial gene transfer (Bengel et al. 2003). In addition to HSV-tk and FIAU, NIS with ^{124}I and human estrogen receptor ligand binding domain (hERL) with 16α-[^{18}F] fluoro-17β-estradiol (^{18}F-FES) have been evaluated for in vivo tracking of hMSC graft (Wolfs et al. 2014, Qin, Lan, et al. 2013).

1.3.3 Computed tomography (CT)

X-ray and CT are the most available and affordable imaging modalities, yet CT fell out of favor as imaging modalities for in stem cell tracking due to the requirement of high concentration, high-density / high-atomic number materials as contrast agents (Frangioni and Hajjar 2004). For example, at least 1/8 of the total cell volume is needed to be solid iron to generate enough contrast above background for CT scanning (Frangioni and Hajjar 2004). However, with recent

development of multi-imaging modality methods, CT has been used in tracking MSC grafts in rabbit (Kedziorek et al. 2013).

1.3.4 Ultrasound (US)

The contrast for ultrasound is achieved by acoustic interfaces (e.g. microbubbles and perfluorocarbons) (Frangioni and Hajjar 2004). Ultrasound has the potential to detect a single cell loaded with a single unit of contrast agent (Klibanov et al. 2004). The advantages of ultrasound include extremely cheap imaging cost, wide availability in most clinics, high spatial resolution, and lack of long term side effects. However, ultrasound fell out of favor in recent years due to some limitations like the acoustic "shadowing" effect and limited signal penetrance depth (Klibanov et al. 2004). Despite these limitations, US has been utilized in prostate stem cell monitoring with nanotubes (Wu et al. 2014) and *in vivo* neural progenitor cells tracking with microbubbles (Cui et al. 2013).

1.3.5 Bioluminescence imaging (BLI)

Bioluminescence imaging is one of the complementary optimal imaging methods that utilizes light emitted from a product of an enzyme-mediated chemical reaction. The signal for BLI comes from emission of a photon from luciferin oxidized by the enzyme luciferase in the presence of ATP and oxygen (Shah and Weissleder 2005, Contag et al. 1997). The emitted light is often detected by a charge-coupled device (CCD) camera. From numerous luciferases identified and cloned, two luciferases isolated from two organisms are commonly employed: firefly (*Photius pyralis*) and sea pansy (*Renilla reniformis*). Due to structural and auto-oxidation properties, the luciferase isolated from the firefly is more

broadly used for *in vivo* tracking. The cells have to stably express the gene for luciferase and utilized for long duration monitoring (Welsh and Kay 2005). For *in vivo* BLI imaging, the animals are placed in a dark chamber with a sensitive photodetecter, IVIS Lumina Series Imaging System (PerkinElmer), and D-luciferin is needed to be injected shortly before imaging. In a recent study, human neural progenitor cells (NPC) grafted in mouse brain were tracked *in vivo* for 12 weeks (Bernau et al. 2014). Also, the aforementioned study by Wolfs et al. (Wolfs et al. 2014) has utilized BLI as one of the imaging modalities for their multimodal imaging of hMSC.

However, several limitations are associated with BLI. Since the wavelength of typical BLI utilizes 400-700 nm, the signal is highly susceptible in absorption and scattering in living tissue (Frangioni and Hajjar 2004). This is a major obstacle for it restricts the use of this imaging modality to small animals like mice and rats (Frangioni and Hajjar 2004). Even in mice, false-negative scanning can occur (Rice, Cable, and Nelson 2001). Also, the pharmacokinetics of luciferin has to be taken into account since each organ has a different absorption rate, catalysis rate, and elimination kinetics for luciferin (Lee et al. 2003). Moreover, BLI requires injection of high concentrations of potentially immunogenic substances which makes it unlikely to be used in clinical settings (Frangioni and Hajjar 2004).

1.3.6 Fluorescence light imaging (FLI)

Unlike BLI, FLI uses organic (i.e. green fluorescent protein, near-infrared fluorescent protein) or organic/inorganic approaches (i.e. quantum dots)

(Frangioni 2003). The signal is produced by the fluorescence molecule when the molecule is excited by specific incident wavelength and emits back red shifted light (Frangioni 2003). For *in vivo* monitoring of grafted cells, near-infrared (650-900 nm) fluorescent proteins have demonstrated a great promise due to the relatively high signal penetrance up to 10 mm (Ntziachristos, Bremer, and Weissleder 2003). For both BLI and FLI, single cell resolution can be achieved with intravital microscopy, and even visualizing cell-cell or even cell-protein interaction can be visualized taking an advantage of the multiple fluorophores (Mempel et al. 2006, von Andrian and Mempel 2003). In a recent study, the migration of intestinal stem cells ($Lgr5^+$ cells) has been monitored in single cell resolution with multiphoton intravital microscopy (Ritsma et al. 2014).

Despite the great resolution and the ability to visualize cell-cell interaction, the invasive nature of intravital microscopy prevents it from ever being utilized in neural imaging. For whole body imaging, FLI suffers the same limitations as BLI such as light scattering and signal absorption by surrounding tissue, which limits the depth of tissue to only the surface area. Even with tomographic imaging methods, spatial resolution is limited to approximately 1 mm with signal penetrance up to 100 μm (Ntziachristos et al. 2002).

1.3.7 Magnetic resonance imaging (MRI)

Magnetic resonance imaging holds a great promise as an imaging modality that can be used in non-invasive *in vivo* tracking for stem cell grafts. MRI provides superior resolution, 3-dimensional imaging capability, high safety profile, and the ability to visualize soft tissues. Also, unlike SPECT and PET, MRI is the safest

imaging modality because it does not use radioactive isotopes. Due to these advantages, MRI has been used by most researchers to track stem cells *in vivo*.

1.3.7.1 MRI basics

Magnetic resonance imaging is based on the principles developed for the nuclear magnetic resonance (NMR). Magnetic resonance imaging detects the signal originates from endogenous mobile water protons (^{1}H) or fluorinated molecules (^{19}F). The protons possess spin giving angular momentum (Figure 1-2a), and due to their electrical charge, magnetic momentum (B) arises. When a strong external static magnetic field (B_0) is applied, protons align in the direction of the external magnetic field (Figure 1-2b). When nuclei align with the magnetic field, not only the magnetic moments align with the magnetic field, but they also undergo precession. Precession can be described as wobbling motion of the spinning body around its axis. The alignment process is gradual and associated with the dissipation of energy. When protons align with a static magnetic field, net magnetization (M_0) is created in the parallel direction of the external static magnetic field (z-axis) referred to as longitudinal magnetization. MR signal is produced when electromagnetic waves in the form of radiofrequency (RF or B_1) pulses is introduced perpendicular to B_0 (Figure 1-2c). The resulting magnetization is then on the transverse plane (M_{xy}), and the transverse magnetization precessed about the z-axis creates oscillating electric current that can be detected by an MRI coil. The detected signal is then processed by computer, and an MR image is produced by a magnetic gradient system and a spatial encoding method.

The contrast for MRI is typically generated by manipulating pulse sequences to exploit differences in relaxation properties or proton density. When the external magnetic field is removed, magnetic moments re-align in the external magnetic field direction (B_0). The time it takes to recover net magnetization is called longitudinal relaxation time or spin-lattice (T_1) relaxation (Figure 1-2d). The T_1 relaxation time depends on the mobility of the proton (spin-lattice) or the gyromagnetic ratio of the nucleus. Another method to generate MRI contrast is by utilizing transverse relaxation time (T_2). In contrast to T_1, T_2 measures the diminishing net transverse magnetization in the xy-plane or the loss of spin coherence by dephasing of spins (Figure 1-2e). Two factors affect T_2 relaxation: molecular interactions and local magnetic field inhomogeneity. Combinations of these artifacts result in hastened decay of transverse magnetization referred to as T_2*. The common MRI measures the relaxation of protons. MRI contrast agents generate contrast by inducing either T_1 or T_2 relaxation of juxtapositioned proton generating hyper- or hypointense signal.

1.3.7.2 Labeling methods

There are two methods to label cells: direct and indirect methods (Figure 1-3). Direct labeling method does not involve any genetic modifications (Figure 1-3a). For direct labeling, stem cells are incubated with a contrast agent (e.g. SPIO), and the contrast agent is taken up by the cells. The contrast agent can be coated with polymers or even with surface membrane receptors to enhance the cellular uptake. Although the direct labeling method is relatively easy to employ, there are several limitations. First, the label is diluted as cells divide, and such dilution

limits the monitoring duration. Second, the contrast agent can be released from apoptotic cells and taken up by adjacent cells (i.e. false positive signal) or even localize to the extracellular matrix. The first and second limitations of direct labeling method were well demonstrated in a study involving tracking of *lacZ* expressing neural stem cells labelled with SPIO (Walczak et al. 2007). In this study, the rapid division of neural stem cell grafts resulted in the dilution of MRI contrast. In postmortem analysis, they further demonstrated the lack of MRI contrast in the stem cell-derived neuronal cell populations (Walczak et al. 2007). Third, transfection agents are sometimes used in order to assist cellular uptake of probes by the cells affecting motility, differentiation potential, viability, proliferation, and functionality (Youn and Hong 2012). This limitation can be overcome with an indirect labeling method (Figure 1-3b). Indirect labeling methods utilize molecular cloning strategies. A reporter gene can be expressed in the stem cell, and stem cell grafts can be tracked longitudinally. Depending on the promoter used, the expression of the reporter gene can be restricted in a specific cell type or can be expressed constitutively. Many strategies have been developed including enzymes, receptors, and iron chelating proteins. While the indirect labeling method provides information about viability of the grafted cells and allows longitudinal tracking, epigenetic silencing or immunogenic response by the host can occur (Kircher, Gambhir, and Grimm 2011). Lists of direct and indirect probes are provided in Table 1-3.

The indirect labeling method can be further divided into exogenous (reporter mediated) and endogenous (*de novo*) methods (Figure 1-4) (Vande

Velde, Himmelreich, and Neeman 2013, Vandsburger et al. 2013). The exogenous method requires administration of imaging probe that creates contrast (Figure 1-4a). Just prior to imaging, an appropriate imaging probe is administrated, and either the activation or accumulation of the imaging probe generates contrast. One limitation of the exogenous method might be the pharmacokinetics of the imaging probe (Vandsburger et al. 2013). On the other hand, the endogenous method does not require administration of imaging probe (Figure 1-4b), but continuous expression of reporter gene can result in unforeseen consequences such as cytotoxicity (Vandsburger et al. 2013). In one study, chronic overexpression of H-ferritin (FTH1) resulted in a neurodegeneration phenotype (Kaur et al. 2007). Therefore, the expression of a reporter gene can be regulated by an inducible promoter such as Tet-On or Tet-Off switches (Figure 1-4c). The controllable expression approach adds an additional safety by minimizing the impact (on proliferation, migration, and differentiation) of constitutive expression of the reporter. However, both exogenous and endogenous methods share some limitations which include; low dynamic resolution because of the lifetime of the signal depends on the clearance of the reporter and genetic manipulation of stem cell is required and clinical application is unlikely.

1.3.7.2.1. Exogenous MRI reporters

Two types of reporters have been investigated for the exogenous method: enzymes and engineered cell surface peptides (Figure 1-5). The first exogenous MRI reporter gene was reported in 1997 (Moats, Fraser, and Meade 1997). In this study, a molecule, Egad, was synthesized containing Gd^{3+} in a cage composed of

galactopyranose ring and tetraazamacrocycle. When the molecule was exposed to β-galactosidase, galactopyranose was removed from the molecule, and the exposure of Gd^{3+} enhanced longitudinal relaxation of water molecules resulting in positive T_1 contrast (Moats, Fraser, and Meade 1997). Various imaging probes have been developed for *lacZ/β-galactosidase* (Vande Velde, Himmelreich, and Neeman 2013). The versatility of *lacZ/β-galactosidase* system is that depending on the imaging probes used, T_1, T_2, or T_2* contrast can be generated. A recent study has demonstrated that β-galactosidase expressing MSC can be tracked *in vivo* by S-Gal™ as an imaging probe which enhanced T_2 and T_2* MR contrast (Bengtsson et al. 2010), yet several limitations were observed for the *lacZ/β-galactosidase* system including the requirements of direct injection of imaging probe, non-specific cellular uptake of the contrast agent, pharmacokinetics of substance, and possible effects on cell viability (Vande Velde, Himmelreich, and Neeman 2013). An alternative approach uses engineered cell surface peptides as a MRI reporters. In one study, an engineered surface protein expressing hemagglutinin (HA), luciferase, and myelocytomatosis (myc) (i.e. HA-fluc-myc) was developed as an MRI reporter (Chung, Kee, et al. 2011) HA and myc serve as the molecular target for antibody conjugated with SPIO. Both human and mouse ESCs expressing HA-fluc-myc have demonstrated significant hypointense signal in proliferating ESC and teratoma (Chung, Kee, et al. 2011). Several surface receptors, such as biotinylated transmembrane receptor (BAP-TM) and anti-polyethylene glycol (PEG) peptide, have also been developed as genetic MRI reporters, and have been evaluated in cancer cells (Tannous et al. 2006, Chuang et al. 2010). In 2010, Westmeyer et al. developed an interesting method utilizing

a secreted enzyme as a genetic MRI reporter. This study demonstrated secreted alkaline phosphatase (SEAP) could be used as a genetic MRI reporter by aggregation of SPIO (Westmeyer, Durocher, and Jasanoff 2010).

1.3.7.2.2 Endogenous MRI reporters

Endogenous MRI reporters utilize a gene or a set of genes that do not require exogenous substrates to generate MRI contrast. The first endogenous MRI reporter identified was transferrin receptor (*Tfrc*) (Koretsky et al. 1996). When TFRC was overexpressed in cells, R_2* contrast was significantly enhanced (Koretsky et al. 1996). Later, improved contrast was generated when transferrin associated SPIO was used, which takes advantage of endogenous approach with the exogenous approach (Weissleder et al. 2000). Although iron is crucial for normal cell function, internal free labile, chelatable and redox-active, iron is strictly maintained by networks of genes (Frey and Reed 2012). Other genes involved in iron homeostasis like transferrin (*Trf*) and ferritin have also been explored. Transferrin is involved in transporting iron into the cell while ferritin is involved in storing iron in the cell. Of all genes involved in iron homeostasis, ferritin has been the most popular with various applications (Vande Velde, Himmelreich, and Neeman 2013). The overexpression of a heavy chain of ferritin (FTH1) has been demonstrated to generate R_1 and R_2 contrast *in vitro* and *in vivo* (Cohen et al. 2005). Following this study, different strategies have been developed: overexpression of either FTH1 or ferritin light chain (FTL1) alone, or both FTH1 and FTL1. One study has expressed human FTH1 as a reporter for *in vivo* tracking of cardiac stem cells (Campan et al. 2011). The cell survival was

monitored up to 4 weeks after grafting using T_2 weighted imaging and T_2* mapping with a multiecho gradient echo sequence (Campan et al. 2011). In order to demonstrate the sensitivity of the system, human FTH1 and TFRC have also been coupled and overexpressed in murine neural stem cells. The overexpression resulted in enhanced transverse relaxivities observed in both R_2 and R_2* (Campan et al. 2011). Ten days after the graft, T_2*-weighted imaging yielded increased contrast only with 2,500 cells (Campan et al. 2011). FTH1 has been used for stem cell tracking such as embryonic stem cells (Liu et al. 2009) and myoblasts (Naumova et al. 2010). These, studies have demonstrated significant MR signal enhancement between 14 to 21 days after injection. However, further investigation is needed for the impact of overexpressing FTH1 on iron homeostasis. The overexpression of TFRC has shown to activate iron overload response, and the overexpression of FTH1 or FTL1 has shown to activate iron deficiency response (Vandsburger et al. 2013). In 1997, another endogenous MRI reporter gene, tyrosinase, was reported (Weissleder et al. 1997). Tyrosinase is the main enzyme involved in melanin production, and the overexpression of tyrosinase results in melanin accumulation. Melanin is excellent in sequestrating paramagnetic ions, which result in T_1 contrast (Weissleder et al. 1997). Although tyrosinase has not been used in stem cells, the interest of using tyrosinase as a MRI reporter has been revisited due to its ability to employ multimodal imaging such as MRI, photoacoustic, and PET (Qin, Cheng, et al. 2013). Recently, divalent metal transporter-1, DMT1 was examined as a novel MRI reporter gene. The overexpression of DMT1 enhanced manganese uptake and resulted in a significant increase in R_1 (Bartelle et al. 2012). Unlike attenuation of MR signal

with iron homeostasis associated genes, DMT1 resulted in signal enhancement, which was correlated with better sensitivity. However, intraperitoneal injection of $MnCl_2$ was needed to achieve better contrast. Also, systemic and cellular impact of exposure to manganese has to be further investigated. Another possible endogenous MRI reporter candidate is MagA. MagA is a membrane iron transporter protein associated in magnetosome formation in magnetotactic bacteria (Bazylinski and Frankel 2004, Nakamura, Burgess, et al. 1995, Nakamura, Kikuchi, et al. 1995). Magnetosome is magnetite-enriched organelle. MagA is involved in transporting iron and forming magnetite (Fe_3O_4) crystals (Nakamura, Kikuchi, et al. 1995). Magnetite crystals are considered to be an excellent MRI contrast agent because they can induce transverse relaxation time (T_2/T_2*). Although the complete reconstruction of a magnetosome in foreign cells has not been achieved, a number of studies have demonstrated that the overexpression of MagA increased MRI contrast (Zurkiya, Chan, and Hu 2008, Goldhawk et al. 2009, Rohani et al. 2013, 2014, Sengupta et al. 2014). Although the biosynthesis of magnetosomes was achieved in non-magnetosome-forming bacteria by an elaborate stepwise recombination method (Kolinko et al. 2014), the complete reconstruction of a magnetosome in a mammalian cell has not been achieved. The biosynthesis of magnetosomes in mammalian cells might provide the cells with superparamagnetic iron while protecting the host cell by isolating magnetite in membrane-bounded magnetosome organelles (Blackwood et al. 2008). However, the lack of mammalian homologs of genes involved in magnetosome formation might cause immune reactions (Vandsburger et al. 2013).

Compared to the constitutive expression of a MRI reporter gene, an inducible system can be advantageous in multiple aspects. First, controllable expression of a MRI reporter can minimize adverse consequences of constitutive expression of a reporter gene (e.g. toxicity, reduced proliferation rate, possible impact on differentiation potential, etc.). Another advantage is the use of a pharmacological inducing agent with well-documented pharmacokinetics. One of the agents, Dox, has been widely used in controllable expression systems and has shown low toxicity and the ability to cross blood-brain barrier as well as the placenta barrier (Bohl and Heard 2004). Inducible MRI reporters have been reported in *in vivo* monitoring of cell grafts. Cohen et al. have demonstrated *in vivo* monitoring of C6 glioma tumors expressing TET-EGFP-HA-ferritin (Cohen et al. 2005). By employing the Tet-Off system, Cohen et al. were able to illustrate the overexpression of murine FTH resulted in significant R_2 relaxation up to 28 days post transplantation (Cohen et al. 2005). In 2008, Zurkiya et al. have demonstrated efficacy of monitoring tetracycline inducible (Tet-On) MagA in human embryonic kidney cell (293FT) transplanted in the striatum of mice (Zurkiya, Chan, and Hu 2008). In a more recent study, nasopharyngeal carcinoma cells expressing human ferritin heavy chain (FTH1) under the regulation of Tet-Off system were used in *in vivo* monitoring of cell grafts (Feng et al. 2012). By doing so, Feng et al. observed a significant increase in transverse relaxivity (R_2) with the overexpression of FTH1. The proliferation, cytotoxicity, apoptosis, and migration of the cell could be assessed. Not only have inducible genetic MRI reporters been employed in the monitoring of cell grafts but, they also have been employed in detection of gene expression. In 2007, Cohen et al.

generated transgenic mice with TET:EGFP-HA-ferritin (tet-hfer) transgene (Cohen et al. 2007). By mating with mice expressing tetracycline transactivator (tTA) under a tissue-specific promoter (e.g. vascular endothelial (VE) cadherin promoter and liver activator protein (LAP) promoter) the expression of the tissue-specific genes were monitored with MRI (Cohen et al. 2007). However, an inducible MRI reporter gene has not been applied in stem cell monitoring.

1.3.8 Chemical exchange saturation transfer (CEST)

Chemical exchange saturation transfer (CEST) or CEST-MRI has recently become an attractive imaging modality with the development of tailored artificial peptides (Ward, Aletras, and Balaban 2000). Unlike MRI, which measures T_1 or T_2, CEST measures the radiofrequency signal generated when molecules (or contrast agent) exchange protons with nearby water molecules. CEST has three major advantages: first, CEST allows imaging of multiple molecules with adequate separation of resonance frequency; second, the contrast can be turned on and off by applying a saturation pulse; third, CEST can be used with and without exogenous contrast agent (Vandsburger et al. 2013). In 2007, a lysine-rich protein (LRP) has been developed as a CEST reporter gene (Gilad et al. 2007). By expressing LRP in neural implanted glioma cell, a robust signal was observed in CEST-MRI (Gilad et al. 2007). Despite the fact that CEST can be employed to monitor multiple molecules and does not require exogenous contrast agent making CEST a good candidate for translational regenerative therapies (Vandsburger et al. 2013), complex post-processing methods need further development and evaluation *in vivo*.

1.3.9 Multimodal imaging methods

Contemporary developments have focused on molecular probes that allow multimodal imaging, which utilizes two or more imaging techniques (e.g. MRI and PET). The improvement of a multimodal imaging probe might overcome some of the limitations associated with a single imaging modality. Many studies have investigated fusion proteins as a multimodal molecular imaging reporter, and there have been multiple studies that have investigated double or even triple multimodal imaging. The early strategy was to combine optical and PET like hrl-mrfp-ttk (Ray et al. 2004) or HSV1-TF/GFP/Fluc (Ponomarev et al. 2004). One genetic reporter, tyrosinase, has demonstrated triple modality molecular imaging (Qin, Cheng, et al. 2013). In this study, Qin et al. transfected human breast cancer cells (MCF-7) with human tyrosinase (TYR). A special probe targeting melanin, N-(2-(diethylamino)ethyl)-^{18}F-5-fluoropicolinamide, was employed for PET imaging while the nature of melanin as iron chelator and enhancer of optical absorption allowed imaging utilizing MRI and photoacoustic methods (Qin, Cheng, et al. 2013). The fact that the overexpression of one single protein was used as a multimodal reporter makes this study especially interesting; however, the impact of the overexpression of tyrosinase and the accumulation of melanin need further investigation.

1.4 Magnetosome as an endogenous MRI genetic reporter

As mentioned above, the magnetosome has the potential to become a valuable tool for *in vivo* monitoring of cell grafts. The magnetosome is a membrane-bound organelle found in magnetotactic bacteria (MTB), first discovered in 1975

(Blakemore 1975). The term magnetotactic bacteria refers to the biological function of the magnetosome to allow these bacteria to navigate in the environment using earth's geomagnetic field to find a favorable niche for food and oxygen (Frankel and Bazylinski 2009). There are many different sizes and shapes in magnetite (Fe_3O_4) and greigite (Fe_3S_4) crystal structures formed inside magnetosomes. The typical size ranges from 35 - 120 nm with three common crystal morphologies: cuboidal, rectangular, and bullet-shaped (Bazylinski and Frankel 2004). Of these, smaller crystals are not permanently magnetic at room temperature (i.e. superparamagnetic) (Bazylinski and Frankel 2004). Unlike magnetic particles (i.e. particles with permanent magnetic moment), paramagnetic particles have positive magnetic susceptibility and are attracted to the magnetic field. Magnetite nanocrystals are considered to be superparamagnetic, which has much larger magnetic susceptibility than the paramagnets. Therefore, superparamagnetic particles are considered to be an excellent MRI contrast agent.

The formation of the magnetosome can be divided into three steps: 1. vesicle formation, 2. iron uptake, and 3. biomineralization (Rahn-Lee and Komeili 2013) (Figure 1-6). The formation of magnetosome starts with invagination of the inner plasma membrane. The newly formed vesicle is attached to the cytoskeletal structure in the cell. Next, the iron is actively transported into the vesicle. Lastly, the iron in the vesicle is actively incorporated into the magnetite crystal, and the shapes and sizes of the crystals are determined by the specific species (Goldhawk et al. 2012).

The formation of the magnetosome is controlled by a set of proteins with specific biological functions. These proteins are unique to MTB and are encoded by genes identified by genomic comparison of four species of MTB with nonmagnetotactic bacteria (Richter et al. 2007). Among 28 genes identified, 18 genes were located within magnetosome genomic island (MAI). There are number of operons in the MAI: magnetosome membrane (Mam), magnetic particle membrane specific (Mms), and a monocistronic MamW (Faivre and Schuler 2008). Also, there are operons outside of MAI, and these are magnetotaxis (Mtx) and magnetosome membrane (Mme) (Goldhawk et al. 2012). The functions of several operons are still under investigation. Some of these operons have clear association with biosynthesis of magnetosomes while some have little or no association. Genes that are associated with magnetosome formation are listed in Table 1-4 with their putative functions. In *Magnetospirillium magneticum* (strain AMB-1), only the genes in the mamAB operon have shown to be essential for the magnetosome formation (Murat et al. 2010). The biosynthesis of the magnetosome and the biomineralization process of magnetite crystals in MTB are still under active investigation.

1.4.1 Use of magnetosome related genes in MRI

The genes involved in biomineralization and iron transport are particularly interesting from the MR imaging perspective. A number of genes demonstrated involvement in biomineralization: *mms6*, *mad* (*10,11,12,23,25*), and *mam* (*G,F,D,C*). Of these, *mms6* identified in magnetite crystals has been extensively studied, (Arakaki, Webb, and Matsunaga 2003). *mms6* regulates the

mineralization of magnetites by binding to iron on the C-terminal domain (Rahn-Lee and Komeili 2013). Although the efficacy of using *mms6* as an MRI reporter has been examined in 293T cell and demonstrated a significant increase of R_2 (Zhang et al. 2010), further investigation is needed for potential application in *in vivo* tracking of cell grafts. If *mms6* is similar to a ferritin system (iron chelator), whereas *magA* and *chapA* act more like a transferrin receptor. When overexpressed, iron transporters might increase the iron content of the cell, allowing the cell to be monitored using MRI. For these reasons, *chapA* and *magA* have been investigated as MRI reporters.

1.4.2 MagA as a candidate for *in vivo* monitoring using MRI

The focus of this study was to evaluate MagA as a genetic MRI reporter for tracking stem cell grafts *in vivo*. The *magA* gene was discovered in a transposon mutagenesis study in *Magnetospirillium magneticum* strain AMB-1 (Matsunaga et al. 1992). The expression of *magA* was regulated by iron, and the expression of *magA* in *E. coli* indicated an increased iron concentration in vesicles (Nakamura, Burgess, et al. 1995). The gene *magA* is encoded by 1,305 nucleotides with a putative promoter located 75 bp upstream of the start codon (Nakamura, Kikuchi, et al. 1995). A nucleotide homology search (BLAST, NCBI) determined *magA* is homologous to Na^+/H^+ transporter, ferrous transporter, CPA2, KefC, and KefB (Table 1-5) (Altschul et al. 1990). In 1995, Nakamura et al. used MagA-luc fusion protein to localize MagA protein in a subcellular compartment in *E. coli* and validated that the protein is localized in a vesicle structure (Nakamura, Kikuchi, et al. 1995). With the earlier study from the same group, the results

strongly support the idea that MagA is a membrane-bound protein (H^+/Fe(II) antiport), and the expression can enhance the iron content of a cell (Nakamura, Kikuchi, et al. 1995). A macro protein domain search (CDD, NCBI) returned 2a37 (member of KefB superfamily) as a highly conserved domain (Figure 1-7a) (Marchler-Bauer et al. 2013). KefB is glutathione-regulated potassium-efflux system (Bakker et al. 1987) with a metal binding domains. The predicted transmembrane structure and protein model were generated using the Phyre server (Kelley and Sternberg 2009), and the model was rendered using Pymol (Figure 1-7b,c) (Guex and Peitsch 1997). Also, the MagA predicted model and c2k3ca (metal transporter templates) were aligned to create a superposition model to illustrate a possible iron binding domain (Figure 1-7d).

Several studies have investigated the application of MagA in MRI cell tracking (Zurkiya, Chan, and Hu 2008, Goldhawk et al. 2009, Rohani et al. 2014, Sengupta et al. 2014). In 2008, Zurkiya et al. demonstrated that the expression of MagA under the tetracycline inducible promoter in 293FT cells can enhance T_2* contrast in a Dox dosage dependent manner (Zurkiya, Chan, and Hu 2008). Moreover, the transplantation of 100,000 cells into the mouse brain can generate significant contrast in a T_2*-weighted image without previous exposure to Dox and iron supplements (Zurkiya, Chan, and Hu 2008). In a more recent study, Rohani et al. compared MagA and FTH1+FTL1 in the ability to enhance the MR contrast *in vivo*. Here, MagA or FTH1+FTL1 lacking iron response element was expressed in human breast/melanoma (MDA-MB-435) cells and used for repetitive imaging of a tumor. MagA expression resulted in similar contrast to

FTH1-FTL1 expressing cells and illustrated contrast enhancement up to 20 days (Rohani et al. 2014). Also, the same group was able to present similar results *in vitro* showing similar contrast from the cells expressing either MagA or FTH+FTL1 (Sengupta et al. 2014).

The main goal of my study was to evaluate the feasibility of using MagA as a noninvasive MRI genetic reporter for monitoring stem cell grafts.

1.5 Discussion

Molecular imaging has revolutionized our understanding about the molecular biology of the cell. With multiple imaging modalities available, an enormous effort has been invested in developing molecular imaging reporters. Each reporter has its own advantages and disadvantages. Compared to direct labeling methods, indirect endogenous labeling methods have advantages that are critical for stem cell monitoring, including the ability to longitudinally monitor the grafted cells and specificity for rapidly dividing cells. A genetic MRI reporter is important for the advancement and clinical translation of regenerative medicine. The application of a genetic MRI reporter includes tracking cell migration, proliferation/viability imaging, neurogenesis imaging, myocardiac stem cell imaging, cancer stem cell imaging, immune cell imaging, and monitoring of gene expression and differentiation (Vande Velde, Himmelreich, and Neeman 2013, Ahrens and Bulte 2013, Youn and Chung 2013). The monitoring of grafted cells is important in terms of evaluating therapeutic efficacy. Due to the limitations associated with current direct and exogenous monitoring methods, a genetic

reporter is likely to become a key to usher in successful translation of regenerative medicine.

Other than previously mentioned concerns (e.g. increasing cytotoxicity and affecting differentiation potential) of expressing a generic MRI reporter, there are other pitfalls that might be associated with using a genetic MRI reporter. First, since the expression of a reporter gene requires genetic modifications, the integration site of the reporter gene might affect its expression, disrupt normal cell function, might be epigenetically silenced, and even promote malignant transformation (Vande Velde, Himmelreich, and Neeman 2013). One way to overcome this problem is by using targeted gene insertion (knock-in). However, the efficiency of generating knock-ins is low. Second, tissue specificity has to be examined especially in stem cells because the expression of the reporter gene later in differentiated cells can be affected by epigenetic silencing. Also, overexpressing a gene, introducing a foreign gene, or increasing iron content in a cell might trigger host immune response, and the immune cells like macrophages might increase iron concentration at the graft site to create a nonspecific signal (Vande Velde, Himmelreich, and Neeman 2013). Third, when an inducible promoter is used, impact on the temporal resolution by the duration associated with translating of the protein and accumulating enough contrast agents, turnover rate of the reporter, and clearance have to be investigated (Vande Velde, Himmelreich, and Neeman 2013).

1.6 Study proposal

As researchers focus more on clinical translation of cell replacement therapy and regenerative medicine, there are increased demands for methods to monitor and study grafted cells. Despite rapid growth in the number of contrast agents and reporters, there are is more room for improvement. The main focus of this study is to evaluate the possible use of MagA in tracking stem cell grafts *in vivo* using MRI. Although there are multiple steps and numerous genes involved in magnetosome formation in bacteria, the whole reconstruction of magnetosomes may not be necessary to achieve the goal of enhancing MR contrast. Our previous report and two recent studies have demonstrated that expression of MagA alone can generate sufficient MR contrast that can be detected by MRI (Zurkiya, Chan, and Hu 2008, Rohani et al. 2014, Sengupta et al. 2014). Therefore, we hypothesize that the expression of MagA can allow monitoring of stem cell graft *in vivo*, and controlled expression of MagA ensures safety from adverse impacts of expression MagA.

Figure 1. Number of literatures

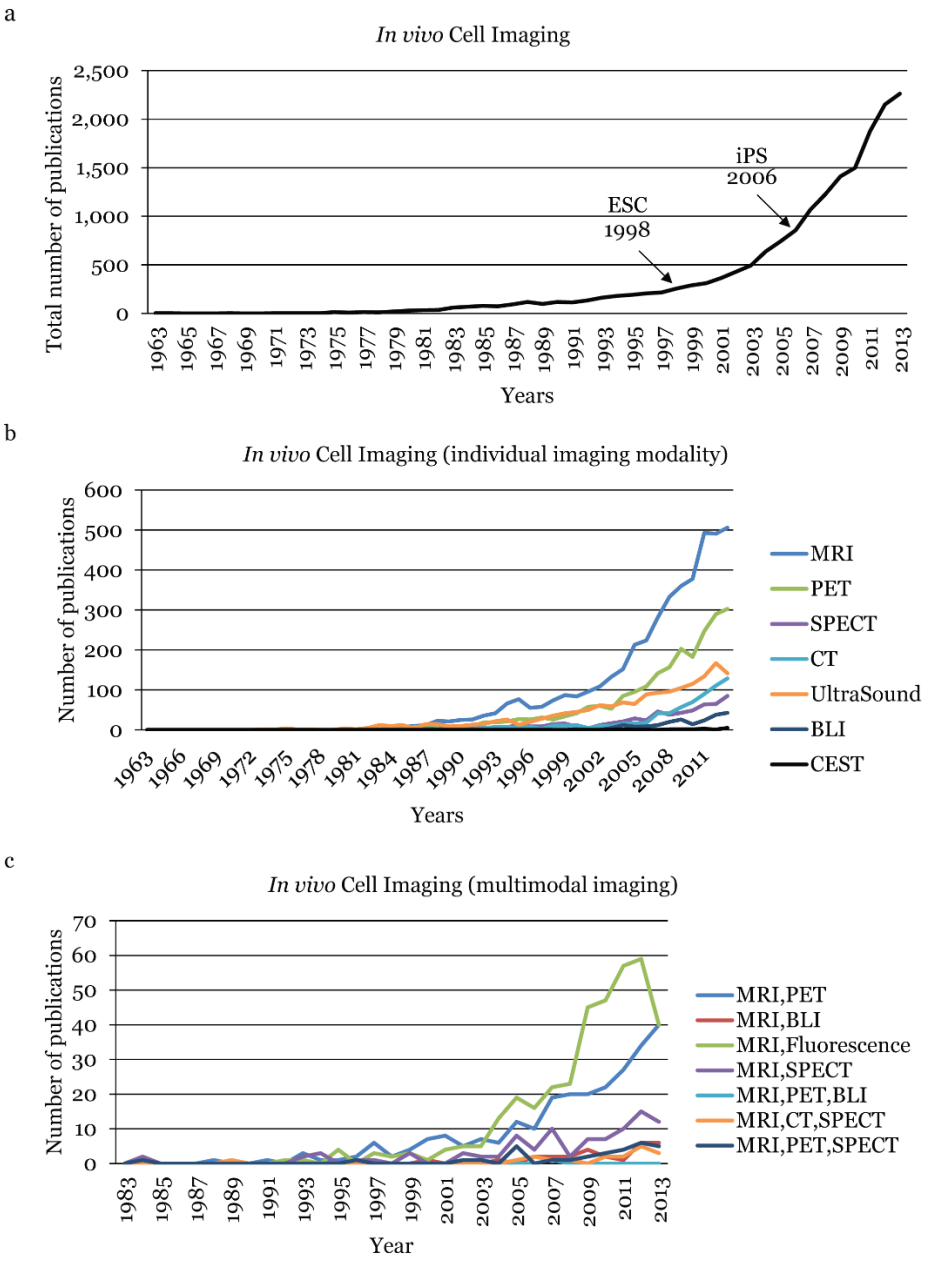

Figure 1-1. Number of publications by year. (a) Total number of publications by year. The PubMed search was conducted using terms *in vivo* cell, imaging, tracking, or monitoring while excluding terms like reviews, methods, and drug delivery. The years when embryonic stem cell (1998) and induced pluripotent stem cell (2006) were developed are indicated by arrows. (b) Number of publication broken down into each imaging modality. (c) Number of publications utilizing multimodal imaging methods.

Abbreviations: PET – positron emission tomography, MRI – magnetic resonance imaging, BLI – bioluminescence imaging, CT – computed tomography, SPECT – single photon emission CT, CEST – chemical exchange saturation transfer

Table1-1. Characteristics of an ideal imaging reporter for *in vivo* stem cell graft monitoring

1.	Nontoxic
2.	Maintenance of pluripotency
3.	High sensitivity
4.	Signal persistency
5.	Specificity
6.	Noninvasive
7.	Longitudinal imaging
8.	No repetitive injection

Table 1-2. Characteristics of imaging modalities

Imaging modality	*Spectrum*	*Probe used*	*Type of visualization*	*Spatial resolution*	*Temporal resolution*	*Signal depth*	*Longi-tudinal*	*In clinic*	*Cost*
SPECT	High energy γ-rays	^{99m}Tc, ^{111}In, ^{123}I, NIS, NET	Whole-body	1 ~ 2 mm	min	Good	+	Yes	$$
PET	Low energy γ-rays	^{18}F, ^{124}I, ^{64}Cu, HSV-tk, NET	Whole-body	1 ~ 2 mm	10 sec ~ min	Good	+++	Yes	$$$$
CT	X-rays	^{125}I, Gd	Whole-body	50 ~ 200 μm	min	Excellent	+	No	$$
US	High frequency sound	Microbubbles, perfluorocarbons	Limited	1~ 2 mm	sec ~ min	mm ~ cm	+	No	$
BLI	Visible light	Luciferase	Whole-body*	3 ~5 mm, 3 ~ 5 μm*	min	1 -2 cm	+++	No	$$
FLI	Near-infrared	QDs, Fluorescent proteins	Intravital microscope	3 ~5 mm, 2 ~ 3 μm*	sec ~ min	< 1 cm	++	No	$$
MRI	Radiowaves	Lanthanides, SPIO**, PEPE, Tyrosinase, β-galactosidase, LacZ, TFRC, FR, MagA	Whole-body	10 ~ 100 μm	min ~ hr	Excellent	+++	Yes	$$$
CEST	Radiowaves	HSV-tk, hPRM1, lanthanides, lipo-CEST	Whole-body	25 ~ 100 μm	min ~ hr	Excellent	+++	No	$$$

*non-*in vivo* or small animal only, **including USPIO, MION, CLIO

Abbreviations: NIS – sodium iodide symporter, NET – norepinephrine transporter, Gd – gadolinium, QD – quantum dots, SPIO – superparamagnetic iron oxide, PEPE – perfluoropolyether, TFRC – transferrin receptor, FR – ferritin, HSV-tk – herpes simplex virus type 1 thymidine kinase, hPRM1 – human protamine-1

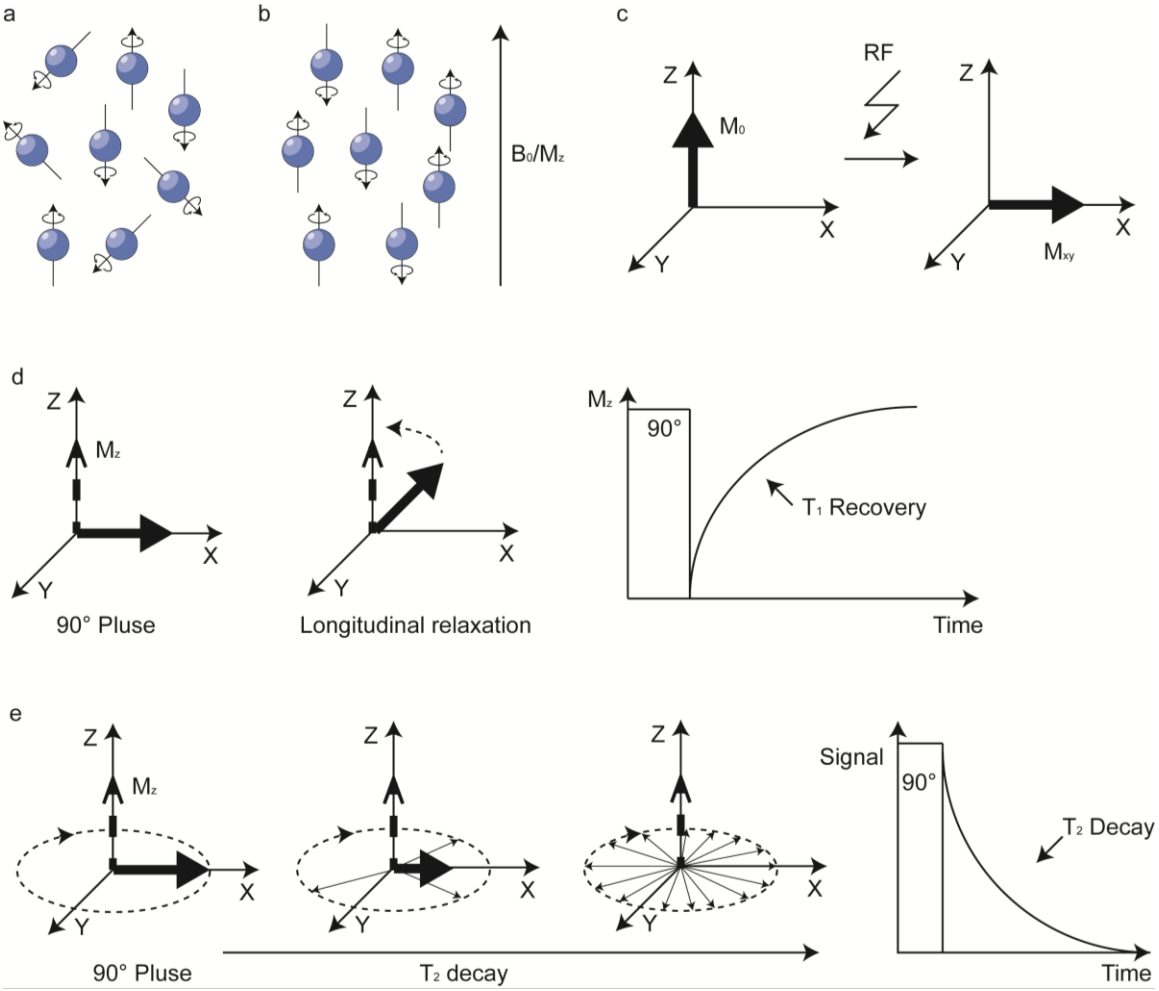

Figure 1-2. Basics of MRI. (a) Protons in equilibrium state show random alignment. (b) In the presence of strong external magnetic field (B_o), more protons align with the magnetic field producing longitudinal magnetization (M_z). (c) An external radiofrequency (RF) pulse can tip the magnetization by 90° causing transverse magnetization (M_{xy}). (d) T1 relaxation is measured by the decay of transverse magnetization and recovery of longitudinal magnetization. (e) When the transverse magnetization is removed, out of phase spins of protons cause the loss of transverse magnetization (T_2 and T_2* relaxation).

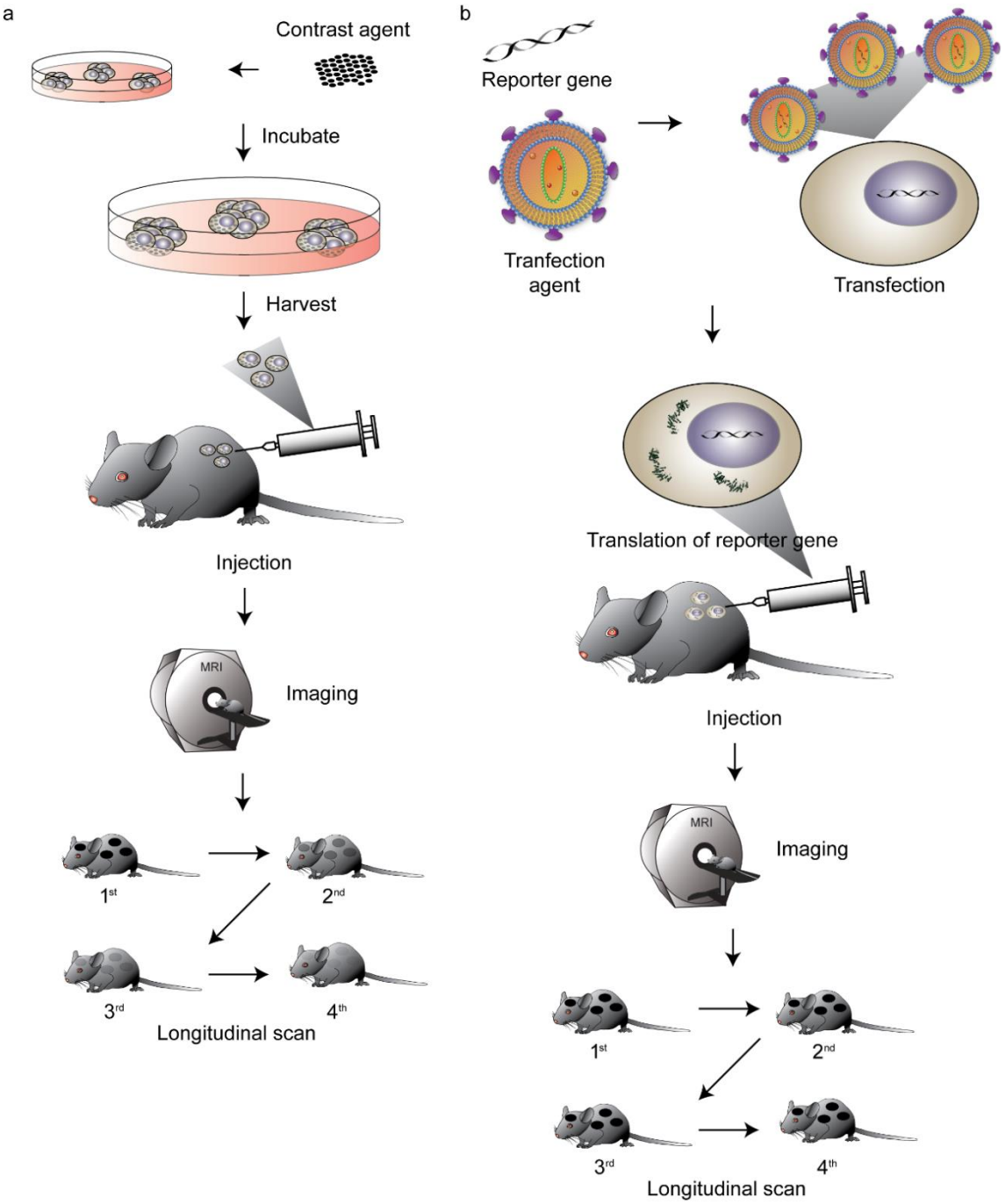

Figure 1-3. Direct and indirect labeling methods. (a) In direct labeling method, cells are incubated with contrast agent (e.g. SPIO). Cells actively take up the contrast agent and are harvested after a specific incubation period. The harvested cells are injected into a study subject, and the cells are tracked by using imaging modality of choice. The major limitation with direct labeling method is the dilution of contrast agent. (b) For indirect labeling method, a reporter gene is transduced to the cells, and cells expressing the reporter gene are injected into a study subject. The major advantage of indirect labeling method is that the contrast agent does not get diluted after cell division allowing, longitudinal monitoring.

Table 1-3. Lists of direct and indirect probes

Probing method	Probe	Imaging modality	Toxicity reported	Research area	FDA approved
Direct	Gd^{3+} or Mn^{2+}	MRI - T_1 (+)	Yes	Viability, migration	Yes
	SPIO, USPIO, CLIO, MION	MRI - T_2 (-)	Yes	Viability, migration	Yes
	PFC	^{19}F MRI	Yes	Viability, migration	Yes
	QD	FLI	Yes	Immunology (homing)	Yes
	Fluorescent probe	Intravital microscope	No	Migration, cell-cell interaction, infiltration, homing	Yes
	^{111}In, ^{99m}Tc	SPECT	Yes	Homing, cell therapy efficacy	Yes
	^{18}F, ^{64}Cu	PET	Yes	Homing	Yes
Indirect	Ferritin / transferrin receptor	MRI - T_2/T_2^* (-)	No	Viability, migration, differentiation	No
	β-galactosidase	MRI - $T_1/T_2/T_2^*$ (-)	Yes	Viability, migration	No
	Tyrosinase	MRI - T_1 (-)	Yes	Viability	No
	MagA	MRI - T_2/T_2^* (-)	No	Viability	No
	Plasma membrane bound reporter peptide	MRI - $T_1/T_2/T_2^*$ (+/-)	Yes/No	Viability, differentiation	No
	Lysine-rich protein	CEST	No	Viability, migration, pH sensing	No
	Fluorescent protein	FLI	No	Migration, cell-cell interaction, infiltration, homing	No
	Luciferase	BLI	No	Migration	No
	HSV-tk (^{18}F)	PET/SPECT	Yes	Viability, migration	No
	NET	PET/SPECT	Yes	Migration, homing	No
	NIS	SPECT	Yes	Migration, homing	No
	Dopamine 2	PET	Yes	Viability	No
	Somatostatin	PET/SPECT	Yes	Viability	No
	DMT1	MRI - T_1 (+)	No	Viability	No

For MRI – (-) for negative contrast and (+) for positive contrast

Abbreviations - MION – monocrystalline iron oxide, USPIO – ultrasmall superparamagnetic iron oxide, CLIO – cross-linked iron oxide, PEPE – perfluoropolyether, SPIO – superparamagnetic iron oxide, NIS – sodium iodide symporter, NET – norepinephrine transporter, QD – quantum dots, DMT1 – Divalent metal transporter 1

References by row
Gd (Louie et al. 2000), Mn (Sterenczak et al. 2012), SPIO (Patel et al. 2010, Neri et al. 2008), USPIO (Boni et al. 2014), CLIO (Kircher et al. 2003), MION (Sibov et al. 2014), PFC (Hitchens et al. 2014, Ahrens and Zhong 2013), QD (Walling, Novak, and Shepard 2009), fluorescent probes (Sutton et al. 2008), SPECT (Jin et al. 2005, Gildehaus et al. 2011), PET (Qin, Cheng, et al. 2013), ferritin/transferrin receptor (Rohani et al. 2014, Liu et al. 2009, Moore et al. 1998), β-galactosidase (Walczak et al. 2007, Louie et al. 2000, Furth et al. 1994), tyrosinase (Alfke et al. 2003, Qin, Cheng, et al. 2013), MagA (Zurkiya, Chan, and Hu 2008, Goldhawk et al. 2009, Rohani et al. 2014, Sengupta et al. 2014), plasma membrane bound reporter peptide (Severance, Chakraborty, and Kosman 2004), lysine-rich protein (Gilad et al. 2007), fluorescent proteins (Li et al. 2010), luciferase (Wolfs et al. 2014, Bernau et al. 2014, Oh et al. 2013, Hwang do et al. 2008), HSV-tk (Chuang et al. 2010, Bengel et al. 2003), NET (Moroz et al. 2007), NIS (Wolfs et al. 2014, Huang et al. 2001), dopamine 2 (Jiang et al. 2011), somatostatin (Wang et al. 2013), DMT1 (Bartelle et al. 2012)

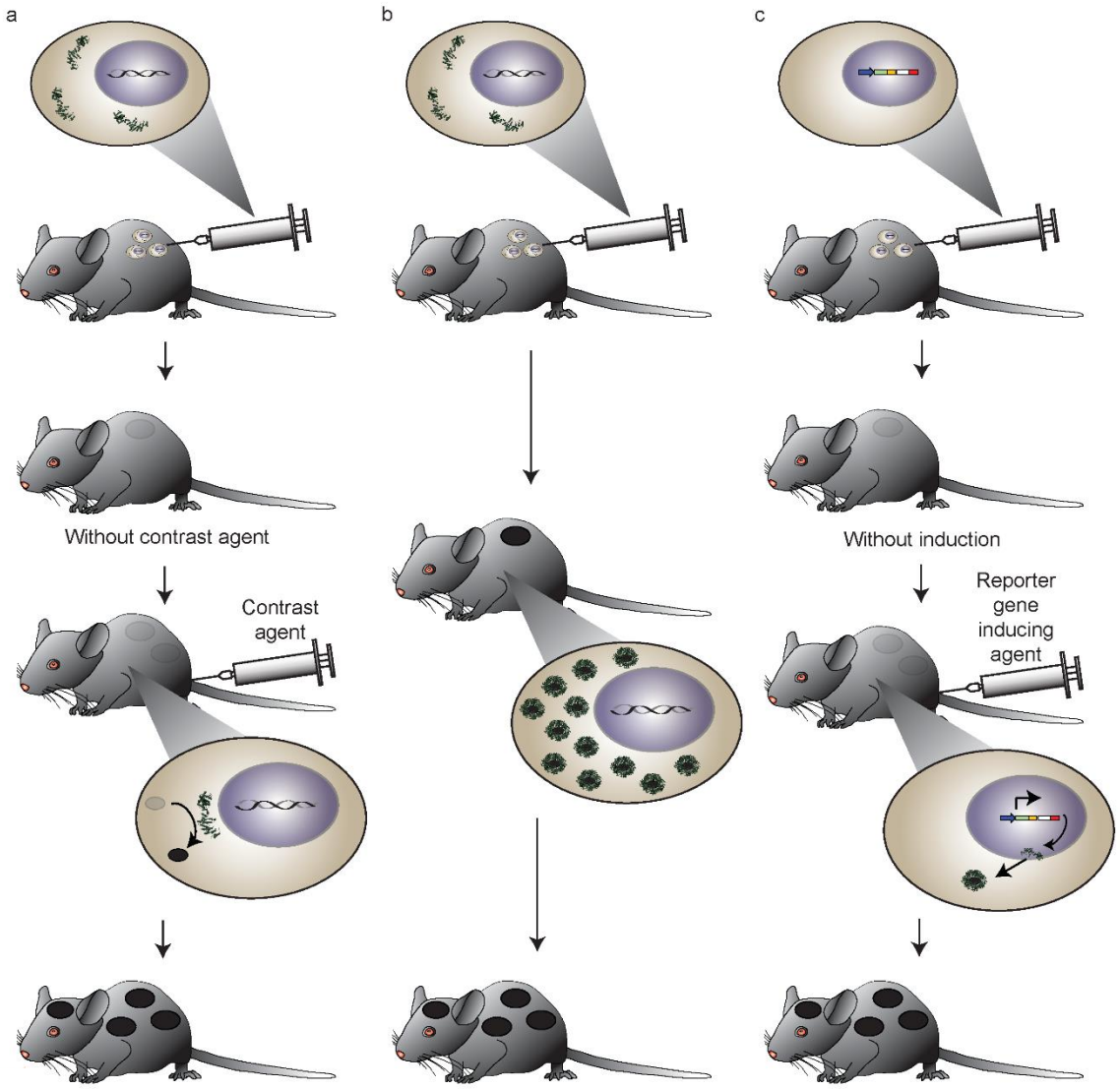

Figure 1-4. Exogenous and endogenous labeling methods. (a) Exogenous labeling method requires injection of a contrast agent. Either the binding of the contrast agent or activation by enzyme generates contrast. (b-c) Endogenous labeling methods. (b) Constitutive expression does not require injection of contrast agent but lacks the mechanism to regulate the expression. (c) An inducible promoter allows expression of the reporter gene when monitoring is required.

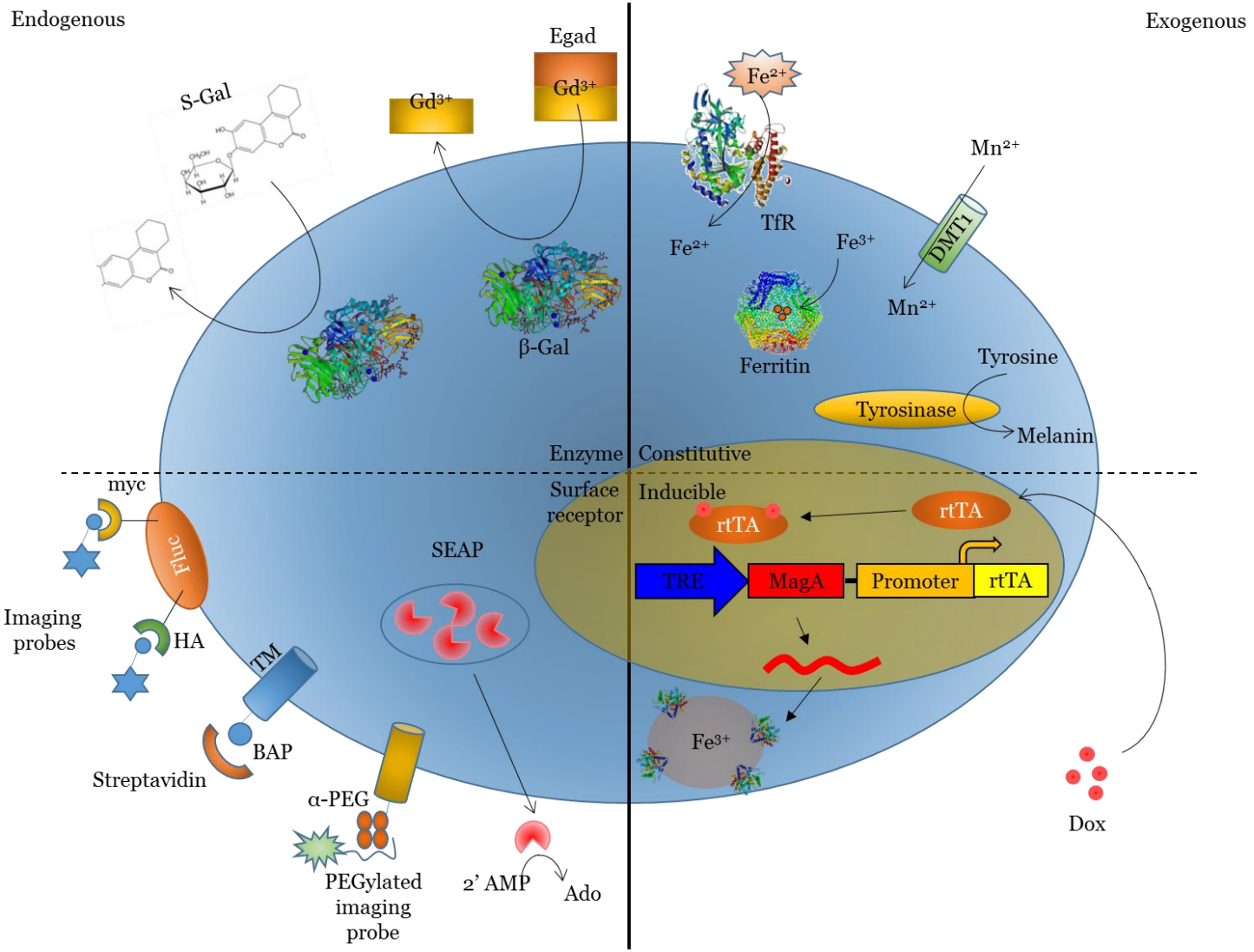

Figure 1-5. Exogenous and endogenous genetic reporters.

Table 1-4. Magnetosome associated genes

Gene name	Essential	Process involved
magA, feoB	Somewhat	Iron transporter
chpA	Yes	Copper-dependent, high affinity iron transporter
mamB, M, N	Yes	Cation diffusion facilitator of metal transporter
mamH, Z	No	Major facilitator superfamily of transporter
nir, nap	Yes	Reduction of nitrate to nitric oxide (oxidizing ferrous iron)
mamE, P, T	Yes	Magnetochrome / electron transport chain
mamX	No	Magnetochrome / electron transport chain / iron reductase
mamZ	No	Iron reductase
mms6	No	Regulation of the mineralization of iron
mad25, 23, 10, 11, 12	No	Shape and size regulation of biomineralization
mamG, F, D, C	No	Biomineralization / regulates size of the a magnetite crystal
mamQ	Yes	Biomineralization
mamJ, K	Yes	Cytoskeletal structure
mamI, L	Yes	Vesicle formation

(Lefevre et al. 2013, Matsunaga et al. 1992, Dubbels et al. 2004, Murat et al. 2010, Uebe et al. 2011, Raschdorf et al. 2013, Li et al. 2013, Li et al. 2012, Siponen et al. 2012, Arakaki, Webb, and Matsunaga 2003, Scheffel et al. 2008, Faivre and Schuler 2008, Komeili et al. 2006)

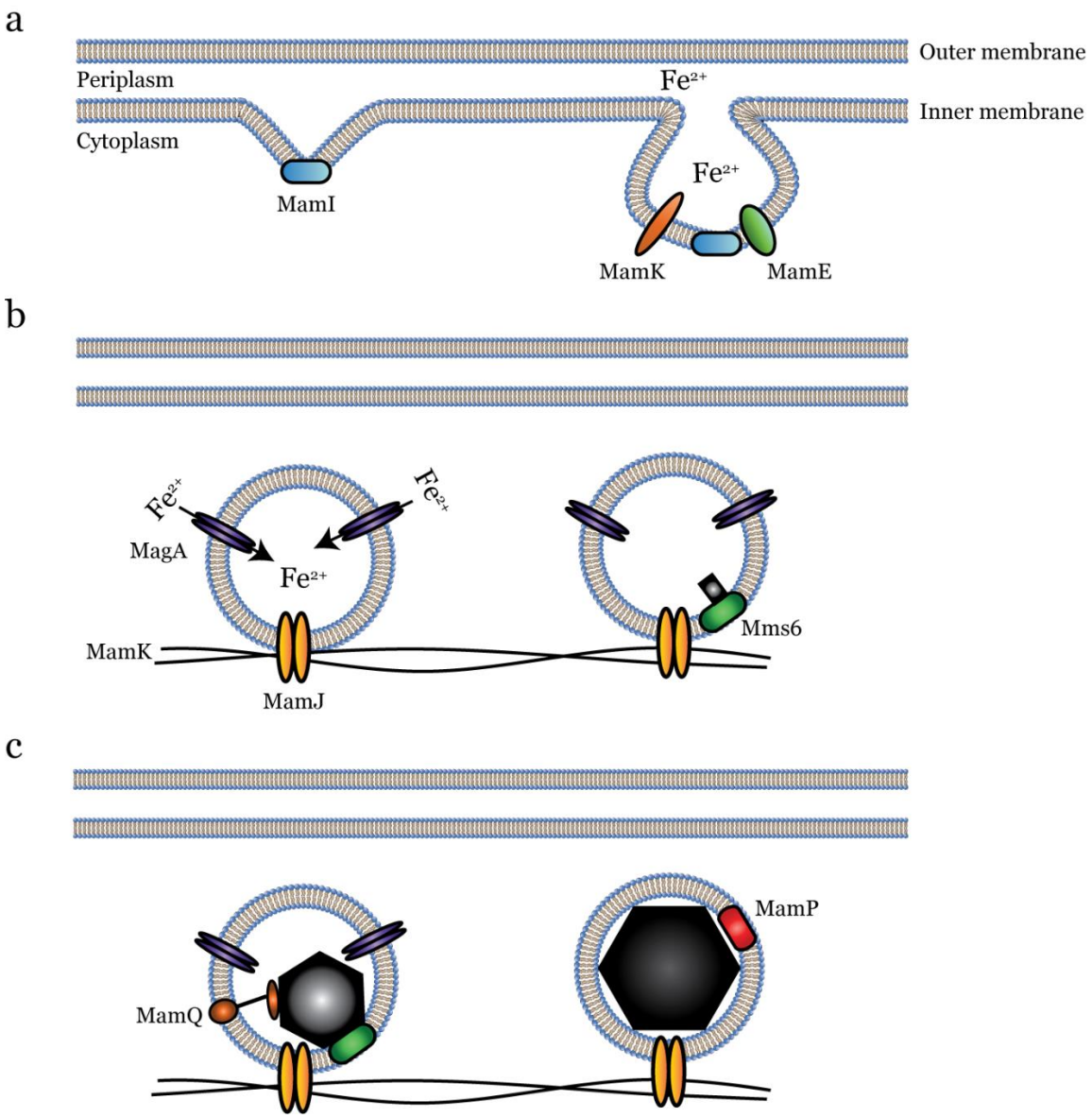

Figure 1-6. A model of a magnetosome formation process. (a) The first step of magnetosome formation is invagination and vesicle formation. The initial invagination process is activated by MamI, L, Q, and B. A vesicle is formed by recruiting additional proteins (e.g. MamK and E). (b) After the vesicles are formed, they are aligned on a chain via interaction between MamK, a cytoskeletal structure, and MamJ, a membrane bound protein. Mm6 is involved in the biomineralization process. (c) A magnetite crystal starts to form with the increase of iron content in the vesicle with many proteins involved in the process (i.e. MamA, G, F, D, and C). MamP appears to be involved in the size restriction.

Table 1-5. *magA* homology BLAST search result

Gene	Organism	Function	Max score	Identity
Na^+/H^+ exchanger	*Magnetospirillum gryphiswaldense*	Sodium/hydrogen exchanger	544	69%
Kef-type K^+ transport system	*Caenispirillum salinarum*	K^+ transporter	402	55%
Ferrous transporter	*Candidatus Odyssella thessalonicensis*	Fe^{2+} transporter	305	44%
Na^+/H^+ antiporter / Ferrous transporter	*Nitratireductor indicus*	Sodium/hydrogen exchanger and ferrous transporter	304	44%
Na^+/H^+ antiporter / Ferrous transporter	*Fulvimarina pelagi*	Sodium/hydrogen exchanger and ferrous transporter	254	40%
CPA2	*Glaciecola chathamensis*	monovalent cation/H^+ antiporter	217	38%
Na^+/H^+ exchanger	*Mariprofundus ferroxydans*	Sodium/hydrogen exchanger	206	35%
KefC	*Francisella sp.*	Glutathione-regulated potassium-efflux	214	31%
KefB	*Nitritalea halalkaliphila*	Potassium transporter	189	31%

Table 1-6. MagA conserved domain

Conserved domain	
TM PBP1	Transmembrane subunit of periplasmic binding protein (PBP)-dependent ATP-Binding Cassette (ABC) transporters
Na^+/H^+ exchanger	Sodium/hydrogen exchanger superfamily
KefC	Kef-type K^+ transport system (inorganic ion transport and metabolism)
2a37	Transporter, monovalent cation/proton antiporter-2 (CPA2) family - transport and binding proteins, cations and iron carrying compounds
RosB	Kef-type K^+ transport system, predicted NAD-binding component (inorganic ion transport and metabolism)
KefB	Kef-type K^+ system, membrane component (inorganic ion transport and metabolism)
NhaP	NhaP-type Na^+/H^+ and K^+/H^+ antiporters (inorganic ion transport and metabolism)

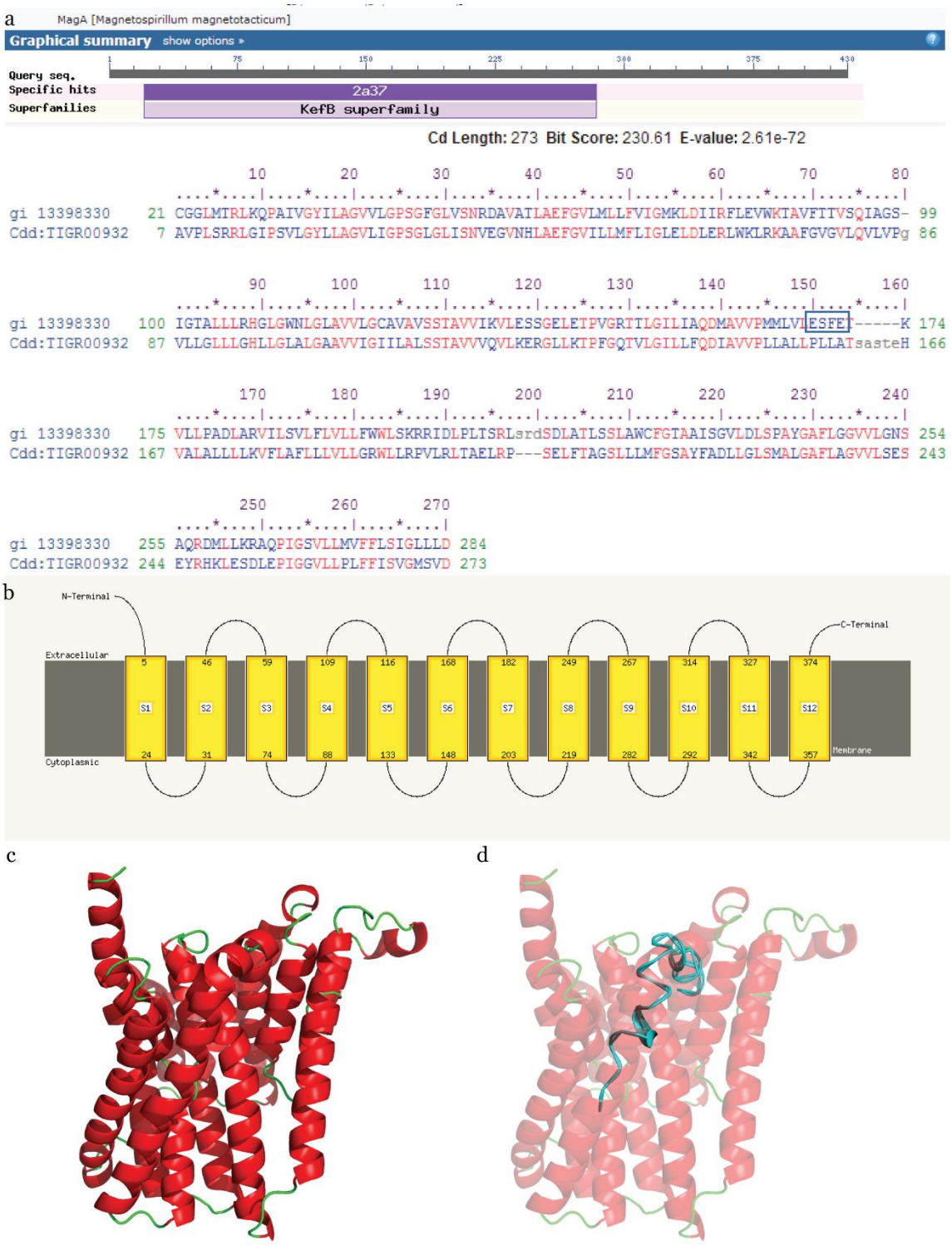

Figure 1-7. MagA protein structure analysis. (a) BLAST search of the MagA protein sequence demonstrates high similarity to 2a37 (KefB superfamily). E-X-X-E, iron binding motif (Severance, Chakraborty, and Kosman 2004), is highlighted in MagA sequence. (b) Phyre server generated transmembrane helix prediction with 12 transmembrane regions. (c) Phyre server generated MagA 3D structure. (d) Superimpose model of MagA and c2k3ca.

Chapter 2

In vitro evaluation of MagA as a genetic MRI reporter for stem cell monitoring

Part of this chapter has been accepted to be published on ***Theranostics***. Cho, I.K., Moran, S.P., Paudyal, R., Piotrowska-Nitsche, K., Cheng, P.H., Zhang, X., Mao, H., Chan, A.W., Longitudinal monitoring of stem cell grafts in vivo using magnetic resonance imaging with inducible MagA as a genetic reporter. 2014.

2.1 Abstract

Cell replacement therapy and regenerative medicine hold a great potential of treating currently incurable diseases such as neurodegenerative diseases. One of the obstacles in making clinical translation is the challenge of non-invasive, *in vivo* assessment of the fate of grafted cells over a long period of time. Here we evaluated MagA as a genetic MRI reporter in mESC. The expression of MagA, a bacterial protein involved in forming iron oxide nanocrystals, was regulated by the Tet-On switch allowing inducible expression. A mES cell-line carrying Tet-MagA (mESC-MagA) was established by lentivirus transduction. Impacts of expressing MagA in mESC were evaluated by proliferation assay, the expression of cytotoxicity markers, teratoma formation, MRI, inductively coupled plasma atomic emission spectroscopy (ICP-OES), and *in vitro* spontaneous differentiation. The expression of *magA in vitro* showed moderate toxicity, significantly induced relaxivity (R_2) with MRI, and showed no impact in pluripotency but showed an increase in early ectodermal lineage specific genes in differentiation. Our results demonstrate that MagA might be useful as a genetic MRI reporter for mESC monitoring.

2.2 Introduction

One of the major obstacles of clinical translation of regenerative medicine are the challenges of monitoring the fate of grafted cells *in vivo*. Besides immunity and functionality of cell grafts, lack of understanding of the fate of implanted cells and their correlation with clinical outcomes have hindered the progress of translation. Thus, there is an urgent need to develop noninvasive

imaging tools that allow longitudinal assessment of cell grafts in aspects of proliferation rate, viability, differentiation, and functional integration.

As described in the previous section, various imaging modalities have been developed for monitoring cell grafts *in vivo*. Among these methods, MRI has the greatest potential because high spatial resolution and high signal penetrance (Table 1-2), which are particularly important for large animal models. However, implanted cells cannot be monitored with MRI unless a contrast agent is used. Metal-chelate exogenous contrast agents and synthetic superparamagnetic iron-oxide (SPIO) nanoparticles have been used to improve contrast (Weissleder 1991, Remsen et al. 1996, Moore et al. 1998, Bulte et al. 1999, Artemov et al. 2003, Bulte et al. 2001, Lewin et al. 2000). Due to dilution of the contrast agents as cells continue to divide, cell grafts can only be tracked for a limited time when using exogenous contrast agents. One alternative to overcome the current limitation associated with using exogenous contrast agent is a developing a transgenic MRI reporter.

An example of a transgenic MRI reporter is the ferritin system (Cohen et al. 2005, Genove et al. 2005, Vande Velde et al. 2011, Vande Velde et al. 2012). Ferritin is an iron chelating protein that is involved in iron storage in cells. Due to low sensitivity and low specificity, the application of the ferritin system in cell tracking has been very limited (Vande Velde et al. 2011, Vande Velde et al. 2012). Another possible candidate is transferrin receptor. However, when transferrin receptor was compared to ferritin, transferrin receptor showed higher toxicity and lower increase in MR contrast (Liu 2009). Therefore, there is a need for an

alternative MRI reporter. Another possible candidate is MagA, which is a bacterial protein transporting iron and forming magnetite (Fe_3O_4) crystals (Nakamura, Kikuchi, et al. 1995). A previous study demonstrated the expression of MagA in mammalian cells and subsequent formation of magnetosomes that resulted in increased MR contrast (Zurkiya, Chan, and Hu 2008). One recent study reported the continuous monitoring of breast cancer cell grafts for up to 34 days after injection into mice (Rohani et al. 2013). Also, compared to the most frequently used ferritin system, MagA generated similar MR contrast as the ferritin system (Rohani et al. 2014).

MagA is one of the key proteins involved in magnetosome formation (Fukuda et al. 2006). Moreover, surprisingly, when MagA is expressed, magnetosomes-like structures are formed in eukaryotic cells.

Although we have demonstrated the feasibility of using MagA as a genetic MRI reporter in 293FT cells, there are still many concerns needed to be addressed when it is applied in stem cells. Since no study has confirmed whether MagA can be employed in stem cell populations, important biological aspects, such as viability, transgene expression, and impact on differentiation, need to be addressed. Also, although MagA expression could increase MR contrast in 293FT cells and other cancer cell lines (Zurkiya, Chan, and Hu 2008, Rohani et al. 2014, Goldhawk et al. 2009), the functionality of MagA as a genetic MRI reporter needs to be addressed in a stem cell population. Moreover, since even ferritin system have exhibited adverse impact in certain cell populations (Picard et al. 1996, Cozzi et al. 2000, Arosio and Levi 2002, Kaur, Rajagopalan, and Andersen 2009,

Kaur et al. 2007), impact on cell functionality has to be independently assessed in stem cell population.

As a way to address these concerns, we have employed the Tet-On inducible system in order to minimize the unforeseen adverse impact of expressing MagA. As a proof-of-concept, mouse ESC (mESC) were used as the experimental model. mESCs are easier to maintain and have a high proliferation rate, which makes it accessible for various characterizations. Also, mESCs are more malleable to genetic modifications, and lentiviral transduction have shown to be effective in establishing stable transgenesis in mESC (Pfeifer et al. 2002, Ma et al. 2003).

Here we show the *in vitro* investigation of MagA as a transgenic MRI reporter in ESCs. A stable mouse ESC (mESC) line expressing MagA under the control of tetracycline inducible promoter, mESC-MagA was established by lentiviral transduction and was used in subsequent studies. The impact of expressing MagA was determined by assessing proliferation, cytotoxicity, and pluripotency. Finally, the impact of iron accumulation and MRI signal was evaluated. The experiments will address the impact of expressing MagA in mESC and the feasibility of using MagA as a genetic MRI reporter.

2.3 Methods

Cells and Vectors

The cell line was established by Karolina Piotrowska-Nitsche, and the lentiviral vector was created by Pei-Hsun Cheng. A wild-type mouse embryonic stem cell

line (mESC-WT), AB 2.2, which was derived from the 129/SvEV strain, was maintained as a stable culture on a single layer of mitomycin-C inactivated mouse embryonic fibroblast (MFF) cells with Dulbecco's modified Eagle's medium (DMEM; Invitrogen) containing 15 % fetal bovine serum (FBS; Atlanta Biologicals), 2 mM L-glutamine (L-Glu; Invitrogen), 0.1 mM β-mercaptothanol (β-Mer; Sigma), 100 U/ml penicillin and 100 μg/ml streptomycin (P/S; Lonza), 0.1 mM of MEM Eagle Non-essential Amino Acid (NEAA; Lonza), and 1,000 IU/ml of human recombinant leukemia inhibiting factor (hLIF; Chemicon). Medium was changed daily and cells were passed every two days at 1:10 to 1:15 ratio. For the passage, mESC were treated with 0.05 % trypsin-EDTA (Life Technologies) and dissociated into single cells.

To generate mouse mESC expressing a fusion gene of *magA* with human influenza hemagglutinin (HA) tag under the control of a tetracycline response element (TRE) (Tet-MagA) (Figure 2-1). The *magA* gene (provided by L.E. Bertani, California Institute of Technology) was cloned as described before (Zurkiya, Chan, and Hu 2008). LV-Tet-MagA was generated by co-transfecting pLV-Tet-MagA with packaging vector pΔ8.9 and envelope vector pVSV-G into 293FT packaging cells (Invitrogen). The culture medium was collected at 48 h post-transfection and used to infect mESC supplemented with polybrene (8 μg/ml) overnight. The viral medium was replaced with fresh medium following day. At 48 h post transduction, 100 μg/ml of zeocin was supplemented in mESC medium for selection, and a single colony was picked manually and expanded to create a clonal cell line (mESC-MagA).

Quantitative real-time PCR (qPCR)

To evaluate successful transduction and differentiation potential, quantitative real-time PCR was conducted. Total RNA was isolated from the cells using TRIzol® (Life Technologies) following standard method. Briefly, cells were suspended in 500 µl of TRIzol® and homogenized with 21G sterile syringe. The homogenized samples were incubated for about 5 min at room temperature, and 100 µl of chloroform (EMD) was added. Samples were vortexed well and incubated about 3 min at room temperature. The samples were centrifuged at 12,000 g for 10 min at 4°C. The aqueous phase was carefully transferred to DNase/RNase inactivated micro-centrifuge tubes, at which point 250 µl of isopropanol (Sigma) was added. The samples were mixed gently and put into a -20°C freezer to allow precipitation of RNA for overnight. The samples were centrifuged at 12,000 g for 30 min at room temperature. The supernatant was removed, and RNA pellets were washed twice with ice cold 750 µl of 75% ethanol followed by centrifugation at 7,500 g for 5 min at 4°C. After the second wash, RNA pellets were briefly allowed to dry about 5-10 min and dissolved in diethylpyrocarbonate-treated water. The RNA concentration was measured on Nanodrop 2000C spectrophotometer (Thermo Scientific). To ensure there was no genomic DNA in the sample, samples were treated with DNase using TURBO™ DNase (Life Technologies) at 37°C for 30 min. The cDNA was synthesized with 500 ng of RNA sample using a High-Capacity cDNA Reverse Transcription Kit (Applied Biosystems). Quantitative real-time PCR was performed using TaqMan® Gene Expression Master Mix (Applied Biosystems) for TaqMan probes, and for

the rest of qPCR reactions, SsoAdvanced™ Universal SYBR® Green Supermix (Bio-Rad) was used. The primer sequences are summarized in Table 2-1. Quantitative real-time PCR amplification was performed using Bio-Rad CFX96 real-time PCR detection system. Gene expression was calculated by comparative CT ($2^{-\Delta\Delta CT}$) normalized to 18S rRNA transcript levels.

Western Blot

Cells were lysed in RIPA buffer. Total protein concentration was determined by DC™ Protein Assay Kit (Bio-Rad). The level O.D. 750 nm was read using Synergy HT Multi-Mode Microplate Reader (Bio-Tek). A total of 30 μg of protein were separated using 4-15% gradient SDS-PAGE (4-15% Ready Gel® Tris-HCL Gel; Bio-Rad) and transferred onto a PVDF membrane using a 15 min protocol on the Trans-Blot Turbo Transfer System (Bio-Rad). The membrane was then blocked for an hour at room temperature in 3% BSA with 0.05% Tween-20. Subsequently, the membrane was probed with primary antibodies overnight at 4°C (mouse anti-HA.11 clone 16B12 monoclonal 1:1,000 (Covance), mouse anti-α-tubulin clone DM1A monoclonal (Sigma)). After washing several times with PBST (PBS with 0.05% of Tween 20), the membrane was incubated with secondary antibody (HRP-conjugated goat anti-mouse 1:10,000 (Abcam)), and visualized with the Western Lighting™ Ultra chemiluminescence substrate kit (PerkinElmer) using the ChemiDoc™ XRS+ System (Bio-Rad). The quantification of MagA-HA was performed using Image Lab™ software (Bio-Rad) and MagA-HA expression was normalized to α-tubulin.

Immunocytochemistry

Cells were fixed with 4% paraformaldehyde (PFA) for 15 min. The fixative solution was removed, and the cells were washed with PBS for 3 times. Cells were then incubated with a blocking buffer which consists of 0.20% Triton X-100, 3 mM sodium azide, 0.1% saponin, 2% BSA, and 5% donkey serum in PBS for 30 min to an hour at room temperature. After the blocking step, cells were incubated with primary antibody for overnight at 4°C. After 3 washes with PBS, cells were incubated with secondary antibody for 30-45 min at room temperature. Hoechst staining was done (0.12 μg/ml) to visualize the nucleus. The list of antibodies used for *in vitro* experiment is summarized in Table 2-2.

Teratoma formation test

All protocols involving animals were approved by Emory University's Institutional Animal Care and Use Committee. A total of $1x10^6$ cells were injected subcutaneously at the front shoulders of nude mice (Crl:NU(NCr)-*Foxn1*^{nu} CD-1 nude mice; Charles River). The development of teratoma was monitored daily following Emory University's Tumor Burden Scoring Guideline. In order to evaluate the iron content after Dox induction, mice were fed 5 mg/ml of Dox and 0.5 mg/ml of FC for 3 days before euthanasia. Teratomas were removed and fixed in 4% paraformaldehyde overnight. We performed hematoxylin and eosin (H&E) staining and Prussian blue staining for iron on the tumor sections.

Cell proliferation rate / cytotoxicity assay

The cell proliferation rate was evaluated by total cell count before and after Dox treatment. Cytotoxicity was assessed using the Muse™ Annexin V & Dead Cell Assay (EMD Millipore). A total of $1X10^4$ cells were treated with 1 μg/ml Dox or 25 μM FC or both in 24-well cell culture plates for 3 days. Cells were harvested at the end of the incubation period, and cytotoxicity was measured via externalization of phosphatidylserine (PS) which readily conjugated with annexin V. The late apoptotic stage was evaluated with 7-aminoactinomcin D (7-AAD), which is a fluorescent intercalator that shows spectral shift upon association with DNA. Relative changes, compared to the untreated group were calculated for both cell lines, and all data are presented as standard error of the mean (SEM).

Cell preparation for MRI

Prior to the experiment, MEFs were depleted from the mESC culture by culturing mESC without the MEF up to three passages on gelatin coated 10 cm plates. A total of $3x10^6$ cells were seeded on a gelatin coated 10 cm cell culture plate without MEF. For each treatment, two plates were prepared for each cell line. However, for the mESC-MagA Dox/Iron group, three plates were prepared in order to compensate for the slower growth. Cells were cultured with or without the supplement of 1 μg/ml of doxycycline and 25 μM of FC for 3 days. At the end of treatment, cells were washed two times with PBS with calcium and magnesium and one time with PBS without calcium and magnesium to remove any residual FC. Cells were then trypsinized and collected. Collected cells were fixed with 4% PFA for approximately 30 min. A total of 7-9 x 10^7 cells were resuspended in 90 μl DMEM.

Cell pellet MRI

A special sample preparation method was utilized in order to improve MRI scan (Figure 2-1). The sample preparation method helped to minimize the air-sample interference, the impact of magnetic field inhomogeneity, and the number of cells per scan. Also, this special sample preparation method allowed multiple sample scan at a single scan. The resuspended cell samples were carefully placed in 0.5 ml straws (TS Scientific) with one end sealed with Leica Critoseal® (Figure 2-1a,b). After the samples were placed into the straws, with all the air bubbles removed, the other end was sealed with parafilm. The straws were carefully arranged, with references (DMEM) (Figure 2-1d), in a tube prepared from two 50 ml conical tubes. 1% agarose was poured between straws to remove any air gaps.

MRI of cell pellets

The cell pellets were imaged using a Bruker Biospec 7T MR scanner (Bruker Biospin, Billerica, MA). The multi-slice and multi-TE (MSME) spin-echo sequence were used. T_2 relaxation times were measured with the acquisition parameters: echo time (TE) = 20 to 600 ms in increments of 20 ms; Time of repetition (TR) = 10,000 ms; field of view (FOV) = 30 X 30 mm; image matrix = 128 x 128; and slice thickness = 1 mm, 2 averages.

R_2 (=$1/T_2$) values were derived from T_2 measurements by the curve fitting of nonlinear monoexponential algorithm, $M_{(TE)} = M_0 \exp(-TE/T_2)$ where TE is the echo time, M_0 is signal intensity at TE = 0, and $M_{(TE)}$ is signal intensity at corresponding TE. Image processing and analysis were performed using ImageJ

1.46r (NIH), KaleidaGraph (Synergy Software), SPSS 20 (IBM), and Excel (Microsoft).

Inductively coupled plasma atomic emission spectroscopy (ICP-OES)

Cell pellets were collected after the MRI scan and briefly washed in PBS. Briefly, samples were processed into dry powder and atomized in the nebulizer. The atomized samples were fed directly into plasma flame and light emission was recorded at different wavelengths specific for the element of interest. All the iron contents were normalized to cell pellet weight. Also, iron contents were normalized to the copper content to compensate for inter-sample variations.

***In vitro* spontaneous differentiation evaluation**

In vitro spontaneous differentiation protocol was adapted from 2006 Yamanaka's mouse iPS paper (Takahashi and Yamanaka 2006). For uninduced group, 5,000 cells were grown for 3 days on Mitomycin-C inactivated mouse embryonic fibroblast (MEF) with Dulbecco's Modified Eagle's Medium (DMEM; Invitrogen) supplemented with 15 % fetal bovine serum (FBS; Atlanta Biologicals), 2 mM L-glutamine (L-Glu; Invitrogen), 0.1 mM β-mercaptoethanol (β-Mer; Sigma), 100 U/ml penicillin, 100 μg/ml streptomycin (P/S; Lonza), 0.1 mM of MEM Eagle Non-essential Amino Acid (NEAA; Lonza), and 1000 IU/ml of human recombinant leukemia inhibiting factor (hLIF; Chemicon). The cells were trypsinized, and the live and dead cells were separately counted using Trypan blue staining. Only 60,000 live cells were transferred to a bacteria culture plate to form embryo bodies (EBs) for three days in the same media without hLIF

supplement as aforementioned. Then, EBs were transferred to gelatin-coated plates. The attached embryo bodies were allow to differentiate for three days in hLIF depleted media. At the end of the differentiation, cells were collected for RT-PCR and ICC (Figure 2-2a). For MagA induced group, cells were treated with Dox for three days prior to form EBs. The same number of live cells, 60,000, were transferred for EB formation (Figure 2-2b). Also, cells were treated with Dox after the initial differentiation step in order to investigate whether inducing MagA affects differentiated cells (Figure 2-2c).

Statistical analysis

All data and graphs are presented with standard error (SE). For all MRI data, MRI images were first processed, and signal intensities were extracted using ImageJ (NIH). All statistical analyses were done using one-way analysis of variance (ANOVA) in SPSS 20 (IBM).

2.4 Results

2.4.1 Establishment of a mESC-MagA cell line

In order to express MagA only at the time when MRI is performed, we used a Tet-On inducible expression system to regulate the expression of MagA. A human hemagglutinin A (HA) tag was placed downstream of the *magA* gene and inserted into a lentiviral vector under the control of the tetracycline response element (TRE). The rtTA sequence was inserted downstream of an ubiquitin promoter (*Ubi*), and zeocin, an antibiotic-resistant gene, and was expressed through the

internal ribosome entry site (IRES). The resulting Tet-On MagA lentiviral vector (LV-Tet-MagA) is illustrated in Figure 2-3a. Doxycycline (Dox) in culture medium regulated the expression of MagA. Dox acts like a switch in the system (Figure 2-3b,c). High-titer LV-Tet-MagA was prepared as previously described (Zurkiya, Chan, and Hu 2008) and used to infect mESCs, followed by clonal selection using zeocin. A mESC line expressing the Tet-MagA (mESC-MagA) was established and used for subsequent studies.

2.4.2 Expression profiling

Immunocytochemistry (ICC) evaluated the expression of MagA in mESC using a specific antibody that recognizes the HA since no antibody for MagA was available (Figure 2-4). There was no detectable signal in the wild-type control mESCs (mESC-WT). Immunostaining demonstrated homogeneous expression of MagA in mESC-MagA upon induction by 1 μg/ml of Dox for three days. No expression of MagA was observed without the presence of Dox.

In order to evaluate the expression profile of MagA, gene and protein expression profiles were determined. Inducibility of *magA* expression in mESC-MagA was first tested by using different concentrations of Dox. *magA* transcripts can be induced by supplementing Dox in a mESC-MagA culture, whereas *magA* transcripts were not detectable in mESC-WT (Figure 2-5a). The expression of *magA* followed a linear positive correlation with Dox concentration, and the maximum expression of *magA* was observed at 1 μg/ml of Dox. Western blot analysis showed MagA protein expression level using HA tag. There was no difference in the protein level when 0.25 μg/ml or more of the Dox was used to

induce MagA expression. Both RT-PCR and Western blot analysis demonstrated that the expression of MagA is regulated by the presence of doxycycline.

2.4.3 Evaluation of pluripotency

In order to evaluate if the presence of the Tet-MagA affects pluripotency of ESC, immunostaining using stem cell specific antibodies and a teratoma assay in nude mice were performed (Figure 2-6). Both mESC-MagA and mESC-WT expressed stem cell markers (Figure 2-6a). Teratoma formation assay using nude mice evaluated the impact of pluripotency (Figure 2-6b). A sub-cutaneous injection of $1x10^6$ mESC-WT or mESC-MagA cells developed teratomas. Both mESC-WT and mESC-MagA derived teratoma were able to form all three germ layers demonstrated by H&E stain (Figure 2-6b). The expression of *magA* was induced *in vivo* by feeding the mice with 4 μg/ml of Dox and 200 μM of ferric citrate (FC) for three days. Prussian blue staining showed more intense staining that support the elevated amount of iron compound in mESC-MagA derived tumor compare to mESC-WT (Figure 2-6b). The pluripotency of the mESC-MagA was not affected by the lentiviral transduction and subsequent culturing.

2.4.4 Impact of MagA expression on cellular functions

To determine if the expression of MagA in ESCs had an adverse impact on cellular function, cell proliferation rates and cytotoxicity assays were performed. The proliferation rates of mESC-MagA did not exhibit significant differences from mESC-MagA at Dox concentrations of 0.5 μg/ml and 1 μg/ml, respectively (Figure 2-7a). However, with 2 μg/ml of Dox, mESC-MagA demonstrated a

significant suppression in cell proliferation compared to mESC-WT (Figure 2-7a, $P = 0.032$, $n = 3$). The proliferation of both mESC-WT and mESC-MagA demonstrated negative correlation to the Dox concentrations, while mESC-MagA was more sensitive to Dox than mESC-WT (Figure 2-7b "a = -0.17 versus -0.07"). Based on gene and protein expression and proliferation rate, 1 μg/ml of Dox was used in subsequent studies to maximize MagA expression with minimal cellular impact. Cytotoxicity was evaluated based on changes in the annexin V and 7-aminoactinomycin D (AAD) positive cell populations as measured by the Annexin V & Dead Cell Assay using Muse™ (EMD Millipore) (Figure 2-7c). Dox alone did not increase annexin V and 7-AAD positive population in mESC-MagA. With 25 μM of FC added to the media, both mESC-WT and mESC-MagA showed significant reduction in annexin V^+ and 7-AAD^+ cells (0.921 ± 0.02 and 0.700 ± 0.006, $P < 0.001$, $n = 3$). However, when both Dox and FC were added to the media, mESC-WT showed significant reduction in annexin V^+ and 7-AAD^+ cell populations (0.769 ± 0.02, $P < 0.001$), but mESC-MagA showed a two fold increase in annexin V^+ and 7-AAD^+ cell populations (2.07 ± 0.02, $P < 0.001$). The expression of MagA decreased proliferation rate while the expression of MagA in the presence of ferric citrate increased apoptotic cell marker expression.

2.4.5 *In vitro* evaluation of MagA as MRI reporter

To examine whether MagA induces MRI contrast, we measured changes in transverse relaxation rate R_2 in mESC-MagA and mESC-WT cell pellets with and without the Dox/FC supplementation. When mESC-MagA was treated with Dox/FC, R_2 values significantly increased compared to those of non-induced

mESC-WT (5% increase, $P < 0.001$) and mESC-WT supplemented with Dox/FC (5.63% increase, $P = 0.029$), respectively (Figure 2-8a). We then used ICP-OES to measure iron content of the cell pellets after MRI scans. There was a significant increase in iron content in mESC-MagA treated with Dox/FC compared to all other groups (Figure 2-8b). mESC-MagA supplemented with Dox/FC had twice as much iron (14.1 μg/g) as mESC-WT supplemented with Dox/FC (7.36 μg/g, $P = 0.029$, $n = 4$). Cell phantom MRI scan demonstrated MR contrast increase when MagA was induced by Dox/FC treatment, and ICP-OES showed increased iron content of the cell pellets when mESC-MagA was treated with Dox/FC.

2.4.6 *In vitro* spontaneous differentiation

In order to further investigate the impact of MagA on pluripotency, we conducted an assay for spontaneous differentiation *in vitro*. When mESC-MagA was treated with Dox, ESC colonies were visibly smaller than an untreated group (Figure 2-9a). The number of Live/Dead cells was evaluated by Trypan blue staining in order to seed equal numbers of live cells for embryo body (EB) formation (Figure 2-9b). Compared to mESC-WT culture without Dox treatment (mESC-WT), both mESC-WT Dox and mESC-MagA had significantly less numbers of live cells: 121,042 (mESC-WT Dox) and 98,750 (mESC-MagA) compared to 151,136 (mESC-WT), $P < 0.05$, $n = 4$. The number of live cells in mESC-MagA Dox was significantly lower than mESC-WT without Dox ($P < 0.001$, $n = 4$). Although the actual number of dead cells were similar throughout all four samples, when the ratios of live to dead cells from the total cell population were compared, mESC-MagA Dox group had a significantly lower live cell and significantly higher dead

cell ratio compared to those of the mESC-WT group ($P < 0.05$, $n = 4$) (Figure 2-9c). When the same number of live cells were used for formation of EB, the EBs derived from the mESC-MagA Dox group were smaller compare to all other groups 94.7 ± 2.88 ($P < 0.001$) (Figure 2-10). After differentiation, lineage-specific primary antibodies were used to determine the presence of the three germ layers: Nestin (neuroectoderm), HNF4a (mesoderm), and CD117 (endoderm). All mESC-WT and mESC-MagA (with or without Dox) were capable of differentiating into three lineages based on immunostaining using specific antibodies that specify the three germ layers (Figure 2-11). When cells were treated with Dox after the initial differentiation stage, cells were also positive for all three germ line specific markers for both mESC-WT and mESC-MagA (Figure 2-12). We performed reverse transcriptase PCR (RT-PCR) with total RNA isolated from *in vitro* differentiated cells in order to determine their differentiation capacity (Figure 2-13). Both mESC-WT and mESC-MagA expressed lineage specific markers which include *T-brachyury* (mesoderm), *GATA-6* (endoderm), *HNF4a* (mesoderm), *Nestin* (ectoderm), and *Map2* (ectoderm). The expression levels of each lineage specific markers were then determined by quantitative real-time PCR (qRT-PCR) (Figure 2-14,15). The expression level of *Nestin* was significantly high in mESC-MagA and mESC-MagA Dox compared to mESC-WT (**$P < 0.001$, $n = 4$). Also, *Map2* expression was significantly higher in mESC-MagA Dox (*$P < 0.05$, $n = 4$). The expression of *T-Brachyury* was also significantly elevated in mESC-MagA Dox (**$P < 0.001$, $n = 4$). Although the expression of *HNF4a* has demonstrated doxycycline responsive expression, it was not statistically significant compared to mESC-WT.

When the expression levels of lineage specific markers were compared in the samples treated with Dox after the initial differentiation stage, there was no difference in gene expression among the marker genes (Figure 2-15).

2.5 Discussion

An ideal reporting system for *in vivo* longitudinal cell graft monitoring should address specific issues relevant to clinical translation, such as safety, capacity for long-term monitoring, and specificity for cell viability/activity. By employing a Tet-On inducible system, we were able to control the expression of MagA, hence reducing the risks of continuous accumulation of MagA and iron.

From our characterizations of MagA expression in mESC, we have demonstrated that the expression level of MagA was inversely correlated to proliferation rate but directly correlated to the expression of cytotoxicity markers *in vitro* (Figure 2-7 and 2-9). The mechanism of cytotoxicity could not be clearly elucidated from our data, and further investigation is needed. One possible mechanism might be from iron overload. The increase of cellular iron, if not converted to a stable form, can potentially be harmful to the cell, as ferrous (Fe^{2+}) ion may lead to the production of reactive oxygen species (ROS) (Kehrer 2000). The overexpression of two most popular genetic MRI reporters, ferritin and transferrin receptor, has resulted in opposite cellular responses. Although overexpression of both ferritin and transferrin receptors resulted in increased intracellular iron pool, overexpression of ferritin resulted in the activation of iron deficit cellular response, while overexpression of transferrin receptor resulted in the activation of iron overload response (Vandsburger et al. 2013). As an iron

transporter, MagA is expected to act similar to transferrin receptor (Vande Velde, Himmelreich, and Neeman 2013), and transferrin receptor demonstrated an augmented Fenton reaction due to increased intracellular labile iron pool (Vande Velde, Himmelreich, and Neeman 2013). Fenton reaction is a process where iron catalyst (i.e. Fe^{2+}) is oxidized by hydrogen peroxide and generates hydroxyl radicals and hydroxide ions. Ferric ion (Fe^{3+}) generated in the first reaction is then reduced back to ferrous ion by another molecule of hydrogen peroxide, which forms a superoxide radical and a proton. The free radicals generated from this reaction is very toxic to the cell because they cause non-selective oxidative reactions. In our study, we were able to observe increased cytotoxic response when the expression of MagA was induced by the administration of Dox in the presence of FC (Figure 2-7c) and observed increased iron content in mESC-MagA under the same conditions (Figure 2-8). Both results suggests the cytotoxicity might have resulted from increased iron content in the cell. Also, no significant change in relaxivity when comparing mESC-MagA to mESC-MagA treated with Dox and FC might suggest that the increased iron pool might have resulted from an increased cellular labile iron pool, and only a slight fraction was converted to iron particles such as magnetites. Expression of MagA in 293FT and other cancer cell types showed no significant impact on proliferation and cytotoxicity and showed a greater change in relaxivity (Zurkiya, Chan, and Hu 2008, Rohani et al. 2014). Cell types may play a role in generating MR contrast with other genes involved, which cannot be ruled out from this study. The impact on proliferation and cytotoxicity might be specific to ESCs, and further investigations are needed in other cell types. In prokaryotic cells, there are many genes involved in the

formation of the magnetosome (Bazylinski and Frankel 2004). Therefore, it can be speculated that other genes, or combination of genes, may aid MagA in generating MR contrast and reducing cytotoxicity. It would be worth to investigate whether co-expressing other genes are involved in the magnetosome formation to increase MR contrast.

The overall pluripotency of mESCs was not affected by the lentiviral transduction procedure and the introduction of the *magA* gene in mESC as demonstrated by a teratoma formation assay and the expression of pluripotency markers in cell culture (Figure 2-6a). Also, mESC-MagA were able to differentiate into all three germ layers *in vivo* (Figure 2-6b) and *in vitro* (Figure 2-11). Pluripotent stem cells (PSCs; i.e. ESCs or induced pluripotent stem cells (iPSC)) harbor the risk of developing malignant teratomas when used in cell therapy. However, ESC and iPSC have advantages such as high proliferation rate, enabling differentiation into different cell types, making genetic modification or correction possible. Many studies are focused on developing neural stem cells (NSC) or neural progenitor cells (NPC) derived from PSCs in cell therapy for neurodegenerative diseases (Ma et al. 2012, Carter and Chan 2012, Chen et al. 2014). Therefore, it is important to ensure that the lentiviral transduction procedure and the presence of a reporter gene has no adverse impact on pluripotency. NSCs or NPCs can be used in future studies to establish Tet-On MagA cell lines to evaluate the feasibility of utilizing MagA as a genetic MRI reporter in other stem/progenitor cell types.

Our *in vitro* differentiation study demonstrates that the expression of MagA does pose an impact on differentiation, however. Overexpression of MagA during early differentiation enhanced the expression of the ectodermal marker genes, *Nestin* and *Map-2* (Figure 2-14). Also, the expression of *T-Brachyury* was elevated (Figure 2-14). More quantitative assays such as fluorescence-activated cell sorting (FACS) can be utilized to demonstrate the change in the population in the differentiation process. Several reports suggested that SPIO used in cell labeling affects cell differentiation (Kostura et al. 2004, Bulte et al. 2004, Chen et al. 2010, Chung, Hsiao, et al. 2011, Julke et al. 2013, Choi et al. 2013), and two studies reported enhanced ectodermal lineage differentiation (Chung, Hsiao, et al. 2011, Choi et al. 2013). These studies suggest the importance of controlling the amount of iron in the stem cell population. However, when the expression of MagA was induced at a later stage of differentiation, the differentiation potential was not affected (Figure 2-15). Our data demonstrated that regulation of transgene expression might be necessary in earlier differentiation stage.

Our results showed, for the first time, that expression of MagA can be modulated while sufficient MRI contrast could be generated in mESC. Compared to a direct labeling method using exogenous contrast agents, such as SPIO, the major limitation of a genetic MRI reporter is relatively lower sensitivity (Vande Velde et al. 2011). For short term monitoring, monitoring of fully differentiated cells, or monitoring of cells with slow proliferation rate, exogenous labeling method is still superior and should be considered. However, in case of progenitor and stem cell grafts, fast proliferation rate and asymmetric cell division make

direct labeling methods unsuitable for long term longitudinal monitoring (Walczak et al. 2007). Tet-On MagA can be employed in situations where longitudinal monitoring, which exceeds the current monitoring span of SPIO, or even combination of SPIO for short term and long term monitoring of the cell grafts. The current exogenous labeling methods only allow cell tracking in the limited time frame that span a few days to a few months (Kircher, Gambhir, and Grimm 2011). Therefore, for the studies that require a couple of months or even years of longitudinal monitoring in a larger animal, such as porcine and nonhuman primates, Tet-MagA could be utilized. As an inducible genetic reporter capable of carrying through generations of all progeny cells, Tet-On MagA provides a unique tool for longitudinal stem cell monitoring. The expression of a reporter gene can be controlled in earlier differentiation stage to minimize the impact on proliferation, cytotoxicity, and differentiation, and the reporter gene can only be expressed when the monitoring of the cell is required.

In summary, our results demonstrate that MagA could function in mESCs as a genetic MRI reporter *in vitro*. These findings not only support the feasibility of applying MagA as a genetic MRI reporter in mESC, but also provide a platform for *in vivo* monitoring of cell grafts.

Gene	Forward (5'-3')	Reverse (5'-3')	Probe (5'-3')
*18S rRNA**	Not disclosed		
magA	ATCCGTTTTCTCGAAGTGTGGAA	GCCCGCGATCTGCAAAA	ACGGCGGTCTTCACC
Sox2	CTGTTTTTTCATCCCAATTGCA	CGGAGATCTGGCGGAGAATA	
Nestin	GGTCACTGTCGCCGCTACTC	AAGCGGACGTGGAGCACTA	
Map2	ACCCTGTCTTAGTGCCAGAATCAA	GAACCAACATCTGTAAACCCCTTT	
Brachyury	GCTTCAAGGAGCTAACTAACGAG	CCAGCAAGAAAGAGTACATGGC	
Gata6	TTGCTCCGGTAACAGCAGTG	GTGGTCGCTTGTGTAGAAGGA	
Hnf4a	GCTGTCCTCGTAGCTTGACC	CAGTGTCGTTACTGCAGGCTT	
magA	AGCTGGACATCATCCGTTTT	ATTCCAGCACCTTGATCACC	
β-actin	ACCTGACAGACTACCTCATGAAG	GAGCAACATAGCACAGCTTCTC	

Table 2-1. List of genes and primers used in quantitative RT-PCR

* Forward, reverse, and probe sequences of Eukaryotic *18S rRNA* Endogenous TaqMan® Assay (Applied Biosystems) are not disclosed

Antibody	Dilution	Company	Remarks
HA	1:1,000	Covance	Clone 16B12 monoclonal, MagA-HA
HNF4a	1:100	SantaCruz	Mesoderm specific marker
NES	1:100	Abcam	Neuronal lineage specific marker
CD117	1:500	SouthernBiotech	Endoderm specific marker
MSI1	1:100	Chemicon	Neuronal lineage specific marker
SOX2	1:250	Millipore	Proliferating (ectoderm) specific marker
OCT3/4	1:500	SantaCruz	Pluripotent marker
NANOG	1:400	SantaCruz	Pluripotent Marker
Cleaved caspase-3	1:1,600	Cell signaling	Apoptosis marker/inflammation (indirect)
Alexa 594 anti-rabbit	1:1,000	Vector Laboratories	Secondary antibody
Alexa 594 anti-mouse	1:1,000	Molecular Probes	Secondary antibody
Anti-mouse Cy-5	1:1,000	Jackson ImmunoResearch	Secondary antibody
Peroxidase anti-mouse	1:10,000	Jackson ImmunoResearch	Secondary antibody for western blot analysis
α-tubulin	1:1,000	Sigma	Secondary antibody for western blot analysis

Table 2-2. Antibodies used

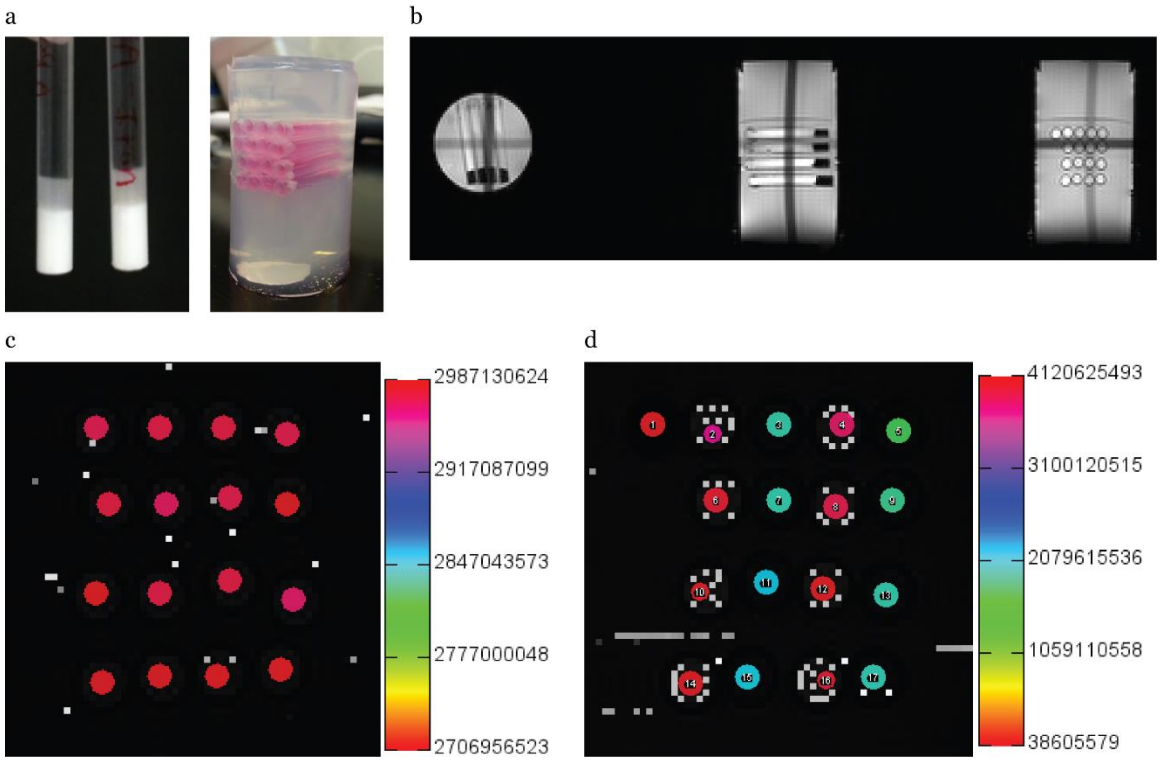

Figure 2-1. Cell pellet MRI. (a) A picture of cell pellets in 0.5 ml straws (TS Scientific), and cell pellet straws in 1% agarose gel. (b) Tri-plot of gel-embedded straws to minimize the air-sample interference. (c) Magnetic field homogeneity test with DMEM showing homogeneous field in T_2 map. (d) Cell pellet test run (column 2 and 4) with the references (column 1 and 3).

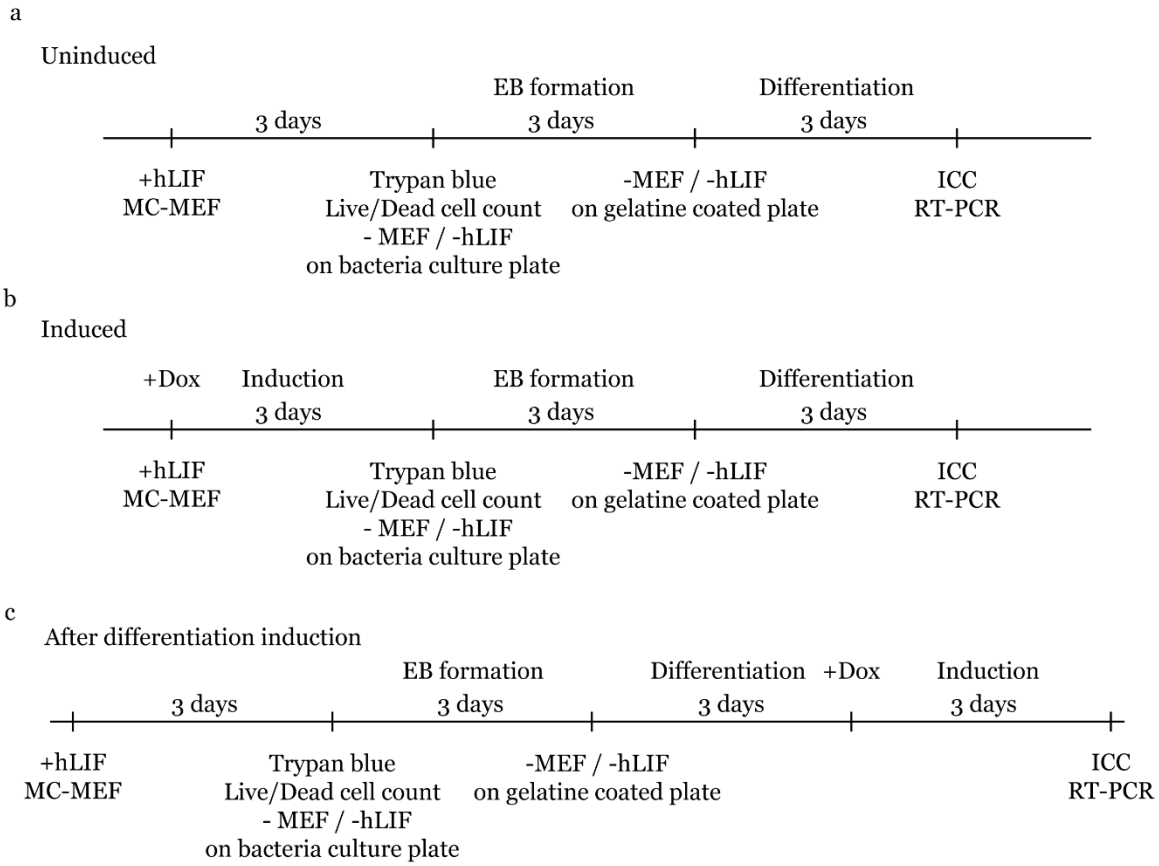

Figure 2-2. Time line of *in vitro* spontaneous differentiation experiment. (a) For uninduced group, 5,000 cells were grown in a normal condition (on MC-MEF and with hLIF supplement) for 3 days. Cells were trypsinized, and live and dead cells were counted. For EB formation, 60,000 live cells were transferred to a bacteria culture plate and grown without hLIF for 3 days. EBs were transferred to gelatin coated plates and allowed to attach to the bottom and allowed to differentiate for 3 days. At the end of differentiation, cells were harvested for ICC and RT-PCR. (b) For induced group, Dox was supplemented with normal growth media, and cells were treated with 3 days. The rest of differentiation protocol was identical to uninduced group. (c) The impact of MagA expression after differentiation was accessed by treating differentiated cells with Dox for three days after the differentiation protocol.

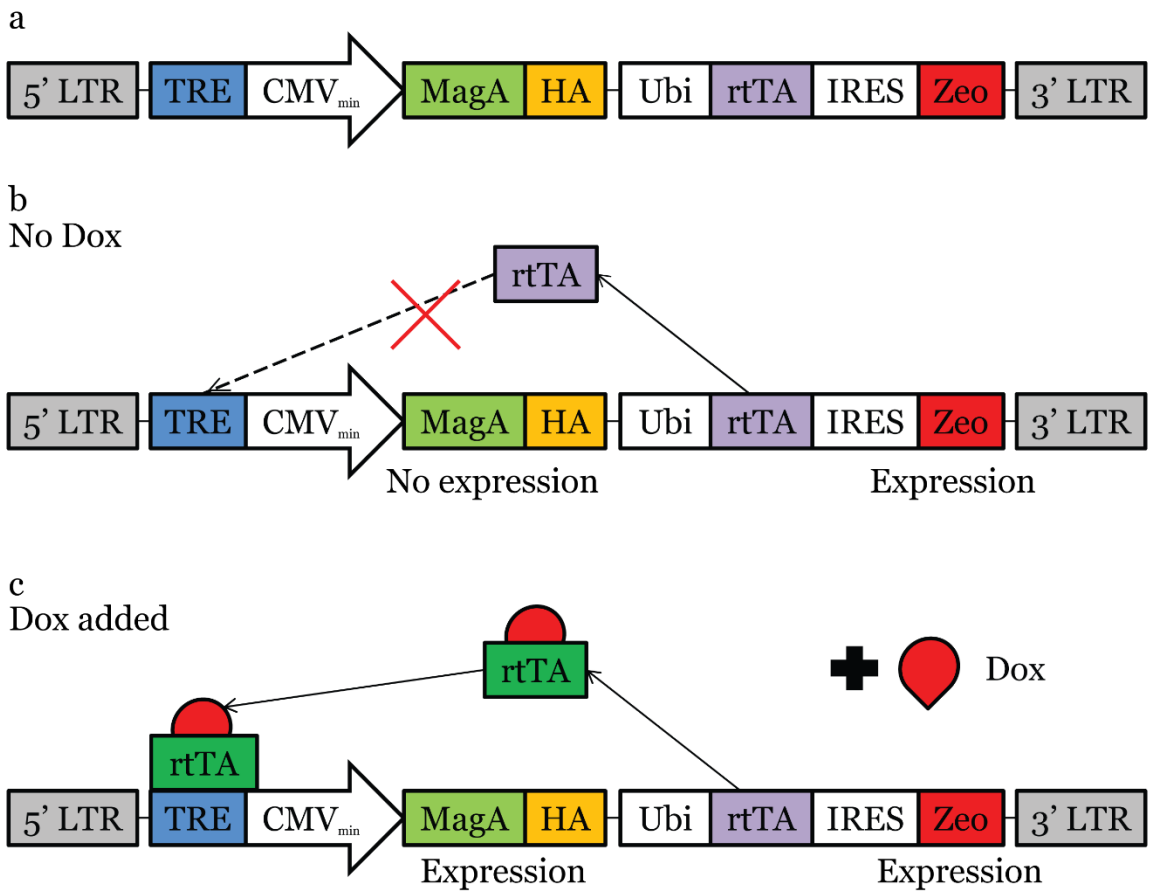

Figure 2-3. Lentiviral vector LV-mCMV-MagA-HA-Ubi-rtTA-IRES-ZeocinR. (a) The Tet-On lentiviral vector construct is represented with HA tagged *magA* under miCMV promoter. The expression of ZeoR was linked to Ubi promoter by IRES, which allowed independent Zeo selection regardless of doxycycline induction. (b) If there is no Dox in the media, rtTA does not bind to TRE, and *magA* gene is not induced. (c) When Dox is added to the media, Dox binds to rtTA allowing rtTA to bind to TRE. It allows to initiate *magA* transgene expression.

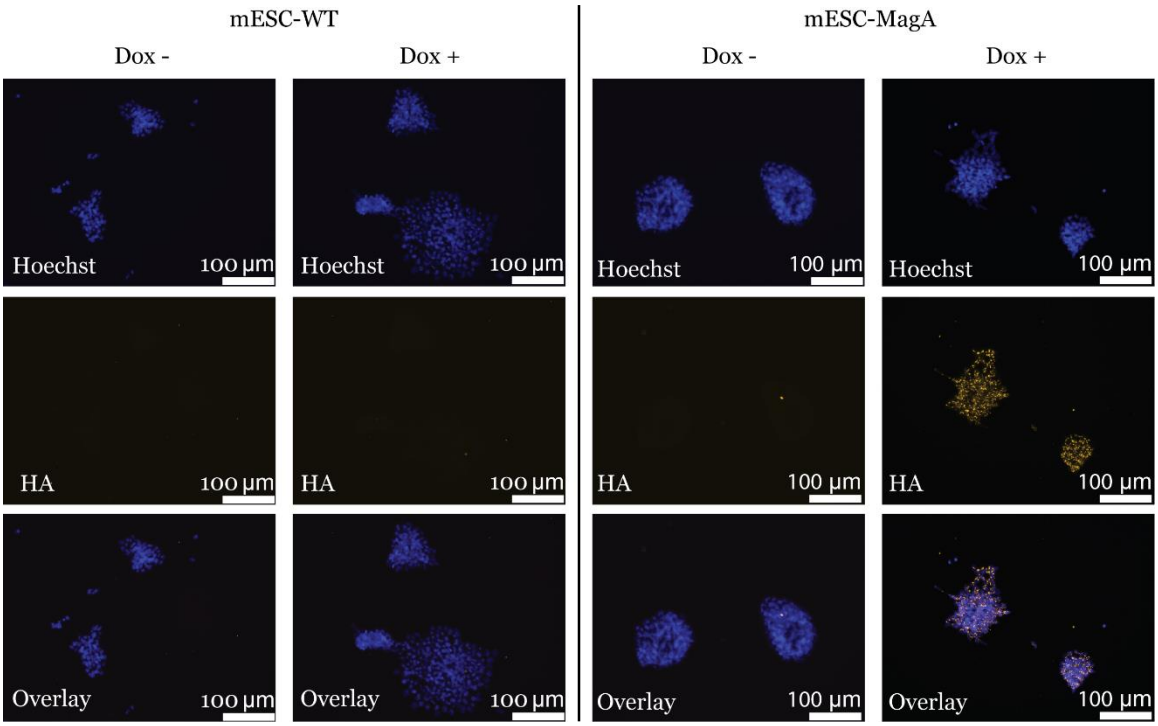

Figure 2-4. Establishment of mESC-MagA. The left column represents mESC-WT with and without doxycycline treatment showing no HA positive cells. The right column represents mESC-MagA with and without doxycycline treatment showing positive cells only when the doxycycline is added.

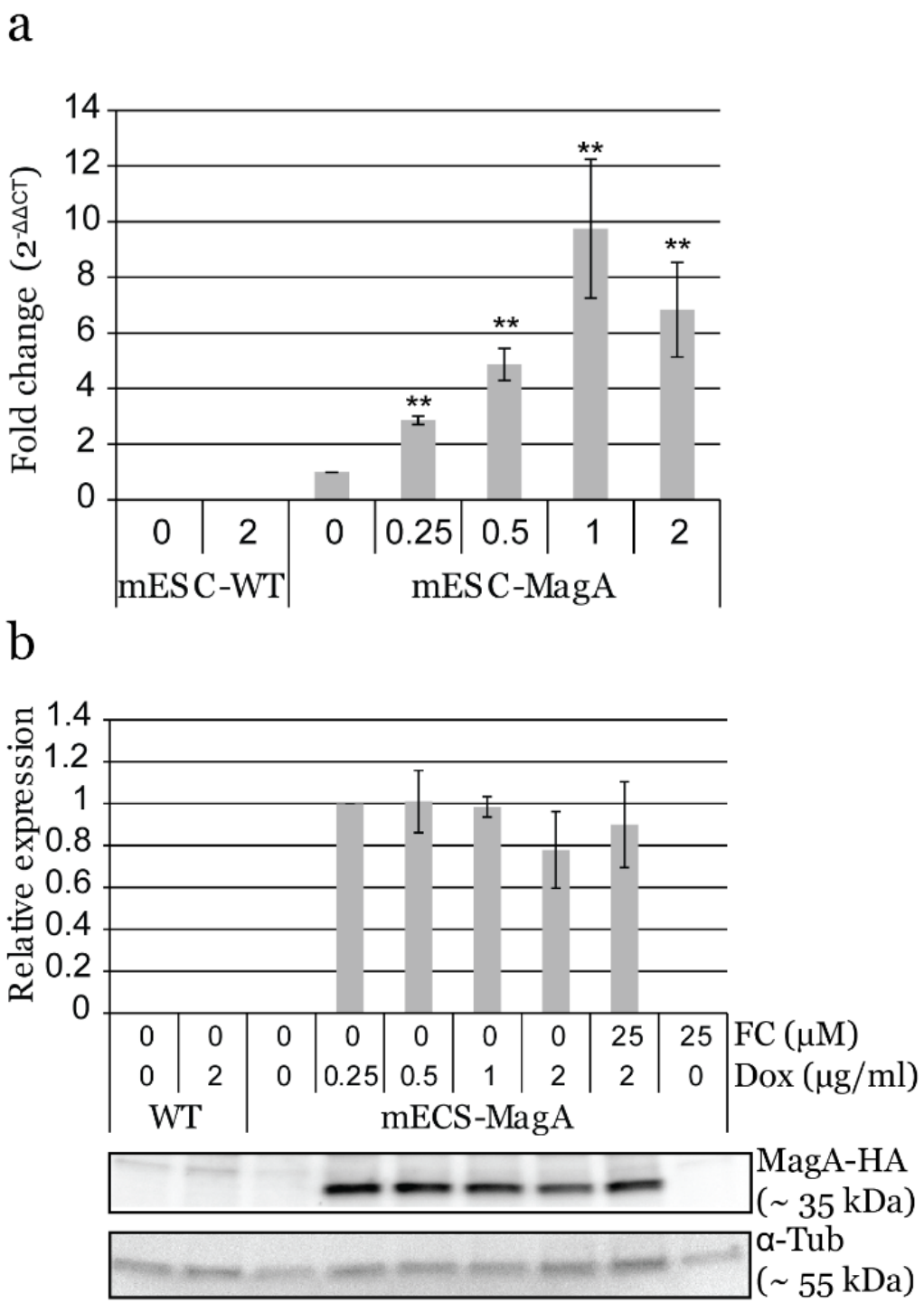

Figure 2-5. The expression profile of MagA. (a) Quantitative real-time PCR (qRT-PCR) analysis of *magA* expression in mESC-MagA demonstrates a positive correlation between the expression of *magA* and the dosage of Dox. Maximum *magA* expression was observed when supplemented with 1 μg/ml of Dox (9.74 ± 2.49, $^{**}P < 0.001$, $n = 3$). (b) Western blot analysis of MagA assessed via HA tag in mESC-MagA demonstrates no differences when supplemented with different dosages of Dox (0.25, 0.5, 1 and 2 μg/ml) as shown in densitometry analysis.

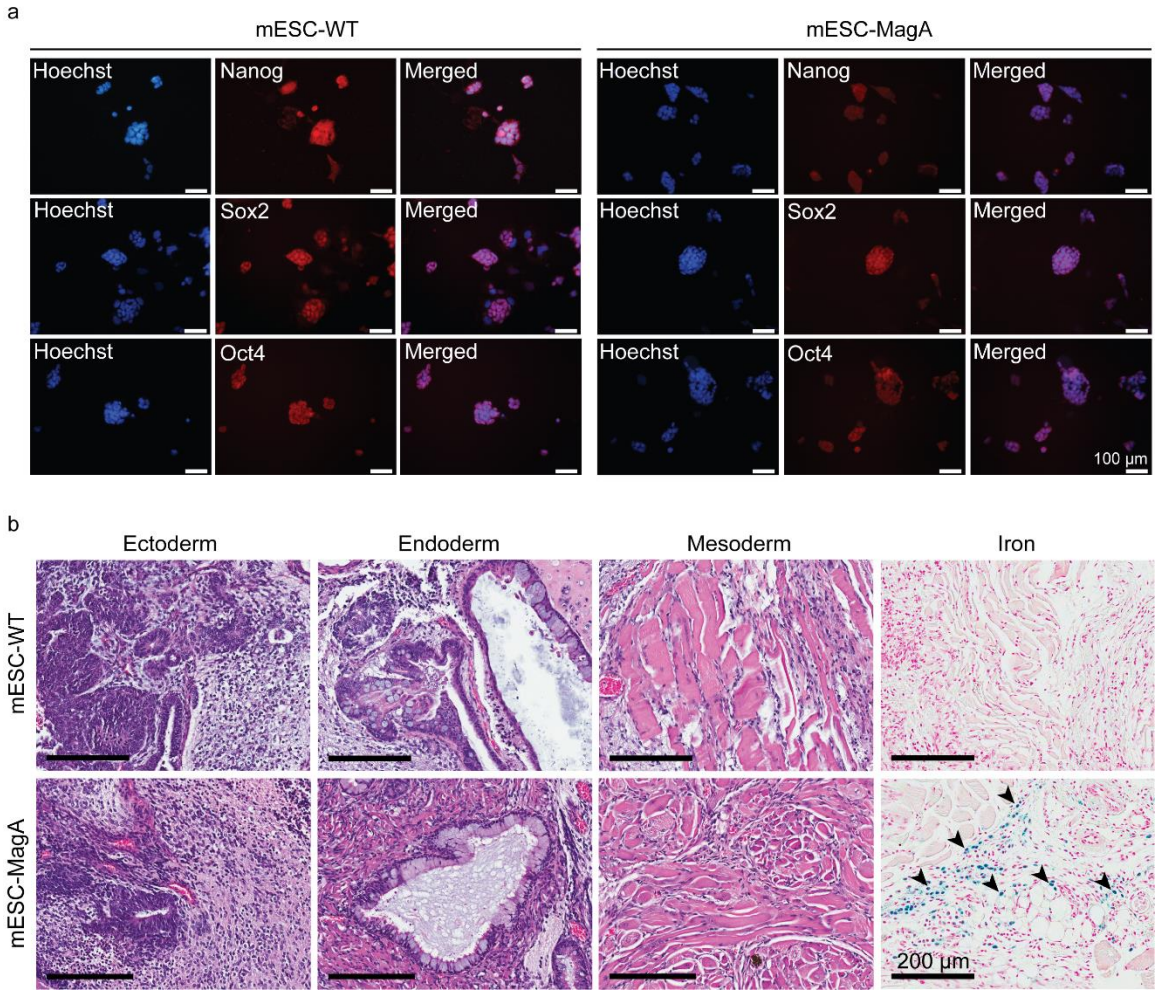

Figure 2-6. Pluripotency of mESC. (a) mESC-WT and mESC-MagA expressing pluripotency markers: Nanog, Sox2 and Oct4. Nucleus is visualized with Hoechst 33342. (b) Teratomas that developed from subcutaneous injection of $1x10^6$ mESC-WT and mESC-MagA cells into a nude mouse shoulder subsequently developed all three germ layers: ectoderm (neural epithelium), endoderm (ciliated epithelium and glands), and mesoderm (striated muscle). Also, Prussian blue-positive cells were observed (indicated by arrow heads) in mESC-MagA teratoma.

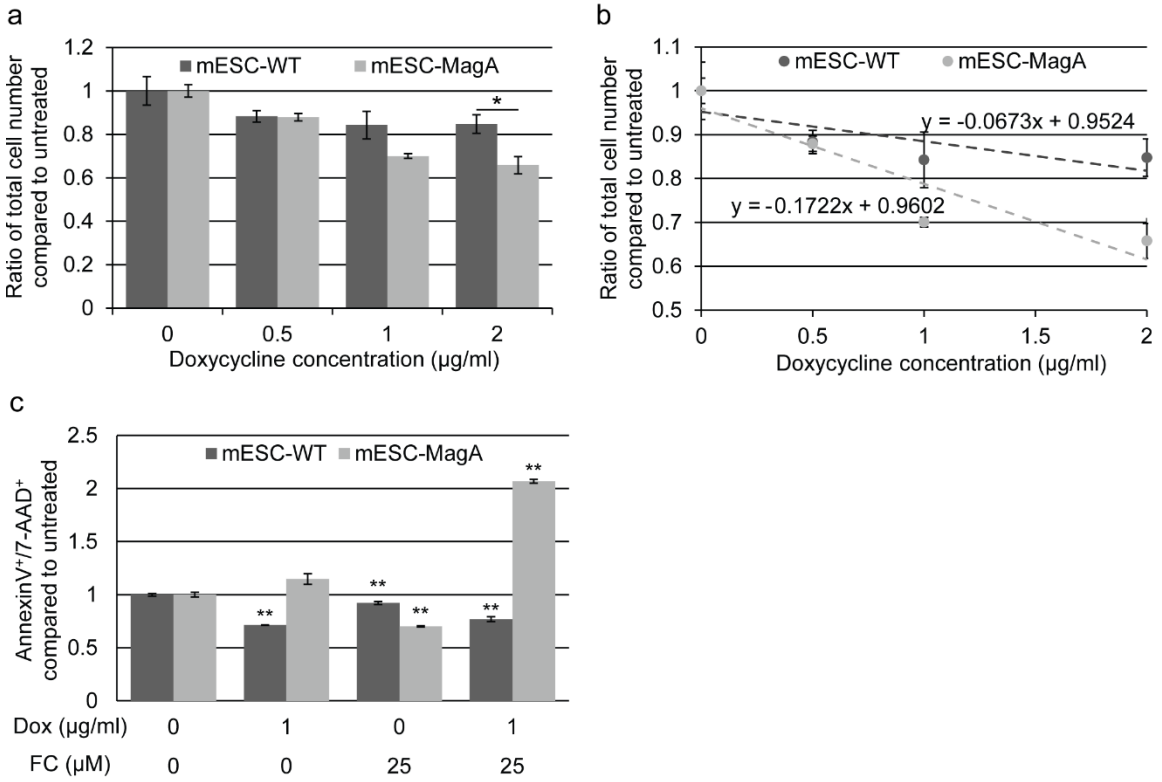

Figure 2-7. Evaluation of impact of expressing MagA in mESC. (a) The cell proliferation rate was determined by total cell count. The proliferation rate showed a negative correlation to the Dox concentration in both mESC-WT and mESC-MagA. We saw no significant suppression in proliferation up to 1 μg/ml of Dox ($P = 0.091$, $n = 3$); however, there was significant suppression at 2 μg/ml ($^{*}P = 0.032$, $n = 3$). (b) The linear correlation demonstrates the sensitivity of both cell lines to Dox. Both mESC-WT and mESC-MagA showed a negative correlation between cell proliferation and Dox concentration. However, mESC-MagA showed a slightly higher negative linear correlation than mESC-WT (a = -0.17 versus -0.07). (c) When mESC-MagA was treated with 1 μg/ml Dox and 25 μM FC, a two-fold increase in annexin V+ and 7-AAD+ cell population (2.07 ± 0.0190, $^{**}P < 0.001$) was observed, while there was no significant increase when mESC-MagA was treated only with Dox. All histogram data are means ± SEM. $^{*}P < 0.05$, $^{**}P < 0.001$ versus appropriate control by ANOVA.

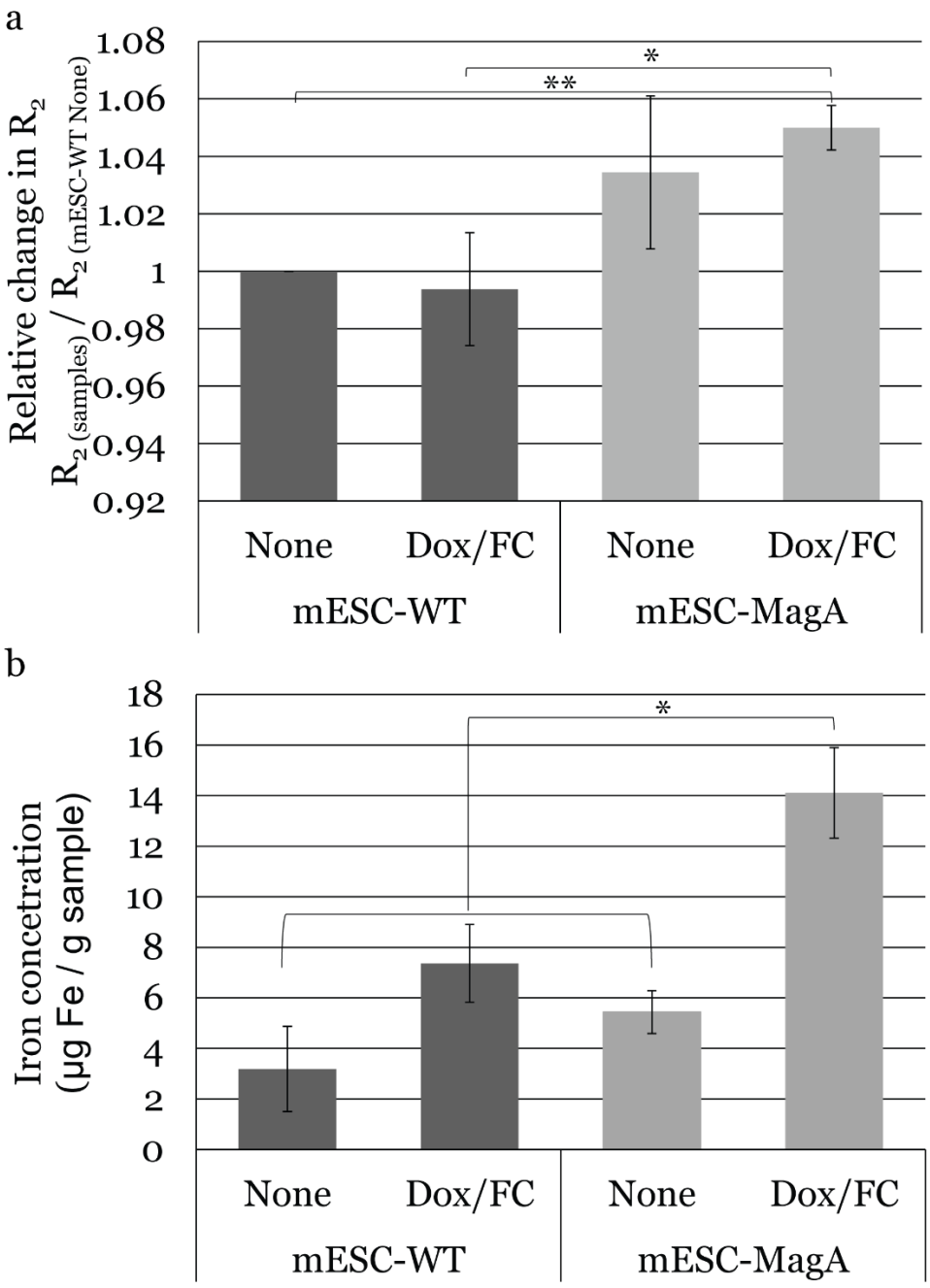

Figure 2-8. MRI of cell pellets and ICP-OES quantifications of iron in mESCs. (a) The cell pellet of mESC-MagA Dox/FC showed significantly induced relaxivity (R_2) compared to mESC-WT both without (5% increase ± 0.007, $^{**}P < 0.001$, n = 5) and with Dox/FC treatment (5.63%, $^{*}P = 0.029$, n = 5). (b) mESC-MagA Dox/FC showed the highest iron content compared to all other groups. Compared to mESC-WT Dox/FC, mESC-MagA Dox/FC had about twice as much iron content (7.36 µg/g and 14.1 µg/g respectively, $^{*}P = 0.029$, n = 4). There was no significant change when mESC-WT Dox/FC was compared to mESC-WT None (P = 0.117, n = 4). All histogram data are means ± SEM. $^{*}P < 0.05$, $^{**}P < 0.001$ versus appropriate control by ANOVA.

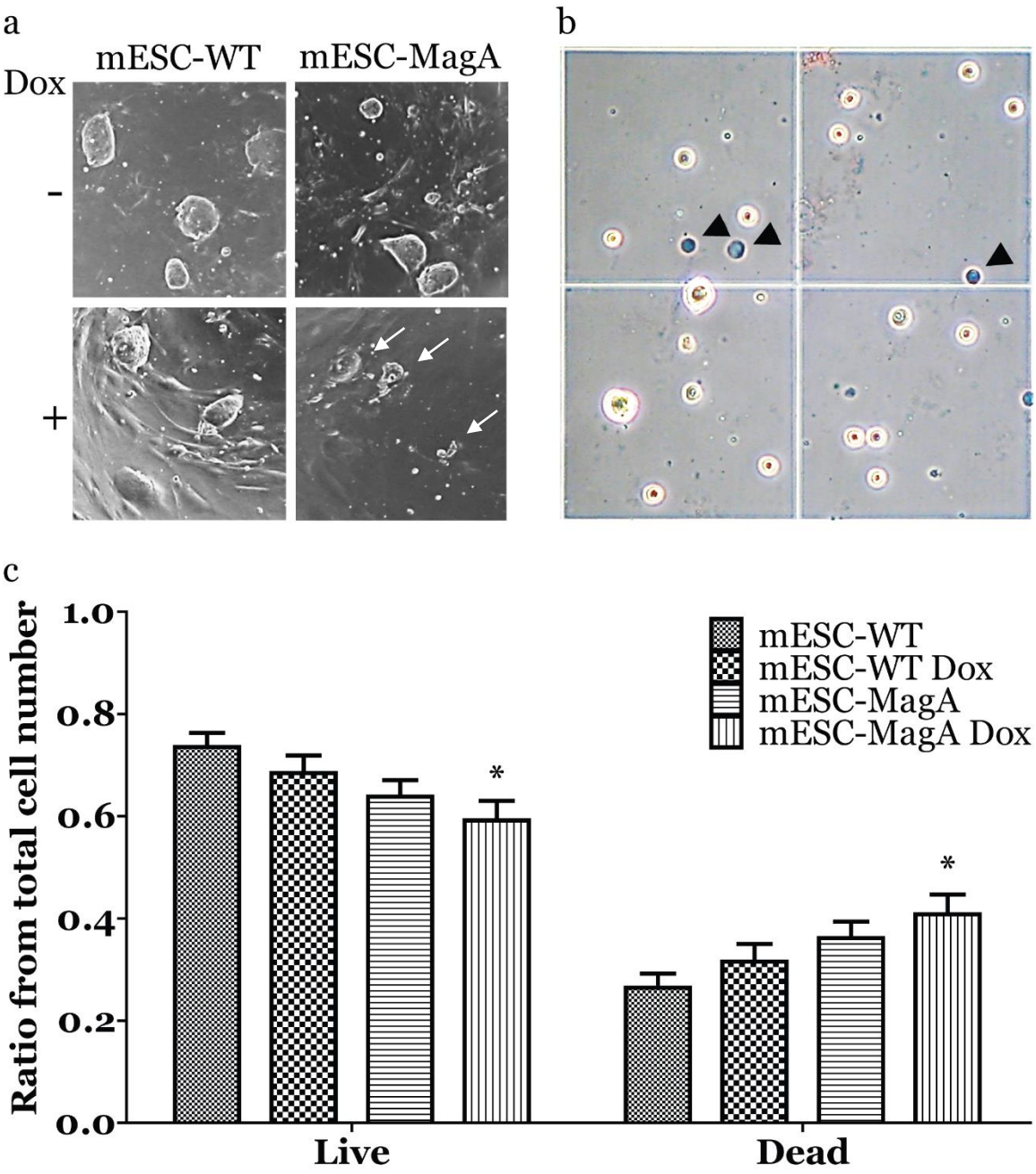

Figure 2-9. *In vitro* spontaneous cell differentiation cell treatment. (a) mESC-MagA treated with doxycycline exhibited the smaller ESC colonies compared to other treatment groups. (b) A representative picture of Trypan blue staining. Dead cells are indicated with the arrows. (c) The ratio of live/dead cell exhibits significantly lower number of live cells and significantly higher dead cells in mESC-MagA Dox group compared to mESC-WT. *$P < 0.05$

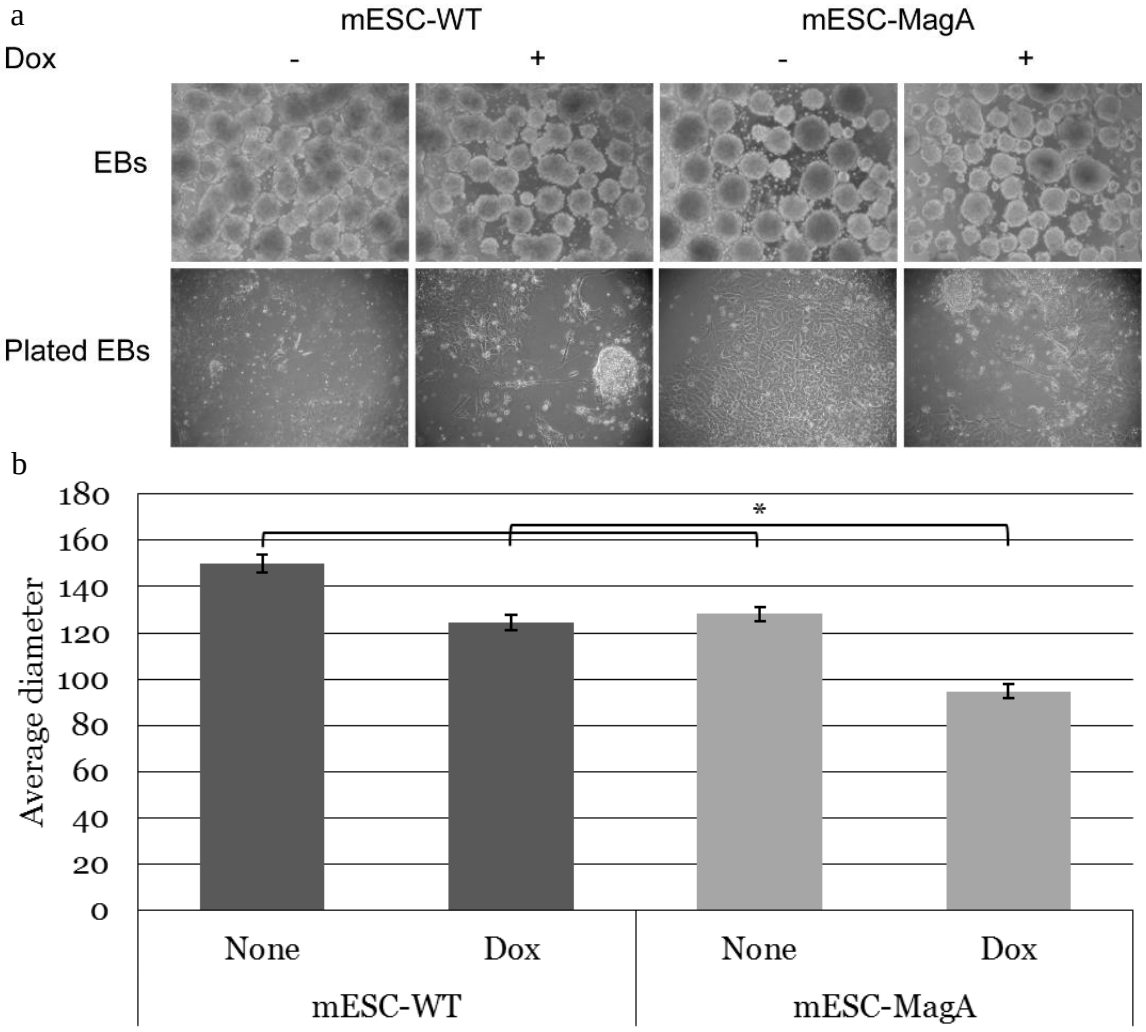

Figure 2-10. EB formation. (a) mESC-MagA treated with doxycycline formed smaller EBs and lower number of EBs. When EBs were transferred to a gelatin-coated cell culture plate, all four groups were able to attach and initiate differentiation. (b) The average size of EBs in mESC-MagA Dox were significantly smaller ($P < 0.001$).

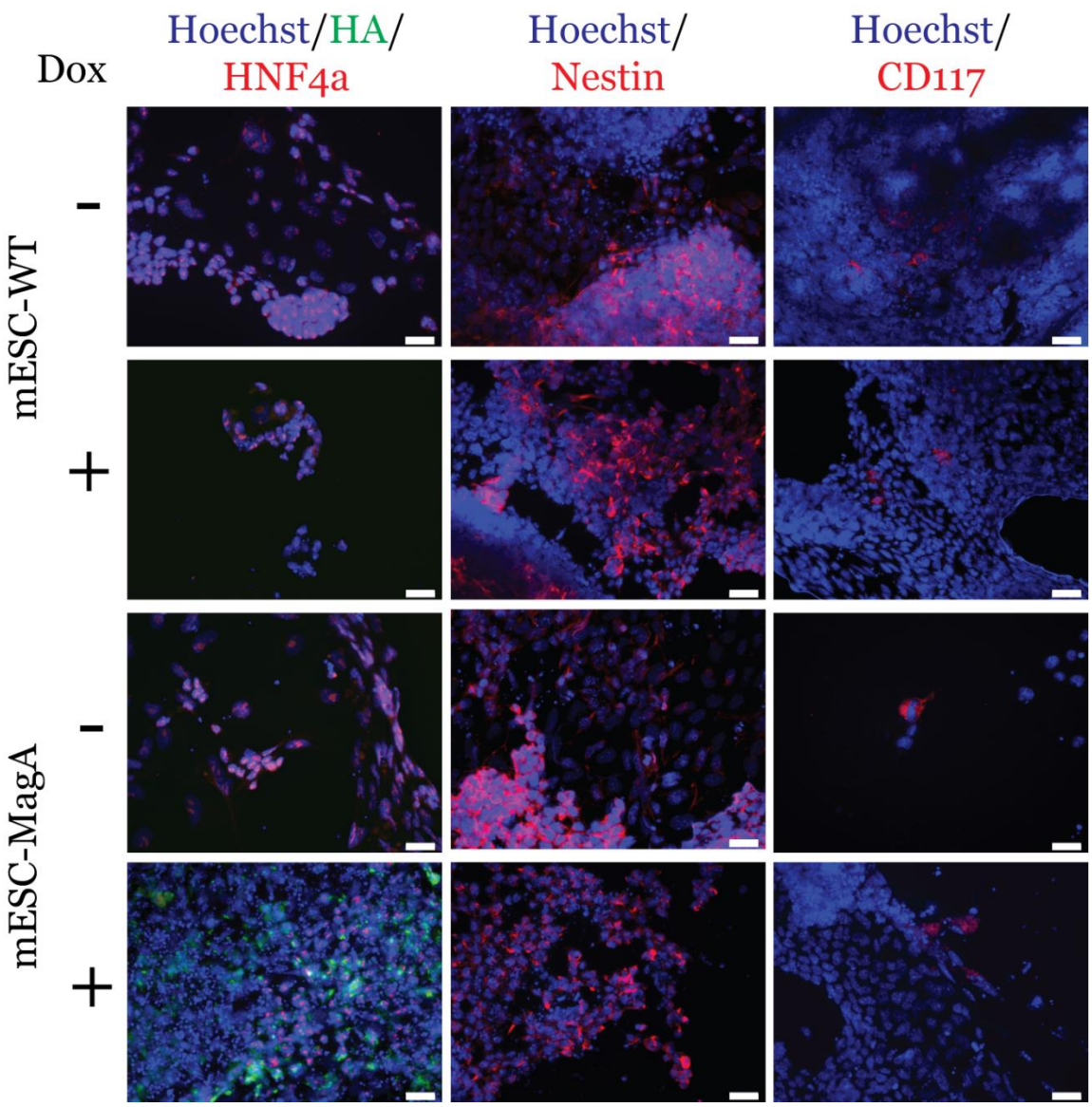

Figure 2-11. Evaluation of differentiation potential with germ line specific markers. All four groups were positive for three germ line specific markers. Scale bars: 20 μm.

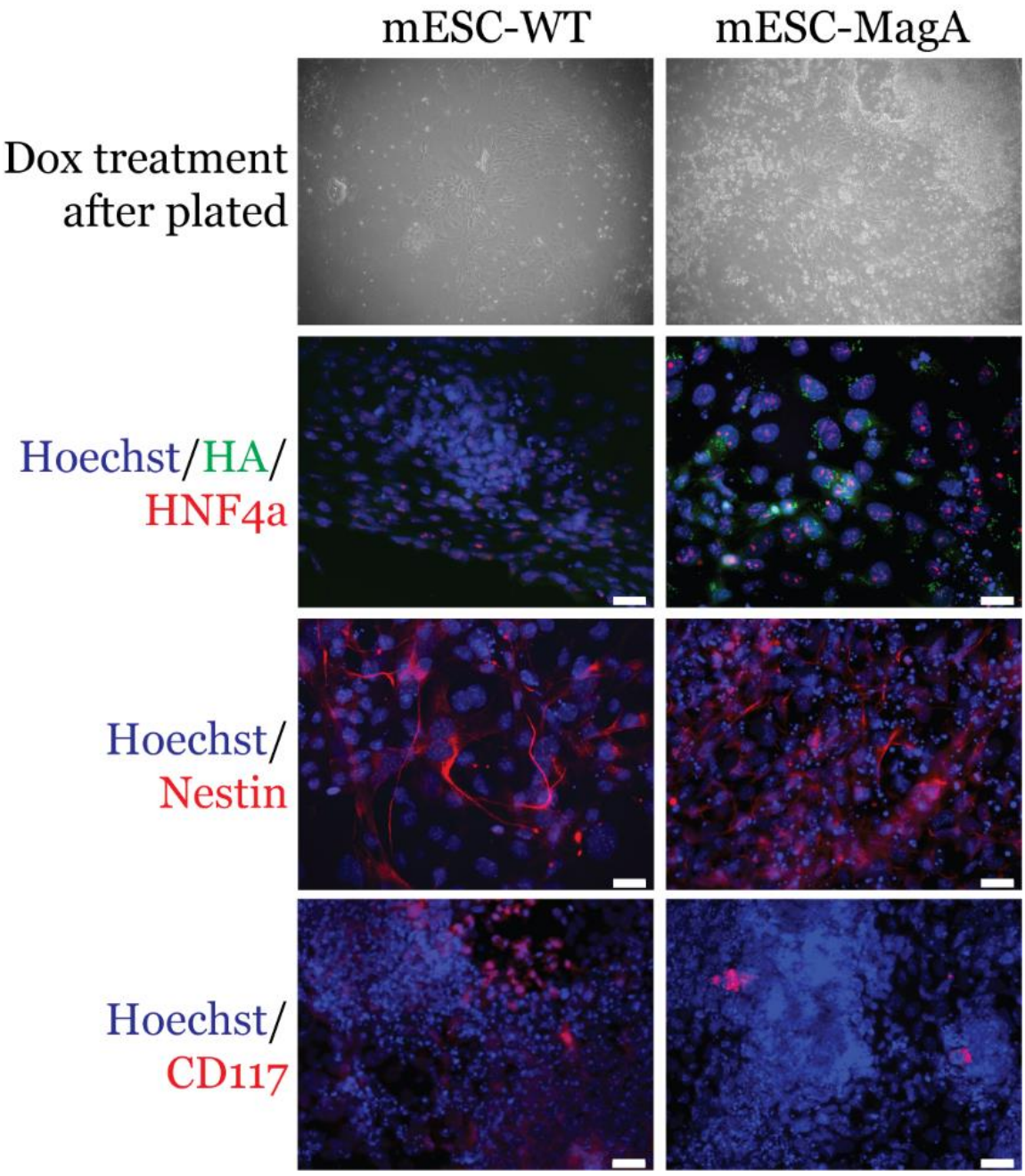

Figure 2-12. Evaluation of differential potential with germ line specific markers. All three germ line specific markers positive cells were observed in the cells treated with doxycycline after cells were differentiated. Scale bars: 20 μm.

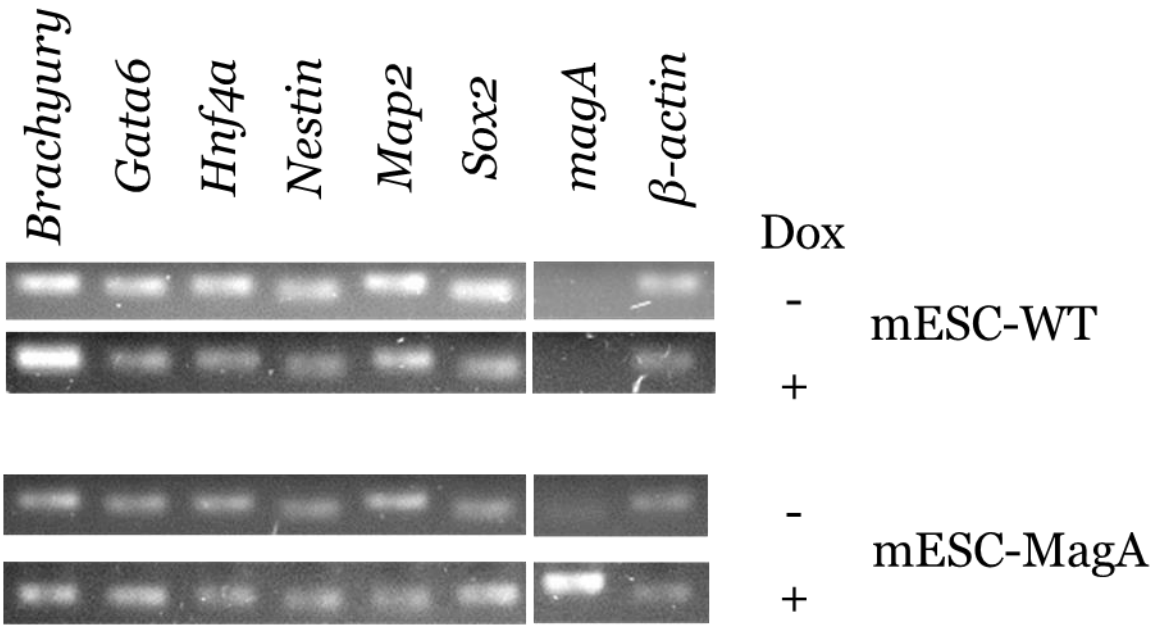

Figure 2-13. Expression of marker genes in differentiated cells. RT-PCR with total RNA isolated from *in vitro* spontaneous differentiation demonstrated positive expression of *Brachyury* (mesoderm), *Gata6* (endoderm), *Hnf4a* (mesoderm), *Nestin* (ectoderm), *Map2* (ectoderm), and *Sox2* (ectoderm) for all four treatment groups. *β-actin* was used as a loading control.

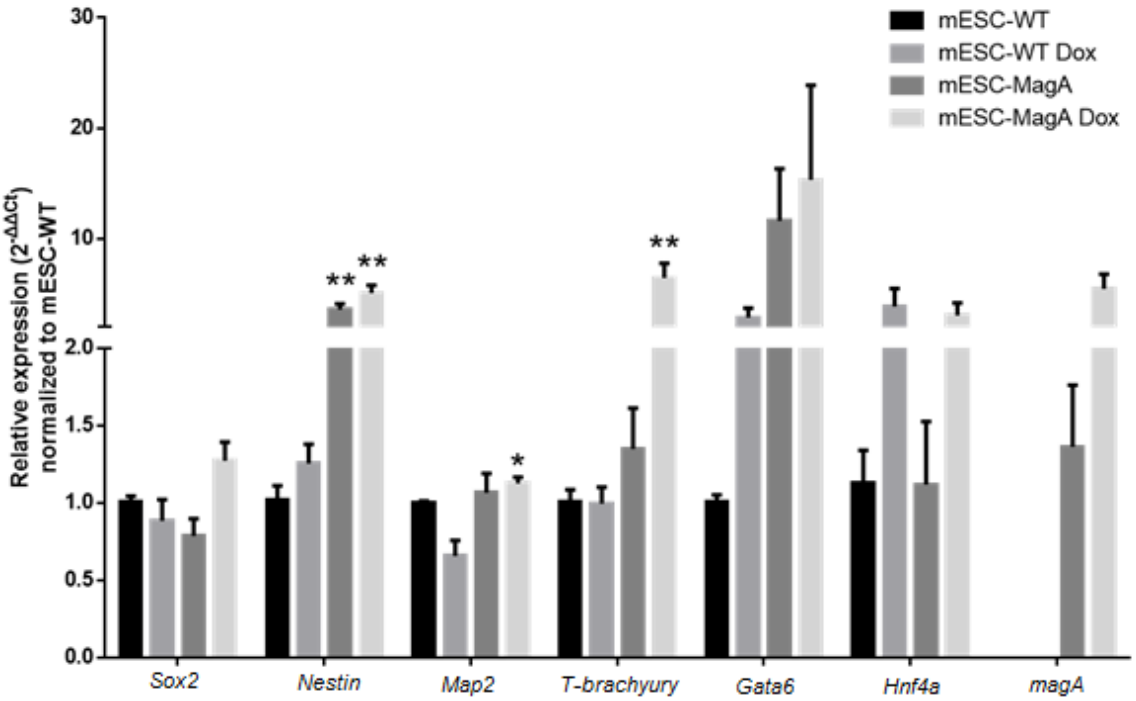

Figure 2-14. Relative expression of germ line specific marker genes were evaluated with qRT-PCR. mESC-MagA showed significantly higher *Nestin* expression, and mESC-MagA Dox showed significantly higher *Nestin*, *Map2*, and *T-brachyury* expression compare to mESC-WT. All data are normalized to mESC-WT except *magA*. All histogram data are means ± SEM. $n = 4$, *P < 0.05, **P < 0.001 versus appropriate control by ANOVA.

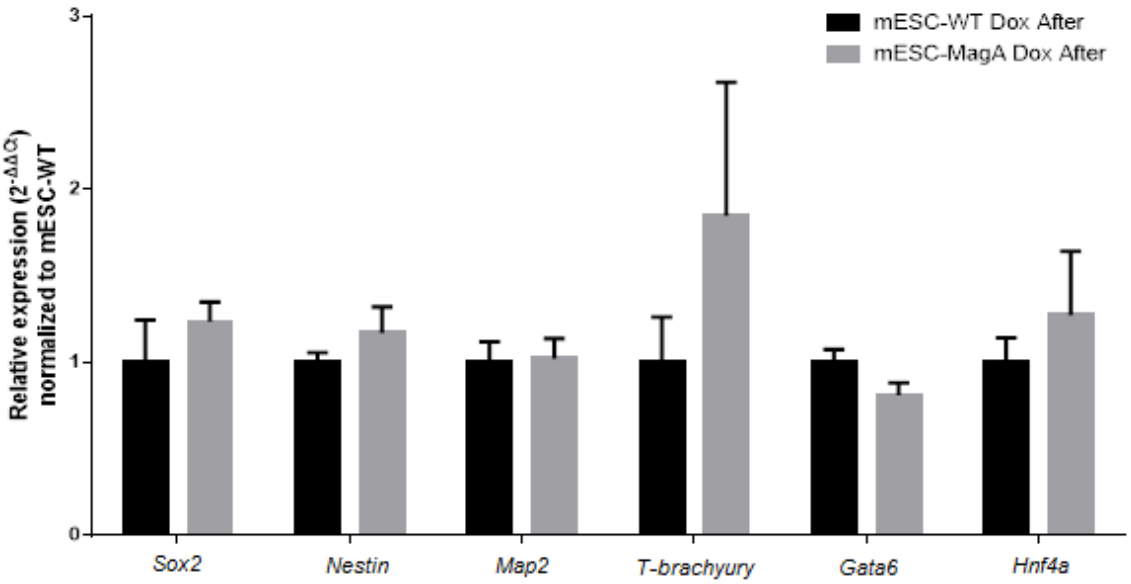

Figure 2-15. Relative expression profile of germ line specific marker genes with the total RNA samples isolated from the cells treated with doxycycline after initial differentiation stage. There was no difference in the expression levels among germ line specific marker genes. All data are normalized to mESC-WT except *mag A*. All histogram data are means ± SEM. $n = 4$.

Chapter 3

In vivo monitoring of stem cell graft using MagA as a genetic MRI reporter

Part of this chapter has been accepted to be published on ***Theranostics***. Cho, I.K., Moran, S.P., Paudyal, R., Piotrowska-Nitsche, K., Cheng, P.H., Zhang, X., Mao, H., Chan, A.W., Longitudinal monitoring of stem cell grafts in vivo using magnetic resonance imaging with inducible MagA as a genetic reporter. 2014.

3.1 Abstract

Stem cell therapy has become a promising therapy choice to cure or treat currently incurable diseases. However, the lack of non-invasive methods to monitor stem cell grafts *in vivo* has been one of the major obstacles in developing and evaluating stem cell therapy. A genetic MRI reporter offers a unique tool to monitor stem cell grafts non-invasively and longitudinally. Here we examined the application of MagA as a genetic MRI reporter in monitoring of mESC grafts *in vivo*. A mES cell-line carrying Tet-MagA (mESC-MagA) was established and used for these studies. First, cell graft of mESC-WT and mESC-MagA in the striatum of brains of immunocompromised mice demonstrated *in vivo* inducibility of MagA. When MagA was induced *in vivo*, mESC-MagA derived tumor demonstrated significant hypointense signal compared to mESC-WT derived tumor. Our *in vivo* longitudinal MRI study with repetitive MagA expression revealed that MRI contrast in intracranial mESC-MagA grafts can be controlled, and the cell grafts can be monitored by MRI upon induced expression of MagA by administrating Dox in the diet. Our results suggest MagA could be used to monitor cell grafts noninvasively and longitudinally by repeated induction, enabling the assessment of cell grafts.

3.2 Introduction

Stem cell therapy holds great promise in curing diseases that currently have no cure. In cell replacement therapy, the goal is to replace the depleted or degenerated cell population. The development of stem cell therapy was historically impeded by the lack of reliable cell sources and was under the

constraint of both technical and ethical issues. With recent developments in stem cell fields including directed stem cell differentiation (Brustle et al. 1999, Reubinoff et al. 2000, Schuldiner et al. 2000), transdifferentitaiton (Selman and Kafatos 1974, Davis, Weintraub, and Lassar 1987), iPSC (Takahashi and Yamanaka 2006), and successful derivation of patient-specific pluripotent stem cells (Chung et al. 2014), cell replacement therapy has become an attractive alternative. iPSC technology provided an alternative route to obtain reliable cell sources and address some of the ethical questions. Cell replacement therapy is especially attractive for degenerative diseases such as amyotrophic lateral sclerosis, Alzheimer's disease, Parkinson's disease, multiple sclerosis, and Huntington's disease. To demonstrate the interest and advancement in stem cell therapy research, there have been many clinical trials using stem cells on multiple disease: macular degeneration (Siqueira et al. 2013), autism (Sharma et al. 2012), amyotrophic lateral sclerosis (Deda et al. 2009), and Parkinson's (Venkataramana et al. 2010). Moreover, although there are still challenges to overcome in iPSC to be employed in clinical studies, such as genomic instability and epigenetic memories (de Lazaro, Yilmazer, and Kostarelos 2014), there have been many pre-clinical studies using iPSC-derived cells (de Lazaro, Yilmazer, and Kostarelos 2014). The recent developments in the stem cell field suggests that the clinical translation of stem cell therapy is within reach.

However, the challenge in long term monitoring of cell grafts *in vivo* remains as a major roadblock in advancing clinical translation. In order to correlate the status of cell grafts and clinical outcomes, a noninvasive imaging

tool that allows longitudinal assessment of viability, proliferation rate, lineage differentiation, and functional integration of cell grafts is needed. Current methods of directly labeling stem cells with contrast agents (e.g. SPIO) have been used for monitoring cell grafts with limited monitoring periods and possible false positives.

Although various imaging modalities can be used to track grafted cells *in vivo*, MRI provides a unique platform with advantages including high signal penetrance and high spatial temporal resolution, and safety to the patient. However, in order to monitor and track cells with MRI, grafted cells have to be distinguished from the surrounding tissues by using contrast agents. Due to limitations associated with exogenous labels (e.g. SPIO), an alternative method was investigated. To achieve the long-term monitoring of cell fate *in vivo* by MRI, a genetic reporter that can produce imaging contrast in the progeny of implanted cells would be ideal. Moreover, in order to reduce unnecessary accumulation of the reporter that may result in unforeseen impacts on cell function, an inducible regulation of reporter expression was taken to add an additional insurance compared to a constitutive expression of a reporter. In the previous chapter, we have evaluated inducible MagA as a genetic MRI reporter to generate MR contrast *in vitro*. We have demonstrated that MagA expression induced by Dox increased iron content in mESCs with detectable MR contrast *in vitro*. Here, we aim to determine the efficacy of MagA as a genetic MRI reporter *in vivo*. Intracranial mESC-MagA grafts were monitored longitudinally with repeated induction of MagA by Dox *in vivo*.

3.3 Methods

Preparation of cell grafts in mice

Two sets of experiments were carried out in order to evaluate whether the MR contrast can be generated *in vivo*. Severe combined immune deficient (SCID) mice (CB17/lcr-, Charles River Laboratories) 6 to 8 weeks of age received cell grafts. The first set of experiment was carried out with single status of "OFF" and "ON" status. For both "OFF" and "ON," the initial graft condition was the same. SCID mice were injected with $1x10^4$ cells suspended in 3 μl of PBS with 100 U/ml penicillin and 100 μg/ml streptomycin (P/S; Lonza). Cell suspensions were injected by stereotactic injection into the striatum of the right and left hemisphere (+0.74 mm anterior, ±1.7 mm medial/lateral relative to bregma, and -3.8 mm ventral from the dorsal surface of the skull). mESC-WT cells were injected into the left hemisphere striatum, while mESC-MagA cells were injected into the right hemisphere striatum. The mice in "OFF" group were fed with normal diet for 14 days, and at the end of 14 days, MRI scan was conducted. For "ON" group, mice were on the normal diet for 7 days, and after 7 days, mice were fed with doxycycline and ferric citrate supplemented water (5 mg/ml and 0.5 mg/ml respectively) and doxycycline chow (200 mg/kg, Bio-Serv) for 7 days. At the end of 7 days on the doxycycline diet, MRI scan was conducted. A graphic description and timeline is presented in Figure 3-1.

The second set of experiment was conducted in order to evaluate longitudinal monitoring of grafted cells with repetitive induction of MagA *in vivo*. Both mESC-WT and mESC-MagA were treated with Dox and FC (1 μg/ml and 25

μM respectively) for 3 d in culture. A total of 1x10^5 cells were suspended in 3 μl of PBS with 100 U/ml penicillin and 100 μg/ml streptomycin (P/S; Lonza). Cell suspensions were injected by stereotactic injection into the striatum of the right and left hemisphere (+0.74 mm anterior, ±1.7 mm medial/lateral relative to bregma, and -3.8 mm ventral from the dorsal surface of the skull). mESC-WT cells were injected into the striatum of the left hemisphere, while mESC-MagA cells were injected into the right hemisphere. After 24 hr of transplantation, the first MRI was conducted with the induced MagA expression, "ON." The mice were on a normal diet for 7 days, and the MagA expression was not induced during that period which indicated with MagA expression status, "OFF." To induce expression of MagA *in vivo*, mice were then fed with doxycycline and ferric citrate supplemented water (5 mg/ml and 0.5 mg/ml respectively) and doxycycline chow (200 mg/kg, Bio-Serv) for 7 days, "ON." Schematic diagram depicting experimental procedure and timeline is presented in Figure 3-2.

In vivo MRI of cell grafts in mice

The imaging parameters were the same for both single status experiment and longitudinal repetitive induction experiment. T_2- weighted images were collected with fast spin echo imaging. A fast low angle shot (FLASH) gradient echo (GRE) sequence, was used for obtaining susceptibility weighted contrast. The imaging parameters for spin-echo (SE) were as follow: TE = 12.5 ms, TR = 4000 ms, FOV = 25 x 25 mm, resolution = 196 x 196, and slice thickness = 0.75 mm. Parameters for FLASH-GRE imaging were: TE = 10 ms, TR = 300 ms, FOV = 25 x 25 mm, resolution = 196 x 196 and slice thickness = 0.75 mm.

The region of interest (ROI) was defined utilizing two MRI images, i.e., gradient echo (GRE) and spin-echo (SE), for single status experiments and for first "ON" and consecutive "OFF" scan of longitudinal repetitive induction experiment. The tumor boundary delineation process is presented as an algorithm in Figure 3-3. In short, both GRE and SE MRI images were utilized in delineation process using ImageJ (Figure 3-4a). First, the brightness level was adjusted to remove as much as background and adjacent tissue. Second, the contrast was adjusted to visualize the boundary. Third, tumor boundaries were delineated (Figure 3-4b, 1). Fourth, boundaries defined by GRE and SE were overlaid to find any disagreement (Figure 3-4b, 2). If there were any disagreement, ROIs were adjusted following first and second steps using both GRE and SE MRI images until ROI defined by both GRE and SE MRI images converge (Figure 3-4b, 3). A magnified picture of GRE image is shown in Figure 3-4c in order to demonstrate the clear tumor/brain boundary. Once ROIs for both mESC-MagA and mESC-WT derived tumors were defined, ROIs were saved, and signal intensity was measured from the image. We also considered bony landmarks, brain contour and tumor size (i.e. area) when defining the ROI. To evaluate the previous ROI analysis, we compared the ROI defined only by MRI and histo-adjusted ROI, and they showed similar signal intensity (Figure 3-5). For the last set of the longitudinal repetitive induction experiment, two different MRI images and Nissl staining of the brain sections were used to better define the ROI. Scaling, rotation and possible artifacts from fixation and sampling process were taken account.

Image processing and statistical analysis were performed using ImageJ 1.46r (NIH), SPSS (IBM), Prism 5 (Graphpad), and Excel (Microsoft).

Tissue preparation

Mice were anesthetized and perfused transcardially with 37 ºC PBS followed by ice-cold 4% paraformaldehyde. Intact brains were removed from the skull and post-fixed in 4% paraformaldehyde overnight followed by 30% sucrose. The whole brain was embedded in OCT and stored at -80ºC. Serial sections were cut at 30 μm using a Leica CM3050S Cryostat (Leica, Nussloch, Germany) and immediately captured on to gelatin-coated Superfrost® Plus (Fisher Scientific) slides. Nissl staining was performed to visualize the tumor. For qRT-PCR, brain samples were snap frozen, and stored in liquid nitrogen until RNA extraction.

Quantitative real-time PCR (qPCR)

Total RNA was isolated from tissues using TRIzol® (Life Technologies) following the standard method. Briefly, tissues were suspended in 500 μl of TRIzol® and homogenized with a 21G sterile syringe followed by treatment with TURBO™ DNase (Life Technologies). The cDNA was synthesized with 500 ng of RNA sample using a High-Capacity cDNA Reverse Transcription Kit (Applied Biosystems). Quantitative real-time PCR was performed using TaqMan® Gene Expression Master Mix (Applied Biosystems). For *magA*, a custom-made TaqMan® probe was used (F- 5'-ATCCGTTTTCTCGAAGTGTGGAA-3', R-5'-GCCCGCGATCTGCAAAA-3', and P-5'- ACGGCGGTCTTCACC-3'). For normalization, eukaryotic *18S* rRNA (Applied Biosystems) was used as an endogenous control. Quantitative real-time PCR amplification was performed

using the Bio-Rad CFX96 real-time PCR detection system. Gene expression was calculated by comparative 1/ΔCT normalized to *18S* rRNA transcript levels.

Immunohistochemistry

For immunohistochemical staining of brain sections, a layer of PBS was placed onto a slide for 10 min at room temperature, then a solution of freshly prepared 1% sodium borohydribe in PBS was applied for 20 min inside the fume hood. Tissue sections were washed thoroughly with PBS. Freshly prepared 10% methanol and 0.3% H2O2 in PBS was applied for 30 min. After a rinse with PBS, preincubation was completed with blocking solution composed of 1% donkey serum, 1% BSA, and 0.3% Triton X-100 for 60 min at room temperature. The primary antibody solution was prepared in blocking solution (mouse anti-HA.11 clone 16B12 monoclonal 1:1,000; Covance) and incubated overnight in a humidified chamber at 4 ºC.

For DAB staining, tissue sections were washed 3 times with PBS after incubation with primary antibody followed by incubation with biotinylated antibody (Vector Laboratories) at a dilution of 1:200 in blocking solution for 90 min at room temperature. After 3 washes with PBS, DAB was reveled using a VECTASTAIN Elite ABC Kit (Vector Laboratories).

For immunofluorescent staining, tissue sections were washed 3 times with PBS after primary antibody incubation, followed by incubation with a secondary antibody (anti-rabbit Alexa 594 1:1,000; Vector Laboratories, anti-mouse Alexa 594 1:1,000; Molecular Probes, anti-mouse Cy-5 conjugated 1:5,000; Jackson

ImmunoResearch) for 90 min. Cell nucleuses were visualized with Hoechst staining (0.12 μg/ml).

Prussian blue staining was performed at the Yerkes histopathology laboratory using the standard protocol to visualize the presence of iron in tumor samples.

Images were captured by using a BX51 microscope equipped with CellSens software.

Statistical analysis

All data and graphs are presented with standard error of the mean (SEM). For all the MRI data, MRI images were first processed, then signal intensities were extracted using ImageJ (NIH). Statistical analyses were completed using one-way analysis of variance (ANOVA) in SPSS 20 (IBM). *P* values less than 0.05 were employed for the threshold for statistical significance.

3.4 Results

3.4.1 *In vivo* induction of MagA

We conducted two sets of experiments to determine if the expression of MagA led to detectable contrast *in vivo*. The first study was to determine whether induction of MagA can generate distinctive contrast in mESC-MagA compared to mESC-WT while no signal contrast was expected when MagA was not induced. MRI scans performed at 14 days after intracranial transplantation of non-induced mESC-WT and mESC-MagA, “OFF,” showed no visible contrast (Figure 3-6a three representative scans are shown). Quantitative of MR contrast showed no

difference in MRI signal between mESC-WT and mESC-MagA derived tumors in the brain (P = 0.3934, n = 4; Figure 3-6b). The second study was to determine whether *in vivo* induction of MagA, "ON," by administration of doxycycline in the diet (water and chow) can generate MR contrast *in vivo*. One week feeding of the recipient mice with sterile Dox chow (Bioserve) and Dox and FC supplemented water induced the expression of MagA *in vivo*. Three representative MRI scans demonstrate the visible contrast in Figure 3-7a. After induction, mESC-MagA derived tumor exhibited hypointense contrast compare to mESC-WT derived tumor. Quantification of the MR contrast demonstrated a significant decrease in MR signal from mESC-MagA derived tumor compared to mESC-WT derived tumor (P = 0.0035, n = 8; Figure 3-7b). Immunofluoresence staining of brain sections confirmed MagA expression in mESC-MagA derived tumors (Figure 3-7c) but not in mESC-WT. The results demonstrated that MagA expression can be regulated by Dox/FC in the diet, and when mice were fed with Dox/FC, mESC-MagA derived tumor showed significant hypointense signal.

3.4.2 Longitudinal repetitive induced expression of MagA *in vivo*

The next study was to evaluate the potential of MagA in a non-invasive longitudinal MRI monitoring of cell grafts. We conducted a series of MRI scans on mESC grafts with induced, "ON," and non-induced, "OFF," expression of MagA controlled by the administration of Dox and FC in rodent chow and water. We performed a total of three scans weekly for three weeks. Based on the experimental paradigm shown in Figure 3-2, the mESC-MagA was treated with Dox/FC for three days before intracranial implantation "ON (-3 days post-

operation or -3 d p.o.)" in mice. The first MRI was performed 24 hours after implantation. Seven days after the first scan, during which no Dox and FC was provided to the mice "OFF (+8 d p.o.)", a second MRI scan was performed. After the second scan, mice were fed with Dox Diet (Bio-Serv) and water supplemented with Dox and FC for seven days "ON (+15 d p.o.)." Mice were then euthanized after the last MRI scan on day 15 after implantation (+15 d p.o.). Figure 3-8 shows representative susceptibility-weighted gradient echo (GRE) images and spin echo (SE) images from three mice.

In order to better define the region of interest (ROI) for analyzing contrast changes, we performed Nissl staining on serial sections of the brain (Figure 3-9). The Nissl staining is a nucleic acid staining method generally used to study morphology and pathology of neural tissue. In this study, Nissl staining is used in order to visualize tumor/brain boundaries because tumors are expected to be more nuclear-dense than brain. We utilized GRE, SE MRI images, and Nissl staining sections side by side and overlaid to define the region of interests (Figure 3-10). When the mean signal intensity of the ROI defined only by MRI was compared to histology-adjusted ROI, similar signal contrast was observed (0.655 ±0.0951 versus 0.657 ± 0.164, n = 3; Figure 3-5).

Figure 3-11a shows representative images of each repetitive scan of a mouse that went through the whole study with MagA expression status indicated by "ON" and "OFF" above images. The corresponding signal intensities are shown below (Figure 3-11b). A significant signal reduction was observed in the hemisphere where mESC-MagA was grafted, compared to mESC-WT (17.6 ± 0.5

versus 19.9 ± 0.9, P = 0.045, n = 4; Figure 3-11b left panel) from the first scan ("ON" -24 hr p.o.). After a week of withdrawal of Dox/FC ("OFF" +8 d p.o.), signals from the mESC-MagA grafts returned to baseline levels, similar to the mESC-WT grafts as MR contrast enhancement disappeared (10.1 ± 0.8 and 10.3 ± 0.9, respectively, P = 0.898, n = 6; Figure 3-11b middle panel). After seven days of induced expression of MagA by Dox with the supplementation with FC ("ON" +15 d p.o.), the mESC-MagA grafts showed a significant signal reduction compared to the mESC-WT grafts (11.8 ± 0.5 versus 14.2 ± 0.6, respectively, P = 0.003, n = 5; Figure 3-11b right panel). This longitudinal imaging study of "ON," "OFF," and "ON" expression of MagA after intracranial transplantation has confirmed the generation of MRI contrast by expressing MagA in cell grafts in mESC-MagA grafts can be induced *in vivo* by a dietary supplement of Dox/FC.

We confirmed the induced expression of MagA *in vivo* by qPCR and immunostaining of serial sections of the brain using anti-HA antibodies. mESC-MagA derived tumors showed MagA expression (Figure 3-12a). At a higher magnification, mESC-MagA derived tumors showed distinct signal (Figure 3-12b, 2) compared to the mESC-WT-derived tumors (Figure 3-12b, 1) or a randomly selected area of the same brain section (Figure 3-12b, 3). A three-dimensional representation of the densitometry of the brain section illustrates the expression pattern of MagA in the mESC-MagA derived tumor (Figure 3-12b, 4). Immunofluorescent staining further demonstrated the specific expression of MagA in mESC-MagA derived tumors (Figure 3-13a). Quantitative measurement and comparison of *magA* transcripts in teratomas derived from both mESC-

MagA and mESC-WT grafts further confirmed the induced expression of MagA in the mESC-MagA grafts (Figure 3-13b). Prussian blue staining revealed more positively stained cells in mESC-MagA derived tumor compared to those sparsely found in mESC-WT derived tumor (Figure 3-14), thus suggesting the increase in iron content in mESC-MagA derived tumor. The MR contrast showed correlation to the MagA expression status and the increased iron content in the tumor derived from mESC-MagA cell graft.

The impact of MagA expression in differentiation capacity as well as the heterogeneity of tumors was assessed by double immunostaining. The co-expression of the lineage specific markers and HA was utilized: HNF4a (mesoderm), Nestin (ectoderm), Musashi (ectoderm), and CD117 (endoderm). Both mESC-WT and mESC-MagA derived tumors were positive for all four lineage specific markers in HA positive cells (Figure 3-15).

3.5 Discussion

Results from this study demonstrate the feasibility of monitoring stem cell grafts longitudinally by a genetic MRI reporter, and controlling MR contrast by using an inducible expression system. Our results demonstrate, for the first time, that expression of MagA can be modulated while sufficient MRI contrast can be generated for monitoring mESC grafts by MRI.

The teratomas developed from the implanted cell grafts are heterogeneous in nature and MR images reveal variation in contrast signal. The heterogeneous nature of the teratoma derived from mESC graft was not unexpected (Figure 3-15); however, we observed variations in MagA expression patterns in IHC (Figure

3-13), heterogeneity in Prussian blue staining (Figure 3-14), and variation in contrast signal in the teratoma (Figure 3-8). Since teratoma consists of diverse tissue types, epigenetic gene silencing in different cell types may influence the expression pattern of MagA upon induction and affect iron uptake and retention in the tumor. In addition, like other tumors, blood supply may not be evenly distributed in the tumor, and the distribution of Dox and FC may vary. As a result, MR contrast generated by the induced expression of MagA is expected to be affected.

According to the cell pellet phantom study, induced expression of MagA in mESC-MagA generated a significant but smaller transverse relaxivity compared to our previous report in 293FT cells (Zurkiya, Chan, and Hu 2008). This finding further suggests differences in cell types that may play a role in the formation of magnetosomes and the uptake or accumulation of iron that affect the generation of MR contrast.

To date, the role of MagA as an iron transporter in magnetosome formation is not fully understood and MagA alone may not allow the formation of a magnetosome (Uebe, Henn, and Schuler 2012). In prokaryotic cells, there are many genes involved in the formation of the magnetosome effectively (Bazylinski and Frankel 2004). It can be speculated that other genes, or a combination of genes, may aid MagA in generating MR contrast. Therefore, to further improve the formation of magnetosome and enhancement of MR contrast, investigation on MagA as well as other genes involved in the formation of magnetosome is a critical next step. However, the effect of epigenetic gene silencing will remain for

ESC- and iPSC-derived teratoma. One possible solution is to use a cell source with a more defined lineage in cell therapy, resulting in a homogenous cell population; thus a more uniform expression pattern of MagA could be achieved with enhanced and homogeneous MR contrast.

Due to the fast growing rate of mESC-MagA and constraints of the mouse model described in this study, we only performed three repeated MRI scans under “ON” and “OFF” expression of MagA as a proof of principle. Future studies using less tumorigenic lineage-specific cell types, such as neural progenitor cells, may enable long-term longitudinal monitoring of cell grafts with MRI to further improve sensitivity and detection threshold of the MagA reporter that was not addressed in this study. Although the sensitivity of the system has not been determined, the fact that mESC-MagA cells exhibit significant hypointense signal with 1×10^5 cells in the first scan has provided a baseline for future studies.

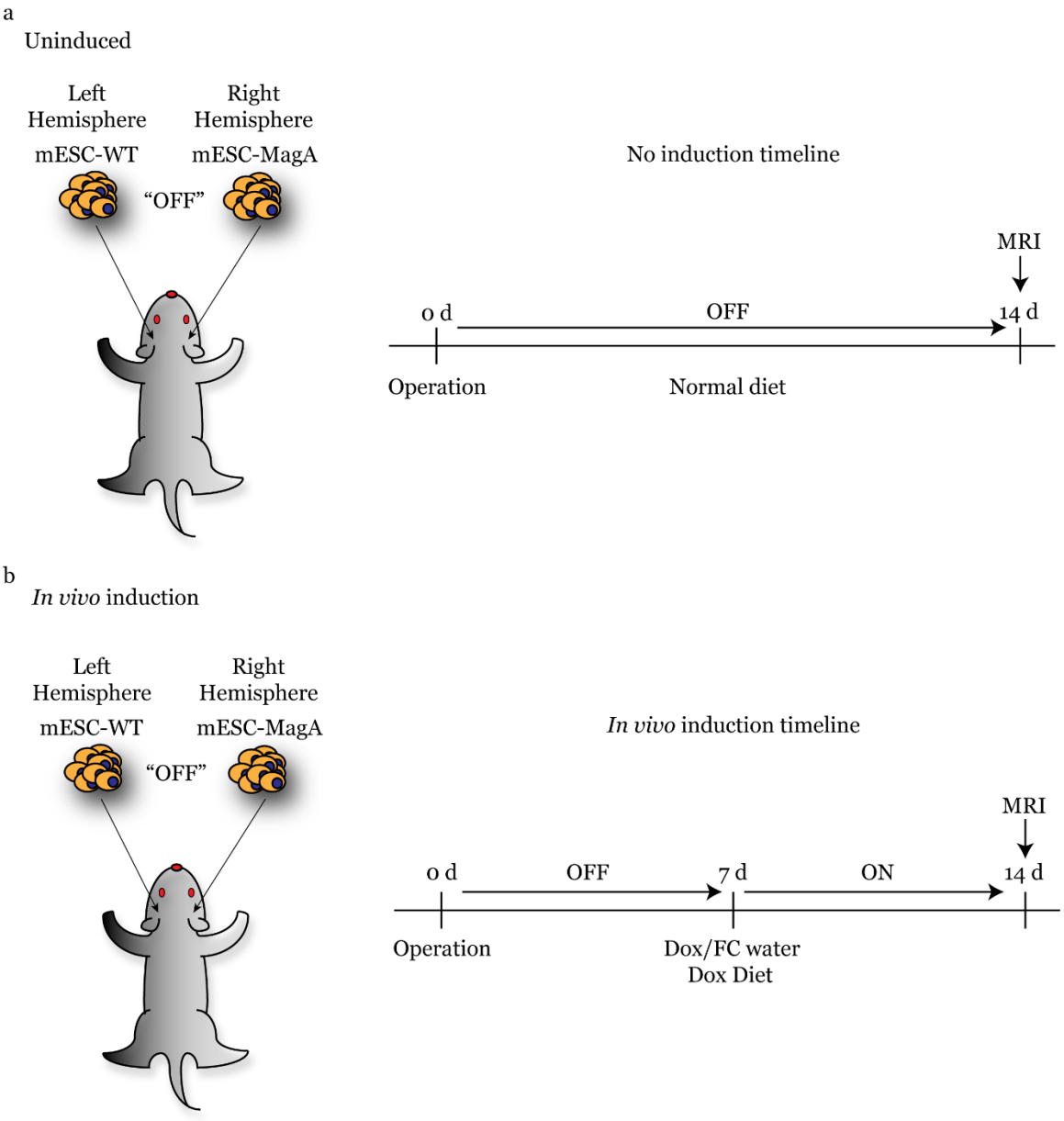

Figure 3-1. Schematic diagram depicting experimental procedure and timeline of single status experiment. (a) Schematic diagram depicting "OFF" graft experiment with the timeline. 1x10^4 cells were grafted in the striatum of mice: mESC-WT in the left hemisphere and mESC-MagA in the right hemisphere. For no induction experiment, "OFF," mice were fed with normal diet for 14 days, and MRI scan was conducted. (b) Schematic diagram depicting "ON" graft experiment, with the timeline. The same number of cells were grafted in the striatum of mice as no induction experiment. However, after 7 days, mice were fed with Dox/FC supplemented water and Dox chow for 7 days inducing MagA in mESC-MagA cell grafts. At the end of induction, MRI scan was conducted and brain was harvested for further analysis.

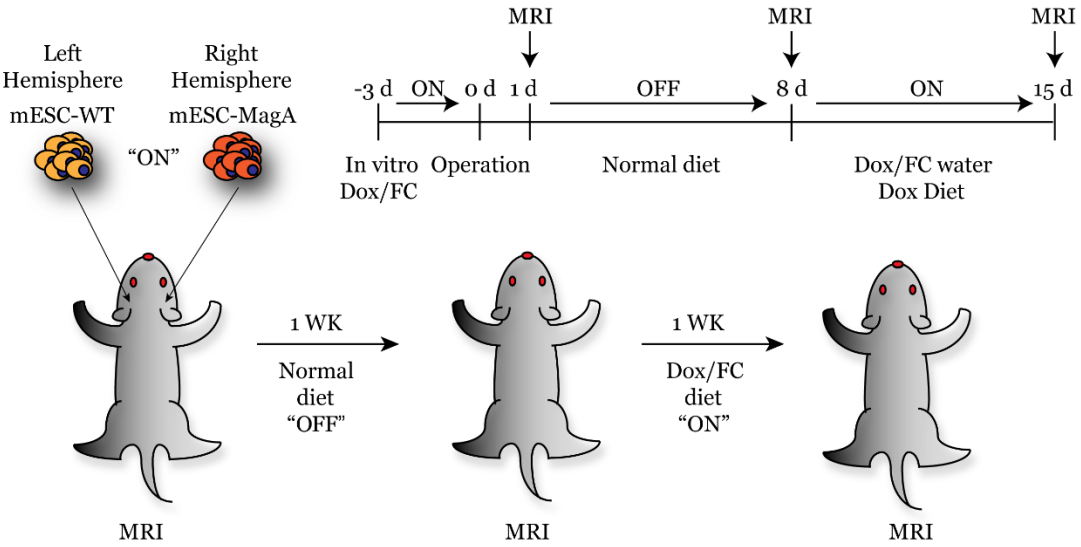

Figure 3-2. Schematic diagram depicting experimental procedure and timeline of longitudinal monitoring of stem cell graft with repetitive induction of MagA *in vivo*. Prior to grafting, cells were induced with Dox and FC (1 μg/ml and 25 μM respectively) for 3 d in culture, denoted as "ON." At the end of *in vitro* induction, a total of 1x10^5 cells were intracranially transplanted in the striatum area of mice. 24 hours after the operation, the first MRI was taken. Mice were put on the normal diet for a week, and the second MRI was taken, which is denoted as "OFF." For the last week, mice were fed with Dox/FC supplemented water (5 mg/ml and 0.5 mg/ml respectively) and doxycycline chow (200 mg/kg, Bio-Serv). The MRI was conducted after the last induction, "OFF." After the last MRI, mice were euthanized, and tissue samples were harvested with appropriate methods.

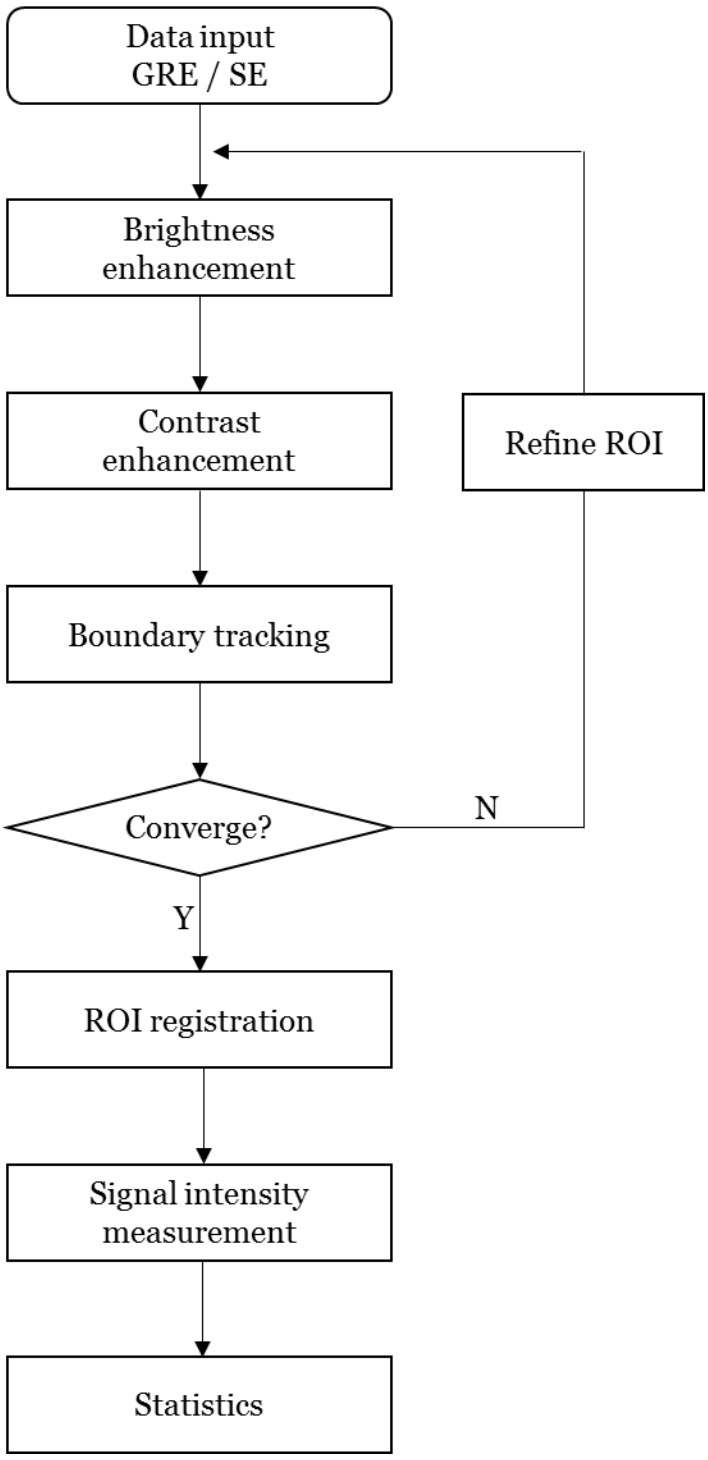

Figure 3-3. An algorithm used to delineate the tumor boundary. For the scans when only the MRI images were available, imaging enhancement and side-by-side comparison of GRE and SE images were used to define region of interest (ROI).

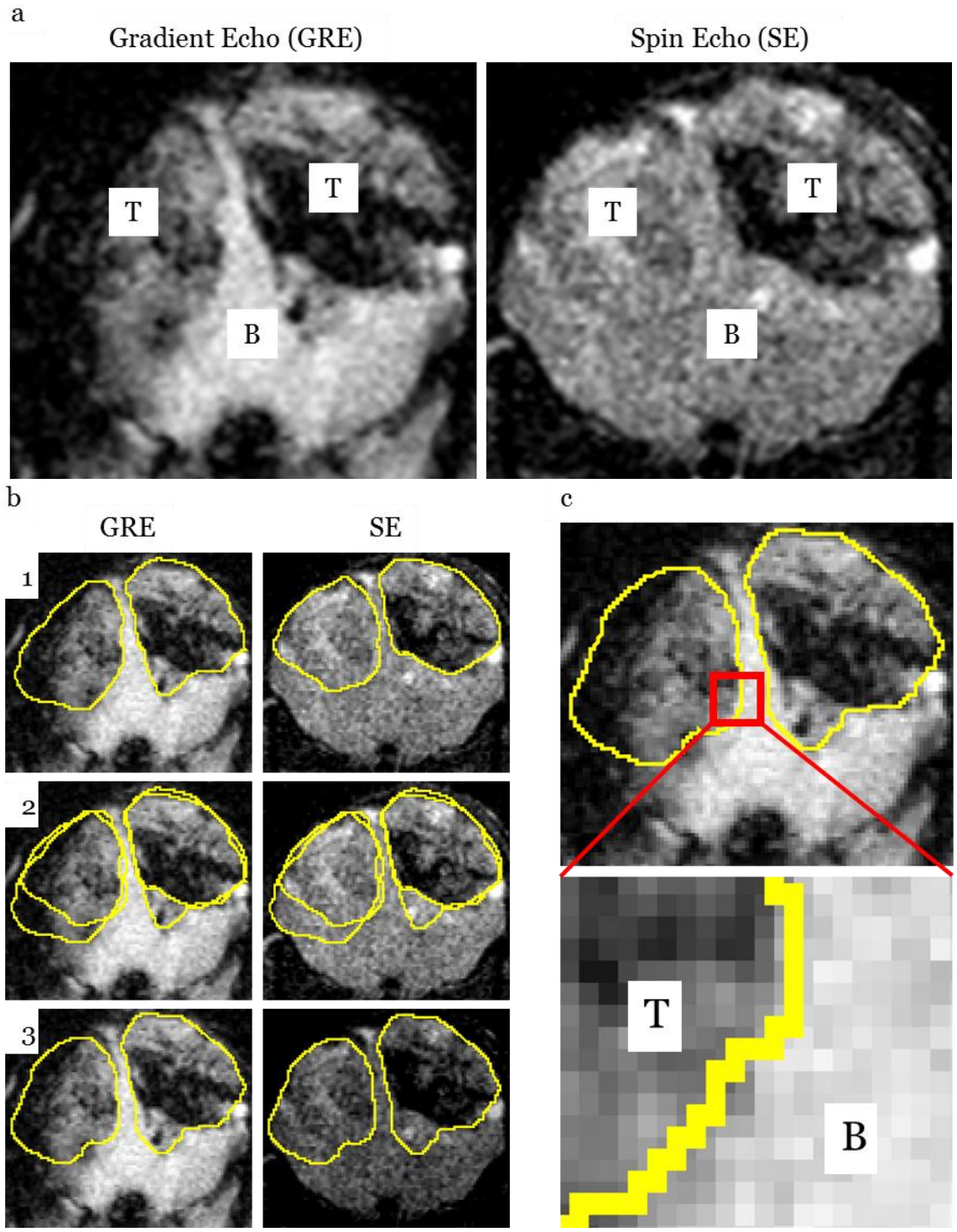

Figure 3-4. An example of tumor boundary delineation process for ROI analysis. (a) GRE and SE MRI images with tumors (T) and brain (B) labeled. (b) First, brightness and contrast adjusted GRE and SE images were independently used to delineate boundary. Second, GRE and SE defined ROI are overlaid to evaluate the boundary. Third, brightness enhancement, contrast enhancement, and pixel by pixel contrast is considered to refine boundary. (c) A magnified GRE image demonstrates clear tumor-brain boundary.

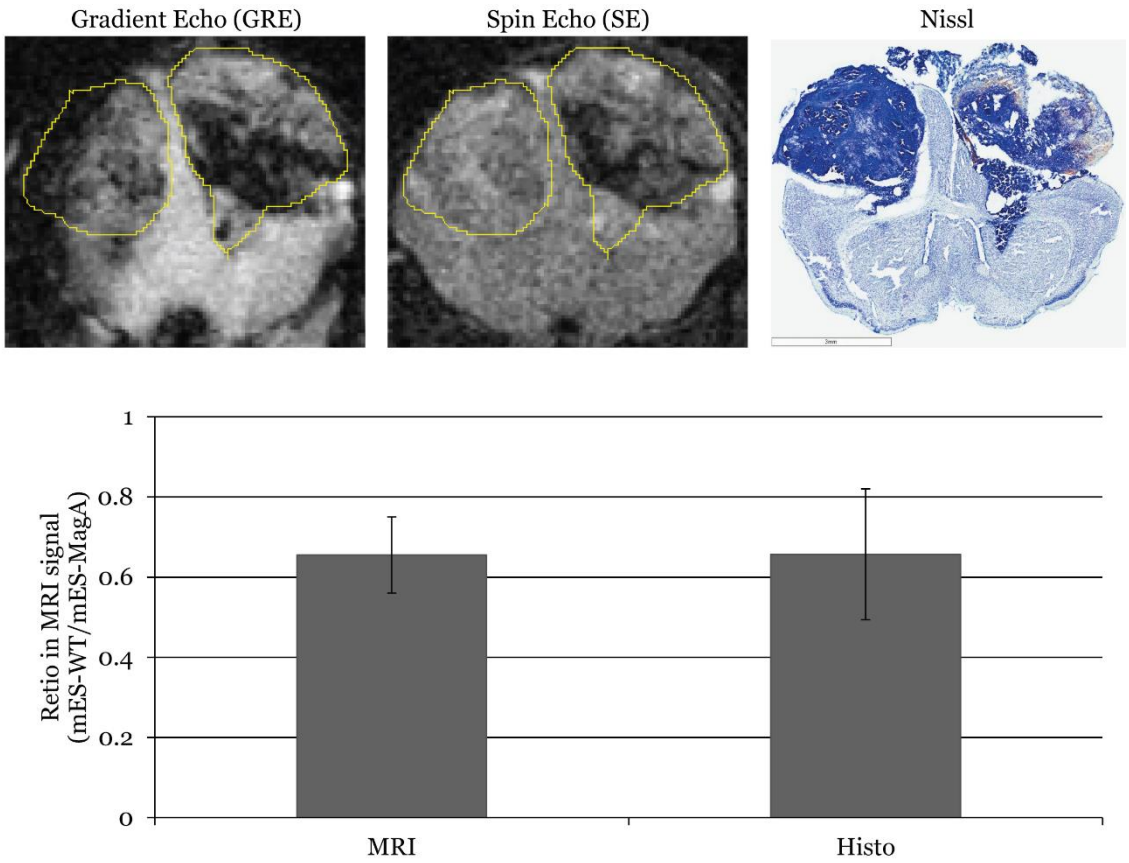

Figure 3-5. MRI only and histo-adjusted ROI analysis. Two MR images (GRE and SE) and Nissl staining histology of the whole brain section were used to evaluate the ROI defined for signal analysis. A comparison between signal intensity analysis using only MRI images to define ROI (MRI) versus histology-adjusted ROI (Histo), which showed similar signal contrast (0.655 ± 0.0951 versus 0.657 ± 0.163, n = 3).

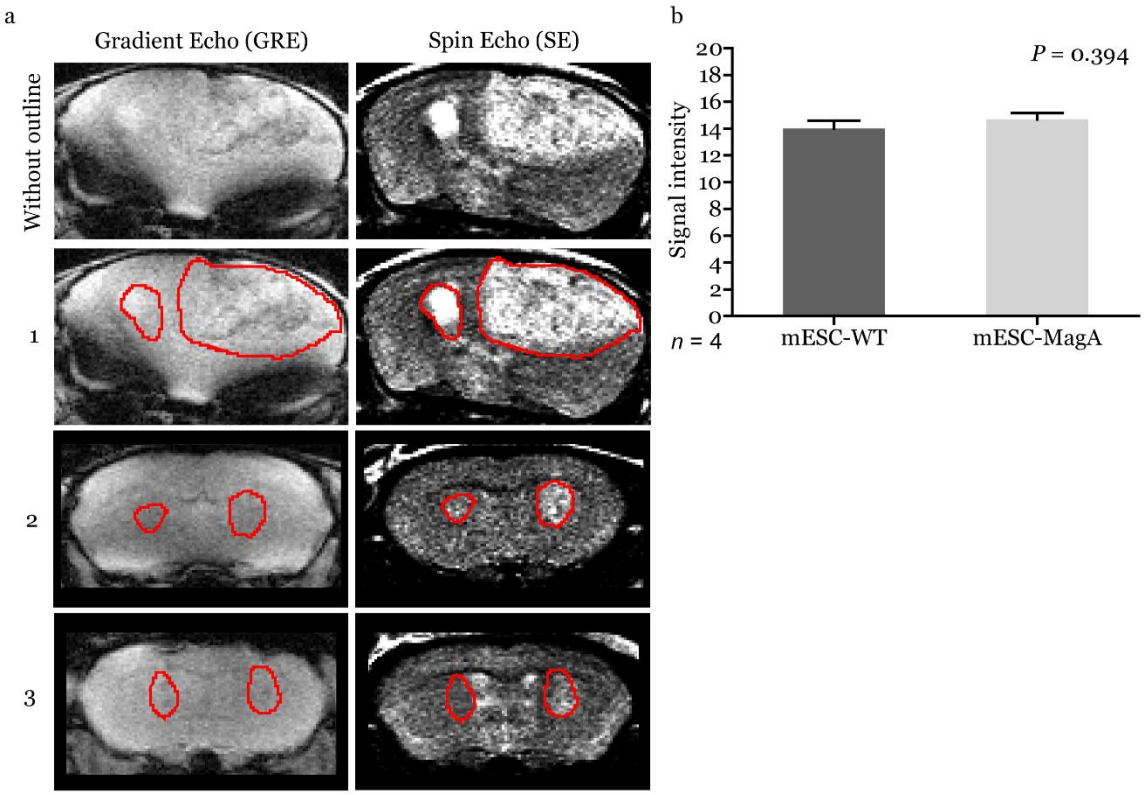

Figure 3-6. No induction, "OFF," *in vivo* cell graft experiment. (a) Representative MRI images from three mice are presented with tumor boundaries highlighted with red lines. Left side is grafted with mESC-WT and right side was grafted with mESC-MagA. Both gradient echo and spin echo images are shown side-by-side. (b) No difference was observed in MR contrast in a mESC-WT and mESC-MagA grafts (P = 0.394, n = 4).

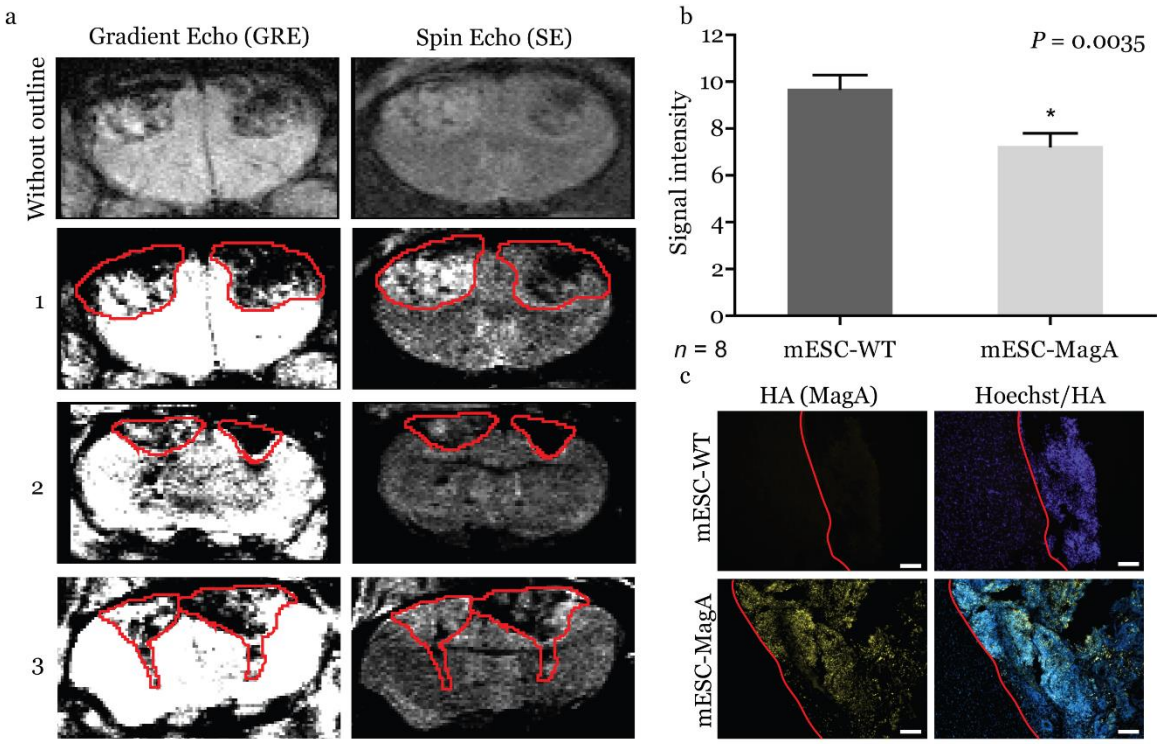

Figure 3-7. *In vivo* induction, "ON," cell graft experiment. (a) Three representative MRI images are presented with tumor boundaries highlighted with red lines. Left side was grafted with mESC-WT, and right side was grafted with mESC-MagA. (b) A significant MR contrast was observed after MagA expression was induced with Dox in the diet for 7 days (P = 0.0035, n = 8). (c) Immunofluorescence analysis using HA antibody confirmed MagA expression in mESC-MagA derived tumor in the brain. The boundary is highlighted with red lines.

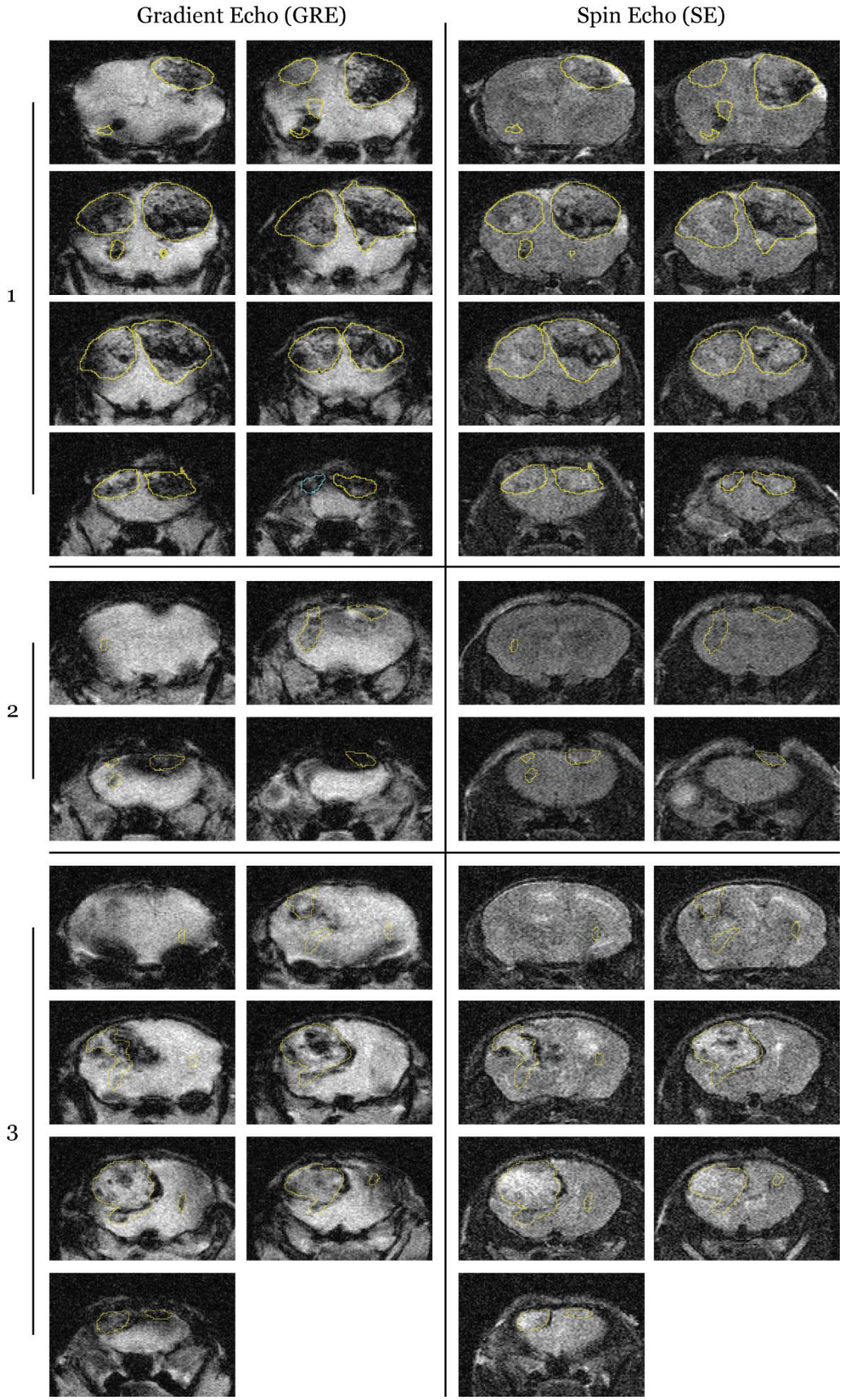
Gradient Echo (GRE)
Spin Echo (SE)
1
2
3

Figure 3-8. MR images of three representative scans from a longitudinal study. GRE images and SE images are shown here with the tumor region outlined with yellow line. The series goes from the posterior to the anterior of the brain starting from the left upper corner to right and going down in a zigzag fashion.

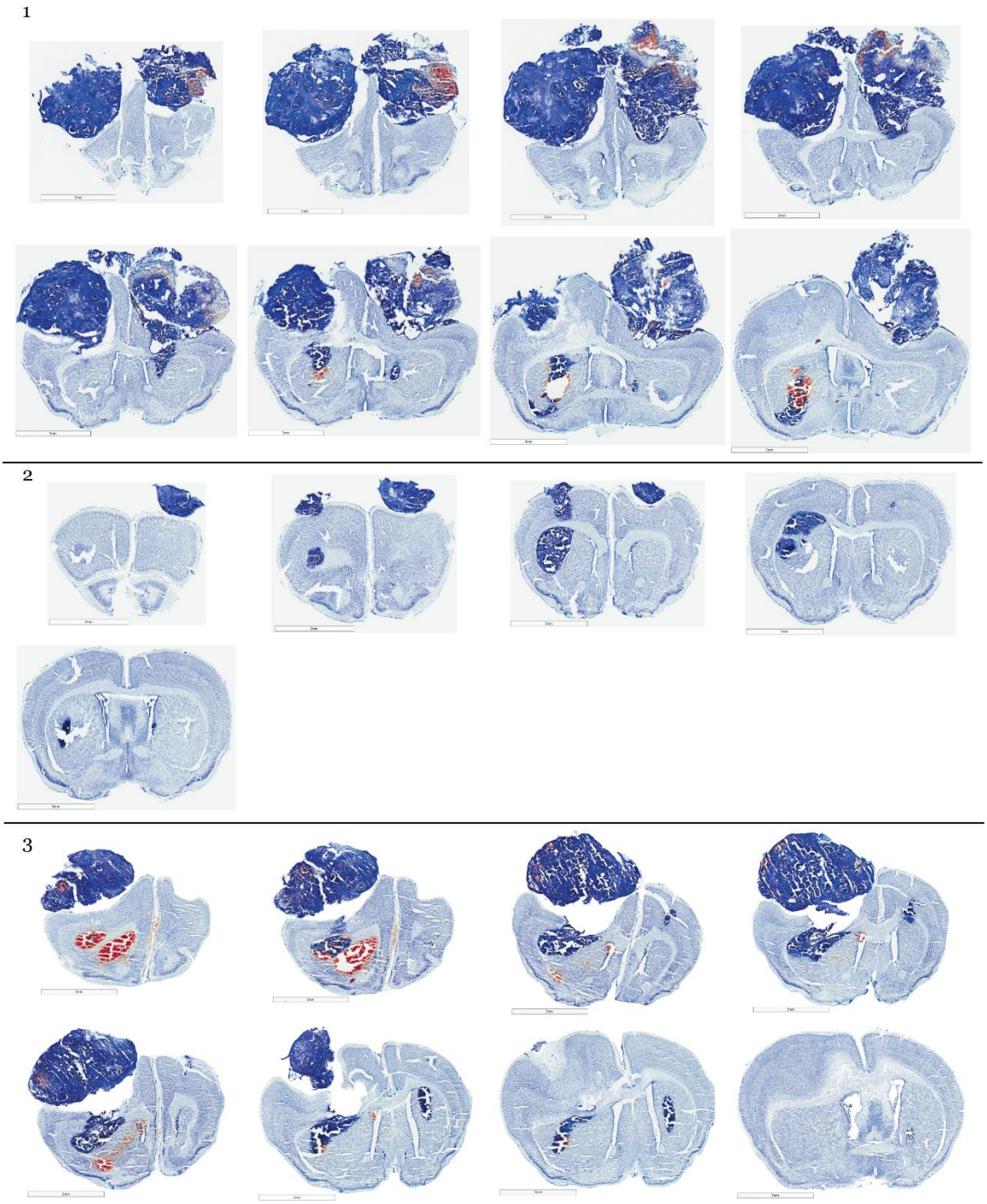

Figure 3-9. Nissl staining of three representative serial brain sections from longitudinal experiment. Three mice brains are presented here. The numbers are the same as the previous MR images from Figure 3-5.

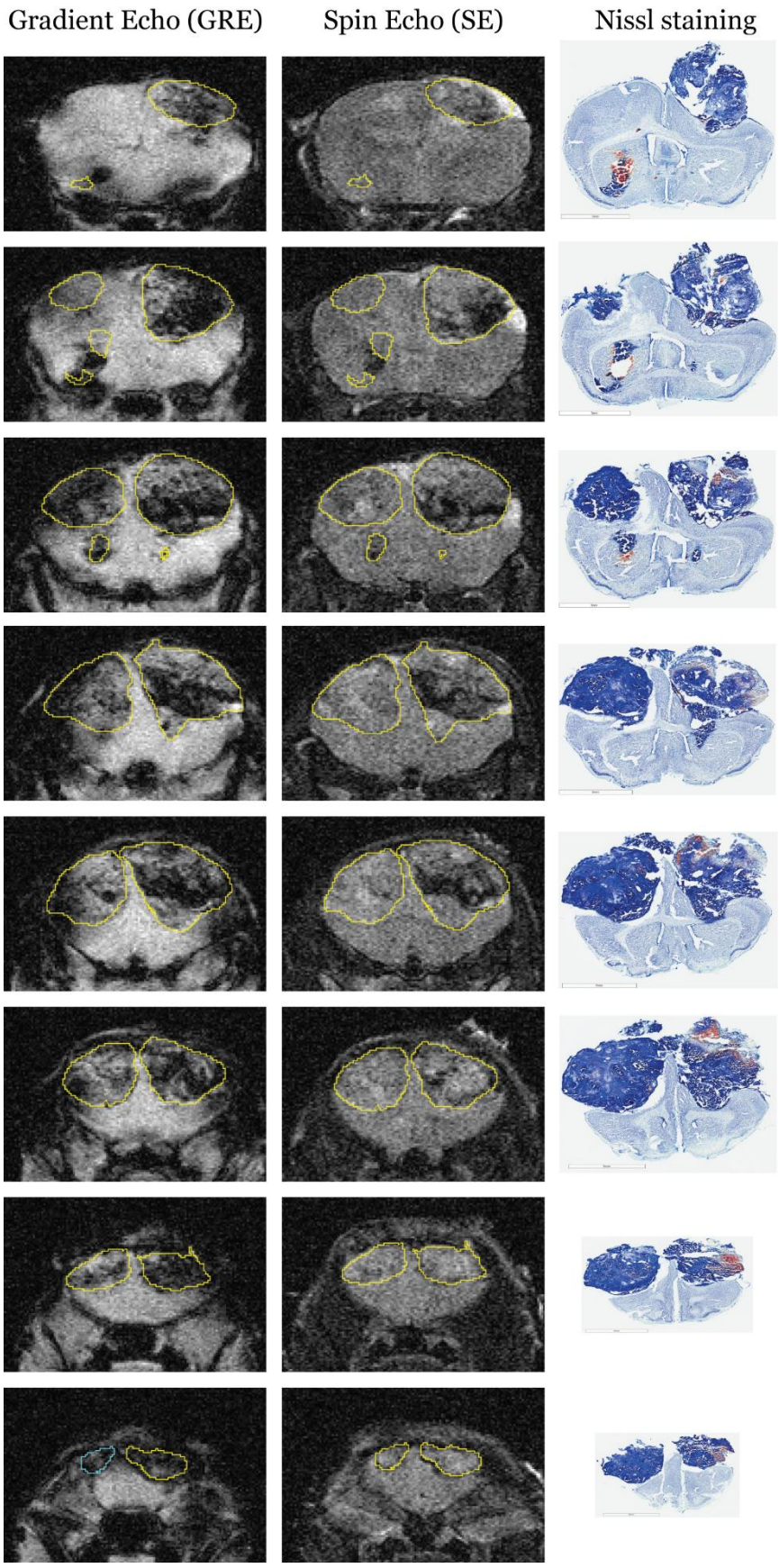
Gradient Echo (GRE)
Spin Echo (SE)
Nissl staining

Figure 3-10. Side by side pictures of MR images (GRE and SE) with Nissl staining images of a single mouse scan. For the ROI analysis, all three images were compared side by side to define ROI. We also considered bony landmarks, brain contour and tumor size (i.e. area) when defining the ROI. Scaling, rotation and possible artifacts from fixation and sampling process were taken account.

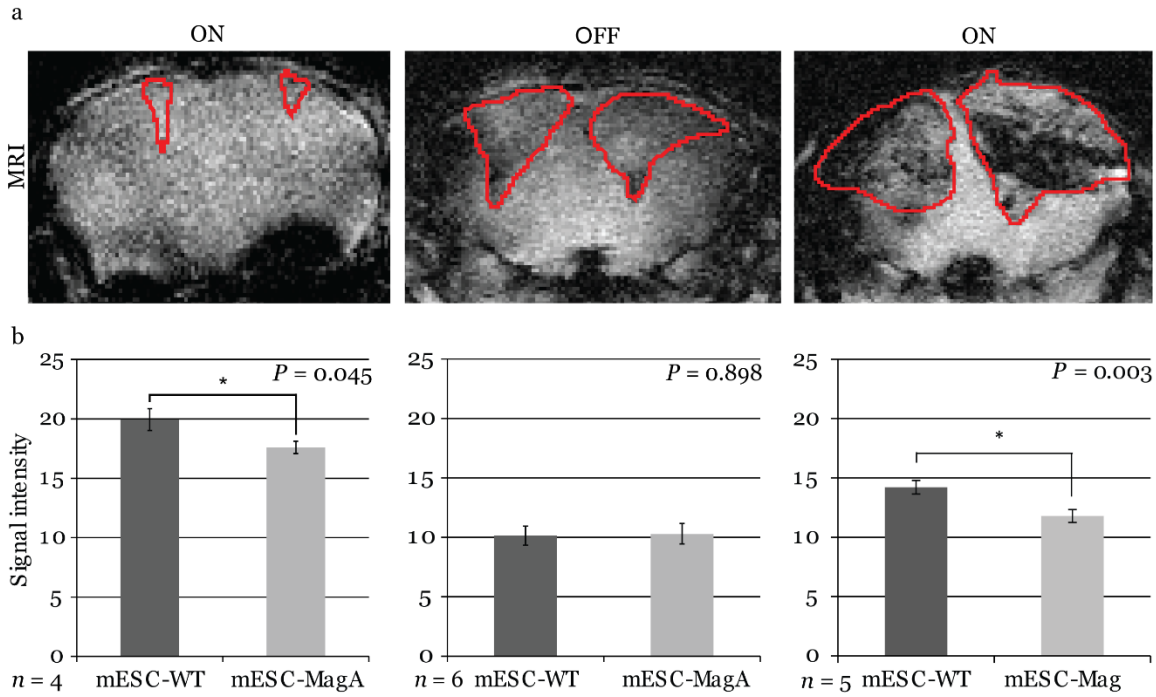

Figure 3-11. Longitudinal monitoring of intracranial implanted cell grafts in mice using inducible MagA reporter by repeated MRI. (a) A representative susceptibility weighted MRI image of a single mouse that went through the whole longitudinal repeated MRI scan. Regions of interest (ROIs) are highlighted with the correlated signal intensity analysis shown in (b). MRI images demonstrate the contrast between mESC-WT and mESC-MagA when MagA was induced ("ON" state, first and last images), but no contrast when MagA was not induced ("OFF" state, middle image). (b) The graphs demonstrate statistically significant hypointense signals in "On" states. A significant MRI contrast was observed at 24 h p.o. (*P = 0.045, n = 4). When MagA expression was not induced, the signal intensity was similar for both teratomas (10.1 ± 0.807 and 10.3 ± 0.859, P = 0.898, n = 6). When MagA expression was induced again in vivo, there was a significant difference in signal intensity, as the hemisphere hosting mESC-MagA graft shows a region with hypointense signal compared to the contralateral hemisphere with mESC-WT graft (11.8 ± 0.542 versus 14.2 ± 0.578 respectively, *P = 0.003, n = 5). All histogram data are means ± SEM. *P < 0.05, **P < 0.001 versus appropriate control by ANOVA.

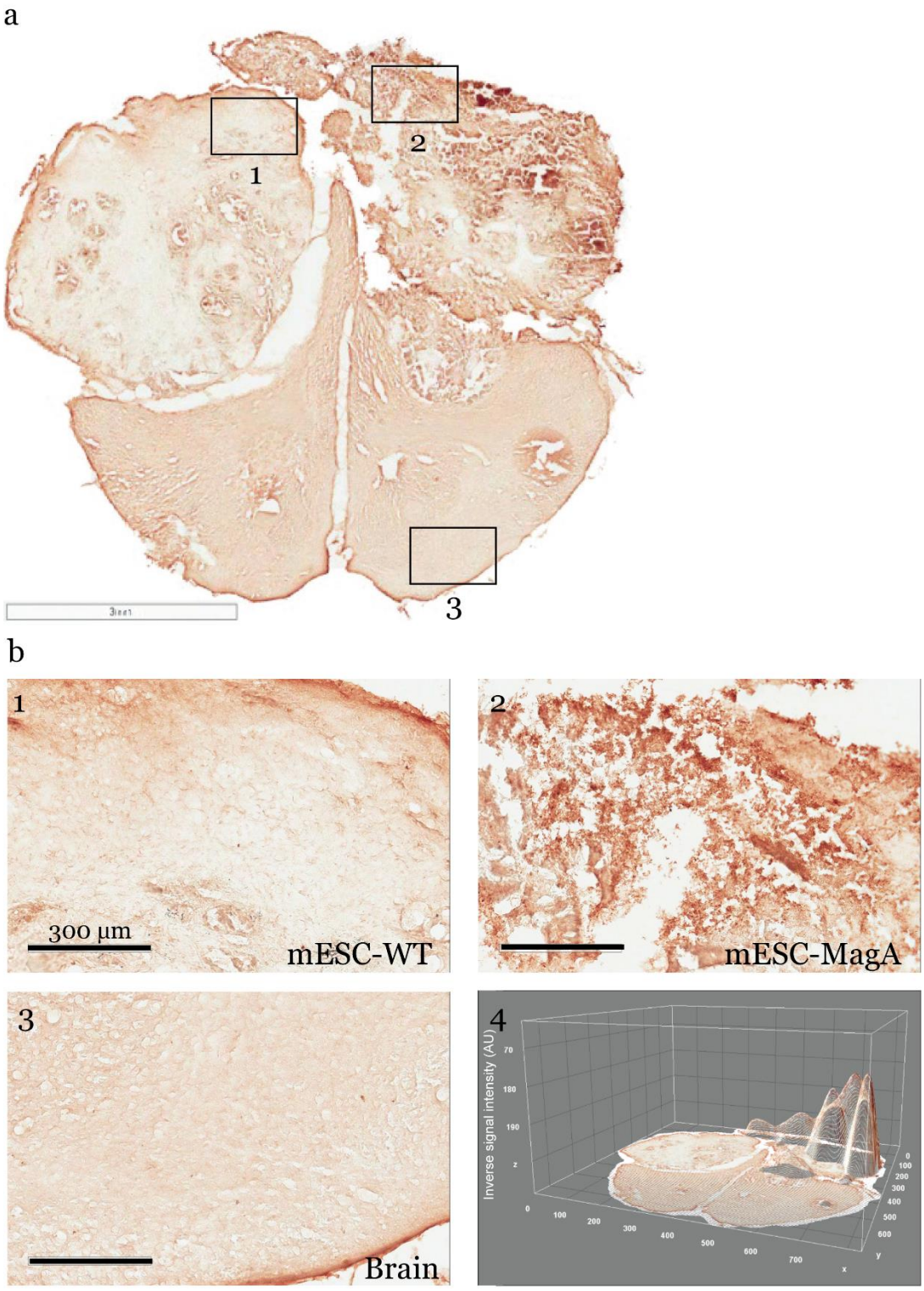

Figure 3-12. DAB staining of brain serial section. (a) Immunohistochemical DAB staining using HA antibody demonstrated MagA expression throughout mESC-MagA tumor. (b) At higher magnification, images of different brain regions (1-mESC-WT, 2-mESC-MagA, and 3-Brain) demonstrated distinct intensity, which was also revealed by three-dimensional image of the brain section.

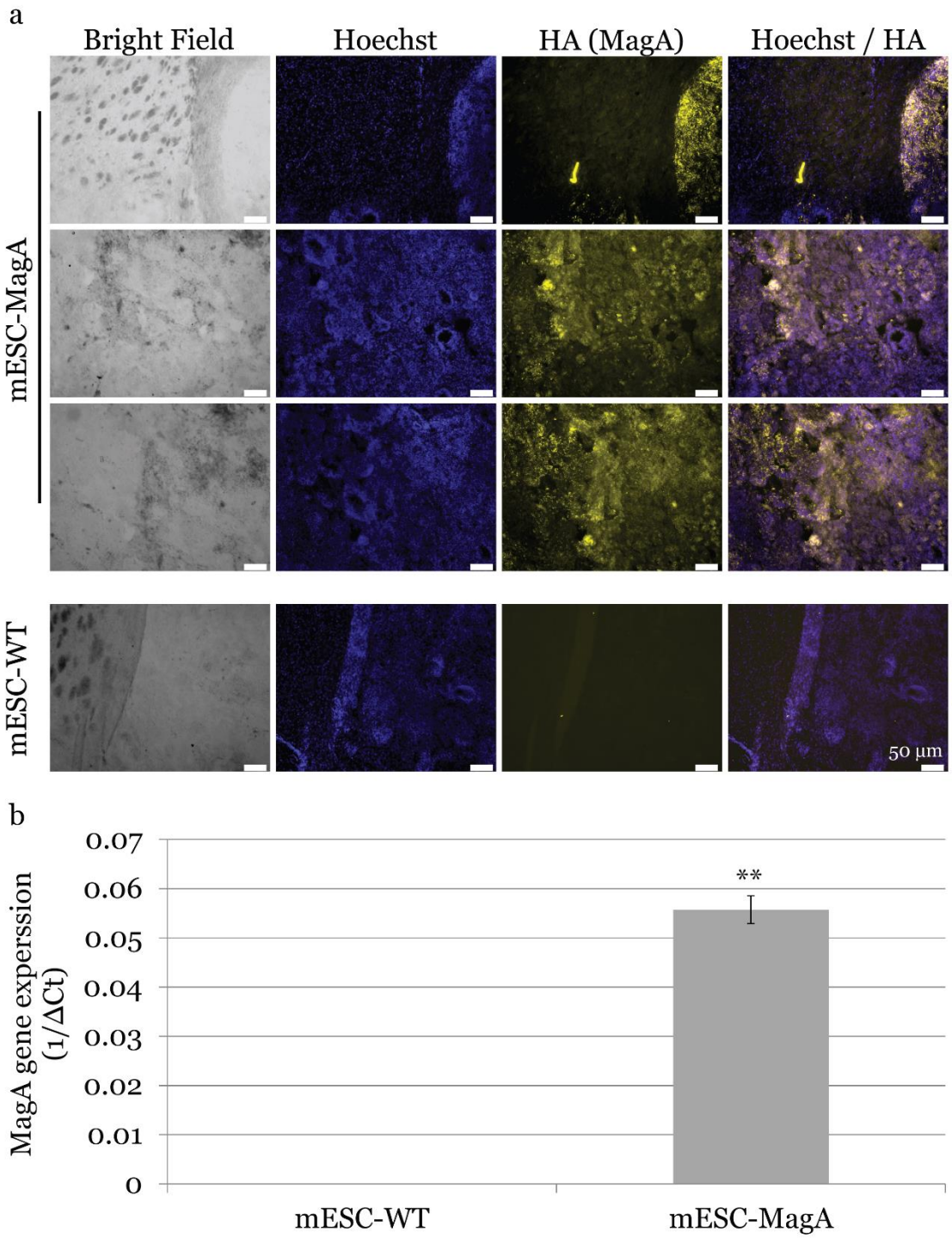

Figure 3-13. Post-mortem tissue analysis. (a) Immunofluorescence analysis using HA antibody demonstrated MagA expression in mESC-MagA derived teratoma. A clear boundary was visible, and MagA expression was only detectable in teratoma developed from mESC-MagA transplantation. (b) Quantitative real-time PCR measurement demonstrates the expression of magA seen only in teratoma developed from mESC-MagA transplantation, while there was no expression in teratoma samples developed from mESC-WT (**$P < 0.001$, $n = 4$).

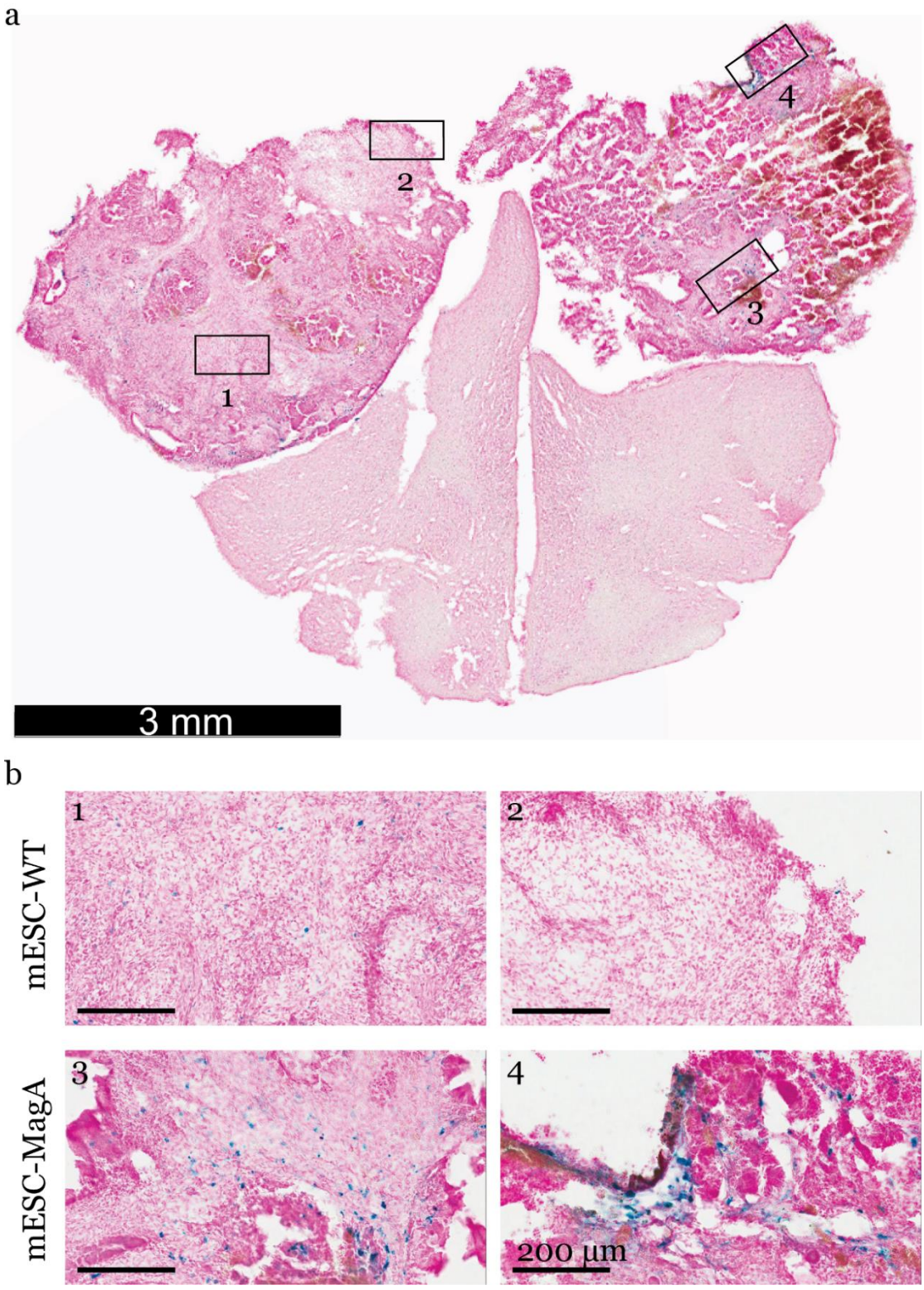

Figure 3-14. Prussian blue staining of brain section. A representative Prussian blue staining of a brain section demonstrated higher frequency of Prussian blue positive cells in mESC-MagA (3 and 4) derived teratoma compared to mESC-WT side (1 and 2).

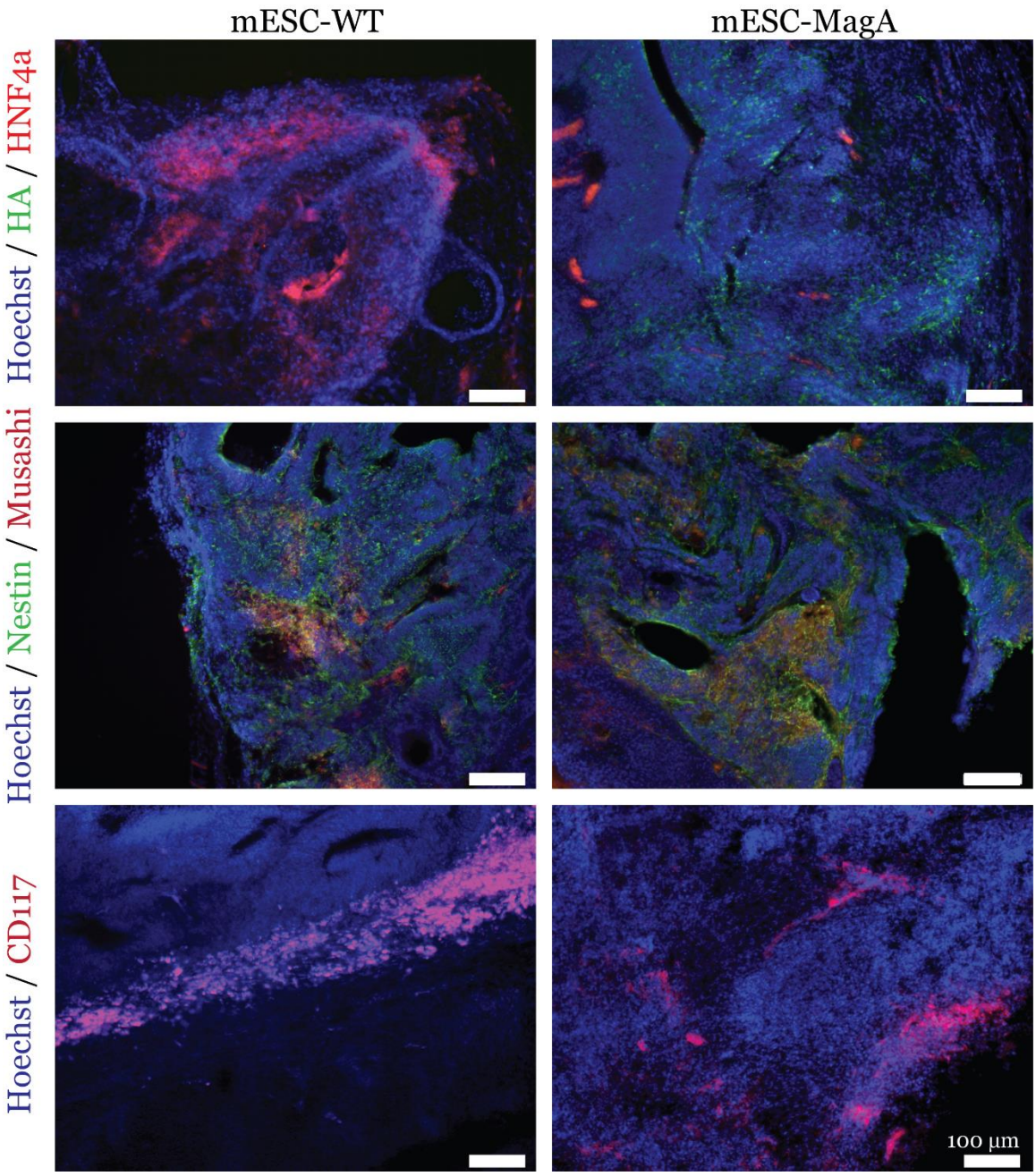

Figure 3-15. mESC-WT and mESC-MagA derived tumors were positive for lineage specific markers. Immunohistochemistry of brain sections revel positive staining of each lineage specific markers: HNF4a (mesoderm), Nestin and Musashi (ectoderm), and CD117 (endoderm). Scale bars: 100 µm.

Chapter 4

Conclusions and future direction

Part of this chapter has been accepted to be published on ***Theranostics***. Cho, I.K., Moran, S.P., Paudyal, R., Piotrowska-Nitsche, K., Cheng, P.H., Zhang, X.,

Mao, H., Chan, A.W., Longitudinal monitoring of stem cell grafts in vivo using magnetic resonance imaging with inducible MagA as a genetic reporter. 2014.

4.1 Discussion

The ability to longitudinally monitor cell grafts and assess their condition is critical for the clinical translation of stem cell therapy in regenerative medicine. Due to limitations associated with direct labeling methods, a genetic MRI reporter is needed that allows non-invasive and longitudinal monitoring of stem cell graft *in vivo*. A reliable genetically engineered MRI reporter is important especially when using large animal models in pre-clinical research. As mentioned in chapter 1, an ideal imaging reporter should satisfy several criteria: nontoxic, maintaining pluripotency, high sensitivity, signal persistency, specificity, noninvasive, longitudinal imaging, and no repetitive injection. Currently, there is no imaging reporter fulfill all of the above criteria. Enormous amount of effort have been focused on improving the existing contrast agents and developing a new reporter. Here we aim to continue our effort in developing a better genetic MRI reporter.

4.2 Summary

Our work demonstrated the use of a genetic reporter for a longitudinal MR imaging of cell grafts with the ability of controlling MR contrast “ON” and “OFF” *in vitro* and *in vivo*. There is no report on the longitudinal monitoring of stem cell grafts using a genetic MRI reporter in an inducible manner, which is critical to minimize potential toxicity of constitutive expression of the reporter. We demonstrated that MagA expressing mESC (mESC-MagA) can generate a

distinctive contrast compare to mESC-WT *in vitro*. By employing Tet-On system, the expression of MagA demonstrated positive correlation to the dosage of Dox. When MagA expression was induced, a significant decrease in cell growth and increase in cytotoxicity was observed in mESC-MagA when compared to mESC-WT. Increase in the expression of ectodermal and mesodermal lineage specific markers in mESC-MagA suggested possible impact of MagA on differentiation. Studies on SPIO also revealed impact on differentiation potential of various stem cells and progenitor cells (Kostura et al. 2004, Bulte et al. 2004, Chen et al. 2010, Chung, Hsiao, et al. 2011, Julke et al. 2013, Choi et al. 2013). Although other studies using either ferritin or transferrin receptor have demonstrated no impact on differentiation, their analysis solely rely on immunohistological analysis, and no quantitative analysis has been reported. Our results demonstrated possible impact of MagA on stem cell pluripotency by inducing ectodermal and endodermal lineage specific markers, which warrants further in depth investigation on the impacts of MagA on stem cell pluripotent potency. Our study employed inducible system which limited the expression of MagA hence minimize the potential adverse impact of the reporter. Our study have demonstrated that MagA generates MR contrast. Also, our data demonstrated increased iron content in the cells *in vitro*. The impact of increased iron content on stem cell property has not yet fully investigated and merit future in depth investigation.

In order to evaluate whether MagA and Tet-On inducible system can be utilized in tracking stem cell grafts *in vivo*, we conducted several intracranial

implantation studies to evaluate the Tet-On MagA system. Our data demonstrated that when MagA was not expressed, there was no distinctive MR contrast generated in mESC-MagA derived tumor when compared to mESC-WT grafts. However, when MagA was induced with Dox and FC, a significant hypointense signal was observed in tumors derived from mESC-MagA grafts. To determine whether grafted mESC-MagA could be longitudinally tracked *in vivo* in repetitive fashion by MRI, we conducted a series of MRI scans on mESC-MagA grafts with "ON" and "OFF" expression of MagA controlled by the administration of Dox and FC. Our data demonstrated that MR contrast was dependent on the expression of MagA. Also, post-mortem analysis confirmed the expression of MagA and increased Prussian blue positive cells in mESC-MagA derived tumors. The tumor formed from both mESC-WT and mESC-MagA demonstrated positive staining for all lineage specific markers, which indicates that the mESC-MagA can differentiate to all three germ lineages.

4.3 Limitations and future directions

Our study demonstrate that MagA can be used as a genetic MRI reporter to longitudinally monitor stem cell grafts in a repetitive fashion. The inducible nature of the construct provided additional safety. Although our study addressed few problems associated with genetic MRI reporter system, there are many more challenges that need to be addressed and improved.

Our study demonstrated the limitations of utilizing a genetic system as a MRI reporter. The major limitation associated with this and other genetic MRI reporters (e.g. ferritin) is the low sensitivity. In recent years, ferritin has become

most frequently used genetic MRI reporter (Vande Velde, Himmelreich, and Neeman 2013). Ferritin has acceptable sensitivity and reduced toxic effects of Fenton reaction (Vande Velde, Himmelreich, and Neeman 2013). A recent study described a direct comparison between ferritin and MagA, and MagA presented stronger augmentation in MR contrast than that of ferritin (Rohani et al. 2014). However, compare to exogenous contrast agents, the contrast generated from genetic MRI reporters is several magnitude lower, yet about 10 cell divisions resulted in 99% loss of signal contrast with SPIO labeling (Liu et al. 2009). Therefore, for short-term study, monitoring of differentiated cells, such as neurons or cells with a slow proliferation rate, direct labeling method could work. A single cell resolution has been achieved utilizing MION (monocrystalline iron oxide). However, with the sensitivity achieved with current genetic MRI reporters, a single cell resolution may not be achieved. Therefore, with the current sensitivity, genetic MRI reporters will find a niche in monitoring immunological rejections, tumor development, or migration of cells out of the graft site. Also, in the case of pluripotent stem cells or progenitor cells, a genetic reporter will be more suitable compare to direct labeling approach because these cells can continue to proliferate and divide asymmetrically (Walczak et al. 2007).

Our system clearly demonstrated the possibility of longitudinal monitoring of mESC grafts, which have high proliferation rate. Moreover, adverse impact of labeling cells with SPIOs including increased cytotoxicity, inhibiting migration, cell cycle aberration, and affecting differentiation potential have also been reported (Bae et al. 2011, Kostura et al. 2004, Bulte et al. 2004). We attempted to

minimize such adverse impact by employing Tet-On regulatory approach to reduce unnecessary expression and accumulation of MagA. The impact of MagA on differentiation potential of mESC has not fully addressed while the expression levels of lineage specific markers in mESC-MagA with induced MagA expression suggest possible impact of MagA on mESC differentiation. The increased level on *Nestin* observed in mESC-MagA even without induction of *magA* may be due to the low level expression of the Tet-On system which have been reported. Nonetheless, this suggest possible influence of *Nestin* or other genes expressions by the expression of *magA*. A better inducible system with tighter regulation of gene expression, such as tamoxifen inducible system, could be employed in order to further reduce the impact of MagA. While impact on differentiation was indicated, in-depth investigation of MagA expression on stem cell property is warranted due to possible impact on differentiation process after transplantation. More quantitative assays such as fluorescence-activated cell sorting (FACS) can be utilized to show correlation of MagA expression to other lineage specific markers expressions. Also, more in-depth study using larger panel of lineage specific markers can be utilized to show differentiation preference with MagA induction.

As a proof of principle, mESC was used to evaluate MagA as a MRI reporter for longitudinal monitoring of stem cell grafts. Future studies will be focused on more lineage specific cell types such as neural progenitor cells (NPC). Proper evaluations should be conducted in each cell type especially on cytotoxicity and differentiation properties. While the search for a perfect

reporting system continues, an inducible genetic reporter such as “Tet-MagA” provides a unique tool for long-term longitudinal tracking of cell grafts and their progeny cells over generations.

4.3.1 Improving sensitivity

First, more powerful MR scanner can be used to increase sensitivity. Studies using ferritin have demonstrated linear increase in contrast enhancement with the increase in field strength (Vymazal et al. 1992). Although other studies have used lower strength MR scanner such as 3T to observed MR contrast with the expression of MagA in cancer cell lines (Rohani et al. 2014, Sengupta et al. 2014), using a more powerful MR scanner might increase the sensitivity by augmenting the MR contrast. However, as a tool for research, empirical evaluation will be need to establish the correlation of field strength and MagA expression.

Second, sensitivity can be improved by expressing other genes involved in magnetosome formation. As presented in chapter 1, magnetosome formation is a multi-gene and multi-step process. MagA is just one of the genes involved in the magnetosome formation, and the expression of other gene or genes might improve the formation of magnetosome thus enhancing the sensitivity. While magnetite crystals believed to generate MR contrast, their size and shape affect the MR contrast. Other magnetosome associated genes, *mms6* and *chapA*, has also been investigated as a MRI reporter (Zhang et al. 2010, Goldhawk et al. 2012). Therefore, it would be interesting to investigate whether expressing other magnetosome associated genes can improve the MR contrast. In fact, our lab established several cell-lines expressing multiple combinations of magnetosome

associated genes, which warrants future studies utilizing this approach. Other than magnetosome associated genes, overexpressing endogenous genes such as ferritin may improve the sensitivity. The teratoma developed from the cell grafts appears to be heterogeneous. This could be due to variation in vascularization in the teratoma that affect the distribution of Dox and FC. Another possible reason for heterogeneous contrast is that some cell types may be better at facilitating MagA function and enhance MR contrast. As demonstrated with the cell pellet phantom scan, mESC-MagA cells induced a significant but smaller transverse relaxivity compared to our previous report with 293FT cells (Zurkiya, Chan, and Hu 2008). Therefore, it is reasonable to speculate that cell types may affect the formation of magnetosome and the generation of MR contrast.

Third, instead of solely relying on MagA, direct labeling methods may be utilized to enhance the sensitivity. While, the detection threshold of MagA expressing cells has yet to be determined, it is likely that the detection limit of genetic MRI reporter is much lower than that of the exogenous contrast agents. However, in case of proliferating cells, genetic reporters may be more suitable for long term tracking. Since the major limitation of direct labeling method is the continuing dilution of the contrast agent as cell continue to divide, double labeling method with both direct contrast agent and an endogenous labeling methods such as MagA may complement each other.

Fourth, following the current trend of the research, MagA can be developed as a multimodal imaging reporter. Since MagA is not endogenously expressed in mammalian cells, an antibody against MagA can be generated, and

MagA antibody conjugate with PET reporter can be investigated as MRI and PET reporter. Also, polycistronic vector expressing MagA and other fluorescence genes (GFP or RFP) can be investigated as MRI and FLI reporter. A lentiviral vector expressing RFP and MagA has been created, and a clonal cell line has been established, which warrants an immediate future experiment utilizing multimodal imaging methods.

4.3.2 Longitudinal monitoring

Due to the high proliferation rate of mESC-MagA and constraints of the mouse model described in this study, we only performed three repeated MRI scans under “ON” and “OFF” expression of MagA as a proof of principle. Considering SPIO labeled cells have been successfully used to monitor up to several months (Stuckey et al. 2006) and another report has demonstrated that tracking MagA expressing tumor cells for 34 days (Rohani et al. 2014), our study seems to come short on claiming the “longitudinal” monitoring of the stem cell grafts. Future studies using less tumorigenic and lineage-specific cell types, such as neural progenitor cells, may allow long-term longitudinal tracking of cell grafts with MRI. This will provide a better system to investigate sensitivity and the detection threshold of MagA as a genetic MRI reporter that was not addressed in this study. We have established a stable rhesus NPC cell line transduced with Tet-On MagA and are ready for future studies.

4.3.3 Other applications of MagA

Although this study has only focused on the ability of MagA as a MRI reporter for imaging cell grafts, there are other possible applications that MagA can be utilized.

One such application is utilizing MagA in the monitoring of gene expression. Similar to GFP, MagA can be placed under a specific promoter and can be used to monitor gene expression *in vivo*. Ferritin also has been used in monitoring of cell differentiation (Cohen et al. 2007). This possibility is especially exciting for translational research where larger animal models, such as pigs and non-human primates, are used for the evaluation of stem cell therapy. One possible scenario is to investigate the differentiation of NPC grafts in NHP *in vivo*. MagA can be placed under the control of neural cell promoter such as tyrosine hydroxylase promoter, and the differentiation of NPC can be monitored *in vivo* with MRI.

This study and other recently publications, have demonstrated that the expression of MagA increases iron content in cells. Additionally, the overexpression of MagA has reduced the expression of transferrin receptor similar to the overexpression of ferritin (Sengupta et al. 2014). Overexpression of ferritin increased iron deficiency cellular response and decrease expression of transferrin receptor (Sengupta et al. 2014). Therefore, MagA may provide a unique tool in studying iron overload response.

4.4 Conclusion

We have demonstrated the potential application of MagA as a genetic MRI reporter for monitoring stem cell graft in mice by using a Tet-On expression

system to control the expression of MagA, thus controlling the level of MRI contrast. With high spatial resolution and soft tissue contrast provided by MRI, MagA can potentially be developed and used for tracking stem cell graft in large animals such as NHP or porcine, in a non-invasive, longitudinal, and repetitive manner, thus allowing immediate assessment on of cell graft status and its correlation with clinical outcomes. In conclusion, our results suggested the feasibility/possibility of non-invasive, longitudinal, and repetitive monitoring of stem cell graft *in vivo* by using MRI, which is an important step for the advancement of regenerative medicine.

References

Ahrens, E. T., and J. W. Bulte. 2013. "Tracking immune cells in vivo using magnetic resonance imaging." *Nat Rev Immunol* 13 (10):755-63. doi: 10.1038/nri3531.

Ahrens, E. T., and J. Zhong. 2013. "In vivo MRI cell tracking using perfluorocarbon probes and fluorine-19 detection." *NMR Biomed* 26 (7):860-71. doi: 10.1002/nbm.2948.

Alfke, H., H. Stoppler, F. Nocken, J. T. Heverhagen, B. Kleb, F. Czubayko, and K. J. Klose. 2003. "In vitro MR imaging of regulated gene expression." *Radiology* 228 (2):488-92. doi: 10.1148/radiol.2282012006.

Altschul, S. F., W. Gish, W. Miller, E. W. Myers, and D. J. Lipman. 1990. "Basic local alignment search tool." *J Mol Biol* 215 (3):403-10. doi: 10.1016/s0022-2836(05)80360-2.

Arakaki, A., J. Webb, and T. Matsunaga. 2003. "A novel protein tightly bound to bacterial magnetic particles in Magnetospirillum magneticum strain AMB-1." *J Biol Chem* 278 (10):8745-50. doi: 10.1074/jbc.M211729200.

Arenas, E. 2002. "Stem cells in the treatment of Parkinson's disease." *Brain Res Bull* 57 (6):795-808. doi: S0361923001007729 [pii].

Arosio, P., and S. Levi. 2002. "Ferritin, iron homeostasis, and oxidative damage." *Free Radic Biol Med* 33 (4):457-63.

Artemov, D., N. Mori, B. Okollie, and Z. M. Bhujwalla. 2003. "MR molecular imaging of the Her-2/neu receptor in breast cancer cells using targeted iron oxide nanoparticles." *Magn Reson Med* 49 (3):403-8. doi: 10.1002/mrm.10406.

Au, K. W., S. Y. Liao, Y. K. Lee, W. H. Lai, K. M. Ng, Y. C. Chan, M. C. Yip, C. Y. Ho, E. X. Wu, R. A. Li, C. W. Siu, and H. F. Tse. 2009. "Effects of iron oxide nanoparticles on cardiac differentiation of embryonic stem cells." *Biochem Biophys Res Commun* 379 (4):898-903. doi: 10.1016/j.bbrc.2008.12.160.

Auricchio, A., P. D. Acton, M. Hildinger, J. P. Louboutin, K. Plossl, E. O'Connor, H. F. Kung, and J. M. Wilson. 2003. "In vivo quantitative noninvasive imaging of gene transfer by single-photon emission computerized tomography." *Hum Gene Ther* 14 (3):255-61. doi: 10.1089/10430340360535805.

Bachoud-Levi, A. C., P. Remy, J. P. Nguyen, P. Brugieres, J. P. Lefaucheur, C. Bourdet, S. Baudic, V. Gaura, P. Maison, B. Haddad, M. F. Boisse, T. Grandmougin, R. Jeny, P. Bartolomeo, G. Dalla Barba, J. D. Degos, F. Lisovoski, A. M. Ergis, E. Pailhous, P. Cesaro, P. Hantraye, and M. Peschanski. 2000. "Motor and cognitive improvements in patients with Huntington's disease after neural transplantation." *Lancet* 356 (9246):1975-9. doi: S0140673600033109 [pii].

Bae, J. E., M. I. Huh, B. K. Ryu, J. Y. Do, S. U. Jin, M. J. Moon, J. C. Jung, Y. Chang, E. Kim, S. G. Chi, G. H. Lee, and K. S. Chae. 2011. "The effect of static magnetic fields on the aggregation and cytotoxicity of magnetic nanoparticles." *Biomaterials* 32 (35):9401-14. doi: 10.1016/j.biomaterials.2011.08.075.

Bakker, E. P., I. R. Booth, U. Dinnbier, W. Epstein, and A. Gajewska. 1987. "Evidence for multiple K+ export systems in Escherichia coli." *J Bacteriol* 169 (8):3743-9.

Bar-Shir, A., G. Liu, K. W. Chan, N. Oskolkov, X. Song, N. N. Yadav, P. Walczak, M. T. McMahon, P. C. van Zijl, J. W. Bulte, and A. A. Gilad. 2014. "Human

protamine-1 as an MRI reporter gene based on chemical exchange." *ACS Chem Biol* 9 (1):134-8. doi: 10.1021/cb400617q.

Bartelle, B. B., K. U. Szulc, G. A. Suero-Abreu, J. J. Rodriguez, and D. H. Turnbull. 2012. "Divalent metal transporter, DMT1: A novel MRI reporter protein." *Magn Reson Med*. doi: 10.1002/mrm.24509.

Bazylinski, D. A., and R. B. Frankel. 2004. "Magnetosome formation in prokaryotes." *Nat Rev Microbiol* 2 (3):217-30. doi: 10.1038/nrmicro842

nrmicro842 [pii].

Bengel, F. M., M. Anton, T. Richter, M. V. Simoes, R. Haubner, J. Henke, W. Erhardt, S. Reder, T. Lehner, W. Brandau, P. Boekstegers, S. G. Nekolla, B. Gansbacher, and M. Schwaiger. 2003. "Noninvasive imaging of transgene expression by use of positron emission tomography in a pig model of myocardial gene transfer." *Circulation* 108 (17):2127-33. doi: 10.1161/01.CIR.0000091401.26280.A0.

Bengtsson, Niclas E., Gary Brown, Edward W. Scott, and Glenn A. Walter. 2010. "lacZ as a genetic reporter for real-time MRI." *Magnetic Resonance in Medicine* 63 (3):745-753. doi: 10.1002/mrm.22235.

Bernau, K., C. M. Lewis, A. M. Petelinsek, H. A. Benink, C. A. Zimprich, M. E. Meyerand, M. Suzuki, and C. N. Svendsen. 2014. "In vivo tracking of human neural progenitor cells in the rat brain using bioluminescence imaging." *J Neurosci Methods* 228:67-78. doi: 10.1016/j.jneumeth.2014.03.005.

Blaber, S. P., C. J. Hill, R. A. Webster, J. M. Say, L. J. Brown, S. C. Wang, G. Vesey, and B. R. Herbert. 2013. "Effect of labeling with iron oxide particles or nanodiamonds on the functionality of adipose-derived mesenchymal stem cells." *PLoS One* 8 (1):e52997. doi: 10.1371/journal.pone.0052997.

Blackwood, Kimberly J, Eric Sabondjian, Donna E Goldhawk, Michael S Kovacs, Gerald Wisenberg, Peter Merrifield, Frank S Prato, Janice M DeMoor, and Robert Z Stodilka. 2008. "Towards Image-Guided Stem Cell Therapy." *Progress in stem cell applications. New York: Nova Science*:153-80.

Blakemore, R. 1975. "Magnetotactic bacteria." *Science* 190 (4212):377-9.

Bohl, D., and J. M. Heard. 2004. "Tetracycline-Controlled Transactivators and Their Potential Use in Gene Therapy Applications." In *Transcription Factors*, edited by Manfred Gossen, Jörg Kaufmann and StevenJ Triezenberg, 509-533. Springer Berlin Heidelberg.

Boni, A., D. Ceratti, A. Antonelli, C. Sfara, M. Magnani, E. Manuali, S. Salamida, A. Gozzi, and A. Bifone. 2014. "USPIO-loaded red blood cells as a biomimetic MR contrast agent: a relaxometric study." *Contrast Media Mol Imaging* 9 (3):229-36. doi: 10.1002/cmmi.1562.

Brenner, W., A. Aicher, T. Eckey, S. Massoudi, M. Zuhayra, U. Koehl, C. Heeschen, W. U. Kampen, A. M. Zeiher, S. Dimmeler, and E. Henze. 2004. "111In-labeled CD34+ hematopoietic progenitor cells in a rat myocardial infarction model." *J Nucl Med* 45 (3):512-8.

Brustle, O., K. N. Jones, R. D. Learish, K. Karram, K. Choudhary, O. D. Wiestler, I. D. Duncan, and R. D. McKay. 1999. "Embryonic stem cell-derived glial precursors: a source of myelinating transplants." *Science* 285 (5428):754-6.

Bulte, J. W., T. Douglas, B. Witwer, S. C. Zhang, E. Strable, B. K. Lewis, H. Zywicke, B. Miller, P. van Gelderen, B. M. Moskowitz, I. D. Duncan, and J. A. Frank.

2001. "Magnetodendrimers allow endosomal magnetic labeling and in vivo tracking of stem cells." *Nat Biotechnol* 19 (12):1141-7. doi: 10.1038/nbt1201-1141

nbt1201-1141 [pii].

Bulte, J. W., D. L. Kraitchman, A. M. Mackay, and M. F. Pittenger. 2004. "Chondrogenic differentiation of mesenchymal stem cells is inhibited after magnetic labeling with ferumoxides." *Blood* 104 (10):3410-2; author reply 3412-3. doi: 10.1182/blood-2004-06-2117.

Bulte, J. W., S. Zhang, P. van Gelderen, V. Herynek, E. K. Jordan, I. D. Duncan, and J. A. Frank. 1999. "Neurotransplantation of magnetically labeled oligodendrocyte progenitors: magnetic resonance tracking of cell migration and myelination." *Proc Natl Acad Sci U S A* 96 (26):15256-61.

Campan, M., V. Lionetti, G. D. Aquaro, F. Forini, M. Matteucci, L. Vannucci, F. Chiuppesi, C. Di Cristofano, M. Faggioni, M. Maioli, L. Barile, E. Messina, M. Lombardi, A. Pucci, M. Pistello, and F. A. Recchia. 2011. "Ferritin as a reporter gene for in vivo tracking of stem cells by 1.5-T cardiac MRI in a rat model of myocardial infarction." *Am J Physiol Heart Circ Physiol* 300 (6):H2238-50. doi: 10.1152/ajpheart.00935.2010.

Carter, R. L., and A. W. Chan. 2012. "Pluripotent stem cells models for Huntington's disease: prospects and challenges." *J Genet Genomics* 39 (6):253-9. doi: 10.1016/j.jgg.2012.04.006.

Casadaban, M. J., J. Chou, and S. N. Cohen. 1980. "In vitro gene fusions that join an enzymatically active beta-galactosidase segment to amino-terminal fragments of exogenous proteins: Escherichia coli plasmid vectors for the detection and cloning of translational initiation signals." *J Bacteriol* 143 (2):971-80.

Chalfie, M., Y. Tu, G. Euskirchen, W. W. Ward, and D. C. Prasher. 1994. "Green fluorescent protein as a marker for gene expression." *Science* 263 (5148):802-5.

Chen, Y. C., J. K. Hsiao, H. M. Liu, I. Y. Lai, M. Yao, S. C. Hsu, B. S. Ko, Y. C. Chen, C. S. Yang, and D. M. Huang. 2010. "The inhibitory effect of superparamagnetic iron oxide nanoparticle (Ferucarbotran) on osteogenic differentiation and its signaling mechanism in human mesenchymal stem cells." *Toxicol Appl Pharmacol* 245 (2):272-9. doi: 10.1016/j.taap.2010.03.011.

Chen, Y., R. L. Carter, I. K. Cho, and A. W. Chan. 2014. "Cell-based therapies for Huntington's disease." *Drug Discov Today*. doi: 10.1016/j.drudis.2014.02.012.

Choi, J. I., H. T. Cho, M. K. Jee, and S. K. Kang. 2013. "Core-shell nanoparticle controlled hATSCs neurogenesis for neuropathic pain therapy." *Biomaterials* 34 (21):4956-70. doi: 10.1016/j.biomaterials.2013.02.037.

Chuang, K. H., H. E. Wang, T. C. Cheng, S. C. Tzou, W. L. Tseng, W. C. Hung, M. H. Tai, T. K. Chang, S. R. Roffler, and T. L. Cheng. 2010. "Development of a universal anti-polyethylene glycol reporter gene for noninvasive imaging of PEGylated probes." *J Nucl Med* 51 (6):933-41. doi: 10.2967/jnumed.109.071977.

Chung, Jaehoon, Kehkooi Kee, Joëlle K. Barral, Rajesh Dash, Hisanori Kosuge, Xi Wang, Irving Weissman, Robert C. Robbins, Dwight Nishimura, Thomas Quertermous, Renee A. Reijo-Pera, and Phillip C. Yang. 2011. "In vivo molecular MRI of cell survival and teratoma formation following embryonic stem cell

transplantation into the injured murine myocardium." *Magnetic Resonance in Medicine* 66 (5):1374-1381. doi: 10.1002/mrm.22929.

Chung, T. H., J. K. Hsiao, S. C. Hsu, M. Yao, Y. C. Chen, S. W. Wang, M. Y. Kuo, C. S. Yang, and D. M. Huang. 2011. "Iron oxide nanoparticle-induced epidermal growth factor receptor expression in human stem cells for tumor therapy." *ACS Nano* 5 (12):9807-16. doi: 10.1021/nn2033902.

Chung, Y. G., J. H. Eum, J. E. Lee, S. H. Shim, V. Sepilian, S. W. Hong, Y. Lee, N. R. Treff, Y. H. Choi, E. A. Kimbrel, R. E. Dittman, R. Lanza, and D. R. Lee. 2014. "Human Somatic Cell Nuclear Transfer Using Adult Cells." *Cell Stem Cell*. doi: 10.1016/j.stem.2014.03.015.

Cohen, B., H. Dafni, G. Meir, A. Harmelin, and M. Neeman. 2005. "Ferritin as an endogenous MRI reporter for noninvasive imaging of gene expression in C6 glioma tumors." *Neoplasia* 7 (2):109-17. doi: 10.1593/neo.04436.

Cohen, B., K. Ziv, V. Plaks, T. Israely, V. Kalchenko, A. Harmelin, L. E. Benjamin, and M. Neeman. 2007. "MRI detection of transcriptional regulation of gene expression in transgenic mice." *Nat Med* 13 (4):498-503. doi: 10.1038/nm1497.

Contag, C. H., S. D. Spilman, P. R. Contag, M. Oshiro, B. Eames, P. Dennery, D. K. Stevenson, and D. A. Benaron. 1997. "Visualizing gene expression in living mammals using a bioluminescent reporter." *Photochem Photobiol* 66 (4):523-31.

Couillard-Despres, S., R. Vreys, L. Aigner, and A. Van der Linden. 2011. "In vivo monitoring of adult neurogenesis in health and disease." *Front Neurosci* 5:67. doi: 10.3389/fnins.2011.00067.

Cozzi, A., B. Corsi, S. Levi, P. Santambrogio, A. Albertini, and P. Arosio. 2000. "Overexpression of wild type and mutated human ferritin H-chain in HeLa cells: in vivo role of ferritin ferroxidase activity." *J Biol Chem* 275 (33):25122-9. doi: 10.1074/jbc.M003797200.

Cui, W., S. Tavri, M. J. Benchimol, M. Itani, E. S. Olson, H. Zhang, M. Decyk, R. G. Ramirez, C. V. Barback, Y. Kono, and R. F. Mattrey. 2013. "Neural progenitor cells labeling with microbubble contrast agent for ultrasound imaging in vivo." *Biomaterials* 34 (21):4926-35. doi: 10.1016/j.biomaterials.2013.03.020.

Davis, R. L., H. Weintraub, and A. B. Lassar. 1987. "Expression of a single transfected cDNA converts fibroblasts to myoblasts." *Cell* 51 (6):987-1000.

de Lazaro, I., A. Yilmazer, and K. Kostarelos. 2014. "Induced pluripotent stem (iPS) cells: A new source for cell-based therapeutics?" *J Control Release* 185C:37-44. doi: 10.1016/j.jconrel.2014.04.011.

Deda, H., M. C. Inci, A. E. Kurekci, A. Sav, K. Kayihan, E. Ozgun, G. E. Ustunsoy, and S. Kocabay. 2009. "Treatment of amyotrophic lateral sclerosis patients by autologous bone marrow-derived hematopoietic stem cell transplantation: a 1-year follow-up." *Cytotherapy* 11 (1):18-25. doi: 10.1080/14653240802549470.

Dubbels, B. L., A. A. DiSpirito, J. D. Morton, J. D. Semrau, J. N. Neto, and D. A. Bazylinski. 2004. "Evidence for a copper-dependent iron transport system in the marine, magnetotactic bacterium strain MV-1." *Microbiology* 150 (Pt 9):2931-45. doi: 10.1099/mic.0.27233-0.

Evans, M. J., and M. H. Kaufman. 1981. "Establishment in culture of pluripotential cells from mouse embryos." *Nature* 292 (5819):154-6.

Faivre, D., and D. Schuler. 2008. "Magnetotactic bacteria and magnetosomes." *Chem Rev* 108 (11):4875-98. doi: 10.1021/cr078258w.

Feng, Y., Q. Liu, J. Zhu, F. Xie, and L. Li. 2012. "Efficiency of ferritin as an MRI reporter gene in NPC cells is enhanced by iron supplementation." *J Biomed Biotechnol* 2012:434878. doi: 10.1155/2012/434878.

Frangioni, J. V. 2003. "In vivo near-infrared fluorescence imaging." *Curr Opin Chem Biol* 7 (5):626-34.

Frangioni, J. V., and R. J. Hajjar. 2004. "In vivo tracking of stem cells for clinical trials in cardiovascular disease." *Circulation* 110 (21):3378-83. doi: 10.1161/01.CIR.0000149840.46523.FC.

Frankel, R. B., and D. A. Bazylinski. 2009. "Magnetosomes and magneto-aerotaxis." *Contrib Microbiol* 16:182-93. doi: 10.1159/000219380.

Frey, P. A., and G. H. Reed. 2012. "The ubiquity of iron." *ACS Chem Biol* 7 (9):1477-81. doi: 10.1021/cb300323q.

Fukuda, Y., Y. Okamura, H. Takeyama, and T. Matsunaga. 2006. "Dynamic analysis of a genomic island in Magnetospirillum sp. strain AMB-1 reveals how magnetosome synthesis developed." *FEBS Lett* 580 (3):801-12. doi: 10.1016/j.febslet.2006.01.003.

Furth, P. A., L. St Onge, H. Boger, P. Gruss, M. Gossen, A. Kistner, H. Bujard, and L. Hennighausen. 1994. "Temporal control of gene expression in transgenic mice by a tetracycline-responsive promoter." *Proc Natl Acad Sci U S A* 91 (20):9302-6.

Genove, G., U. DeMarco, H. Xu, W. F. Goins, and E. T. Ahrens. 2005. "A new transgene reporter for in vivo magnetic resonance imaging." *Nat Med* 11 (4):450-4. doi: 10.1038/nm1208.

Gilad, A. A., M. T. McMahon, P. Walczak, P. T. Winnard, Jr., V. Raman, H. W. van Laarhoven, C. M. Skoglund, J. W. Bulte, and P. C. van Zijl. 2007. "Artificial reporter gene providing MRI contrast based on proton exchange." *Nat Biotechnol* 25 (2):217-9. doi: 10.1038/nbt1277.

Gilad, A. A., K. Ziv, M. T. McMahon, P. C. van Zijl, M. Neeman, and J. W. Bulte. 2008. "MRI reporter genes." *J Nucl Med* 49 (12):1905-8. doi: 10.2967/jnumed.108.053520.

Gildehaus, F. J., F. Haasters, I. Drosse, E. Wagner, C. Zach, W. Mutschler, P. Cumming, P. Bartenstein, and M. Schieker. 2011. "Impact of indium-111 oxine labelling on viability of human mesenchymal stem cells in vitro, and 3D cell-tracking using SPECT/CT in vivo." *Mol Imaging Biol* 13 (6):1204-14. doi: 10.1007/s11307-010-0439-1.

Goldhawk, D. E., C. Lemaire, C. R. McCreary, R. McGirr, S. Dhanvantari, R. T. Thompson, R. Figueredo, J. Koropatnick, P. Foster, and F. S. Prato. 2009. "Magnetic resonance imaging of cells overexpressing MagA, an endogenous contrast agent for live cell imaging." *Mol Imaging* 8 (3):129-39.

Goldhawk, D. E., R. Rohani, A. Sengupta, N. Gelman, and F. S. Prato. 2012. "Using the magnetosome to model effective gene-based contrast for magnetic resonance imaging." *Wiley Interdiscip Rev Nanomed Nanobiotechnol* 4 (4):378-88. doi: 10.1002/wnan.1165.

Guex, N., and M. C. Peitsch. 1997. "SWISS-MODEL and the Swiss-PdbViewer: an environment for comparative protein modeling." *Electrophoresis* 18 (15):2714-23. doi: 10.1002/elps.1150181505.

Haeckel, Ernst. 1868. Natürliche Schöpfungsgeschichte. In *Natürliche Schöpfungsgeschichte*. Berilin: Georg Reimer.

Heyn, C., J. A. Ronald, L. T. Mackenzie, I. C. MacDonald, A. F. Chambers, B. K. Rutt, and P. J. Foster. 2006. "In vivo magnetic resonance imaging of single cells in mouse brain with optical validation." *Magn Reson Med* 55 (1):23-9. doi: 10.1002/mrm.20747.

Hitchens, T. K., L. Liu, L. M. Foley, V. Simplaceanu, E. T. Ahrens, and C. Ho. 2014. "Combining perfluorocarbon and superparamagnetic iron-oxide cell labeling for improved and expanded applications of cellular MRI." *Magn Reson Med*. doi: 10.1002/mrm.25120.

Huang, M., R. K. Batra, T. Kogai, Y. Q. Lin, J. M. Hershman, A. Lichtenstein, S. Sharma, L. X. Zhu, G. A. Brent, and S. M. Dubinett. 2001. "Ectopic expression of the thyroperoxidase gene augments radioiodide uptake and retention mediated by the sodium iodide symporter in non-small cell lung cancer." *Cancer Gene Ther* 8 (8):612-8. doi: 10.1038/sj.cgt.7700354.

Hwang do, W., J. H. Kang, J. M. Jeong, J. K. Chung, M. C. Lee, S. Kim, and D. S. Lee. 2008. "Noninvasive in vivo monitoring of neuronal differentiation using reporter driven by a neuronal promoter." *Eur J Nucl Med Mol Imaging* 35 (1):135-45. doi: 10.1007/s00259-007-0561-8.

Jha, P., D. Golovko, S. Bains, D. Hostetter, R. Meier, M. F. Wendland, and H. E. Daldrup-Link. 2010. "Monitoring of natural killer cell immunotherapy using noninvasive imaging modalities." *Cancer Res* 70 (15):6109-13. doi: 10.1158/0008-5472.CAN-09-3774.

Jiang, H., Z. Cheng, M. Tian, and H. Zhang. 2011. "In vivo imaging of embryonic stem cell therapy." *Eur J Nucl Med Mol Imaging* 38 (4):774-84. doi: 10.1007/s00259-010-1667-y.

Jin, Y., H. Kong, R. Z. Stodilka, R. G. Wells, P. Zabel, P. A. Merrifield, J. Sykes, and F. S. Prato. 2005. "Determining the minimum number of detectable cardiac-transplanted 111In-tropolone-labelled bone-marrow-derived mesenchymal stem cells by SPECT." *Phys Med Biol* 50 (19):4445-55. doi: 10.1088/0031-9155/50/19/001.

Julke, H., C. Veit, I. Ribitsch, W. Brehm, E. Ludewig, and U. Delling. 2013. "Comparative labelling of equine and ovine multipotent stromal cells with superparamagnetic iron oxide particles for magnetic resonance imaging in vitro." *Cell Transplant*. doi: 10.3727/096368913X675737.

Kaur, D., S. Rajagopalan, and J. K. Andersen. 2009. "Chronic expression of H-ferritin in dopaminergic midbrain neurons results in an age-related expansion of the labile iron pool and subsequent neurodegeneration: implications for Parkinson's disease." *Brain Res* 1297:17-22. doi: 10.1016/j.brainres.2009.08.043.

Kaur, D., S. Rajagopalan, S. Chinta, J. Kumar, D. Di Monte, R. A. Cherny, and J. K. Andersen. 2007. "Chronic ferritin expression within murine dopaminergic midbrain neurons results in a progressive age-related neurodegeneration." *Brain Res* 1140:188-94. doi: 10.1016/j.brainres.2006.03.006.

Kedziorek, D. A., M. Solaiyappan, P. Walczak, T. Ehtiati, Y. Fu, J. W. Bulte, S. M. Shea, A. Brost, F. K. Wacker, and D. L. Kraitchman. 2013. "Using C-arm x-ray imaging to guide local reporter probe delivery for tracking stem cell engraftment." *Theranostics* 3 (11):916-26. doi: 10.7150/thno.6943.

Kehrer, J. P. 2000. "The Haber-Weiss reaction and mechanisms of toxicity." *Toxicology* 149 (1):43-50.

Kelley, L. A., and M. J. Sternberg. 2009. "Protein structure prediction on the Web: a case study using the Phyre server." *Nat Protoc* 4 (3):363-71. doi: 10.1038/nprot.2009.2.

Kim, Y. H., D. S. Lee, J. H. Kang, Y. J. Lee, J. K. Chung, J. K. Roh, S. U. Kim, and M. C. Lee. 2005. "Reversing the silencing of reporter sodium/iodide symporter transgene for stem cell tracking." *J Nucl Med* 46 (2):305-11.

Kircher, M. F., J. R. Allport, E. E. Graves, V. Love, L. Josephson, A. H. Lichtman, and R. Weissleder. 2003. "In vivo high resolution three-dimensional imaging of antigen-specific cytotoxic T-lymphocyte trafficking to tumors." *Cancer Res* 63 (20):6838-46.

Kircher, M. F., S. S. Gambhir, and J. Grimm. 2011. "Noninvasive cell-tracking methods." *Nat Rev Clin Oncol* 8 (11):677-88. doi: 10.1038/nrclinonc.2011.141.

Klibanov, A. L., P. T. Rasche, M. S. Hughes, J. K. Wojdyla, K. P. Galen, J. H. Wible, Jr., and G. H. Brandenburger. 2004. "Detection of individual microbubbles of ultrasound contrast agents: imaging of free-floating and targeted bubbles." *Invest Radiol* 39 (3):187-95.

Kolinko, I., A. Lohsse, S. Borg, O. Raschdorf, C. Jogler, Q. Tu, M. Posfai, E. Tompa, J. M. Plitzko, A. Brachmann, G. Wanner, R. Muller, Y. Zhang, and D. Schuler. 2014. "Biosynthesis of magnetic nanostructures in a foreign organism by transfer of bacterial magnetosome gene clusters." *Nat Nanotechnol* 9 (3):193-7. doi: 10.1038/nnano.2014.13.

Komeili, A., Z. Li, D. K. Newman, and G. J. Jensen. 2006. "Magnetosomes are cell membrane invaginations organized by the actin-like protein MamK." *Science* 311 (5758):242-5. doi: 10.1126/science.1123231.

Koretsky, ALYJ, YJ Lin, H Schorle, and R Jaenisch. 1996. "Genetic control of MRI contrast by expression of the transferrin receptor." Proceedings of the International Society of Magnetic Resonance Medicine.

Kostura, L., D. L. Kraitchman, A. M. Mackay, M. F. Pittenger, and J. W. Bulte. 2004. "Feridex labeling of mesenchymal stem cells inhibits chondrogenesis but not adipogenesis or osteogenesis." *NMR Biomed* 17 (7):513-7. doi: 10.1002/nbm.925.

Lang, C., S. Lehner, A. Todica, G. Boening, W. M. Franz, P. Bartenstein, M. Hacker, and R. David. 2013. "Positron emission tomography based in-vivo imaging of early phase stem cell retention after intramyocardial delivery in the mouse model." *Eur J Nucl Med Mol Imaging* 40 (11):1730-8. doi: 10.1007/s00259-013-2480-1.

Lee, K. H., S. S. Byun, J. Y. Paik, S. Y. Lee, S. H. Song, Y. S. Choe, and B. T. Kim. 2003. "Cell uptake and tissue distribution of radioiodine labelled D-luciferin: implications for luciferase based gene imaging." *Nucl Med Commun* 24 (9):1003-9. doi: 10.1097/01.mnm.0000090431.24184.49.

Lee, R. H., M. J. Seo, R. L. Reger, J. L. Spees, A. A. Pulin, S. D. Olson, and D. J. Prockop. 2006. "Multipotent stromal cells from human marrow home to and

promote repair of pancreatic islets and renal glomeruli in diabetic NOD/scid mice." *Proc Natl Acad Sci U S A* 103 (46):17438-43. doi: 0608249103 [pii]

10.1073/pnas.0608249103.

Lefevre, C. T., D. Trubitsyn, F. Abreu, S. Kolinko, C. Jogler, L. G. de Almeida, A. T. de Vasconcelos, M. Kube, R. Reinhardt, U. Lins, D. Pignol, D. Schuler, D. A. Bazylinski, and N. Ginet. 2013. "Comparative genomic analysis of magnetotactic bacteria from the Deltaproteobacteria provides new insights into magnetite and greigite magnetosome genes required for magnetotaxis." *Environ Microbiol* 15 (10):2712-35. doi: 10.1111/1462-2920.12128.

Lewin, M., N. Carlesso, C. H. Tung, X. W. Tang, D. Cory, D. T. Scadden, and R. Weissleder. 2000. "Tat peptide-derivatized magnetic nanoparticles allow in vivo tracking and recovery of progenitor cells." *Nat Biotechnol* 18 (4):410-4. doi: 10.1038/74464.

Li, S. C., L. M. Tachiki, J. Luo, B. A. Dethlefs, Z. Chen, and W. G. Loudon. 2010. "A biological global positioning system: considerations for tracking stem cell behaviors in the whole body." *Stem Cell Rev* 6 (2):317-33. doi: 10.1007/s12015-010-9130-9.

Li, Y., S. Bali, S. Borg, E. Katzmann, S. J. Ferguson, and D. Schuler. 2013. "Cytochrome cd1 nitrite reductase NirS is involved in anaerobic magnetite biomineralization in Magnetospirillum gryphiswaldense and requires NirN for proper d1 heme assembly." *J Bacteriol* 195 (18):4297-309. doi: 10.1128/jb.00686-13.

Li, Y., E. Katzmann, S. Borg, and D. Schuler. 2012. "The periplasmic nitrate reductase nap is required for anaerobic growth and involved in redox control of magnetite biomineralization in Magnetospirillum gryphiswaldense." *J Bacteriol* 194 (18):4847-56. doi: 10.1128/jb.00903-12.

Liu, J., E. C. Cheng, R. C. Long, S. H. Yang, L. Wang, P. H. Cheng, J. Yang, D. Wu, H. Mao, and A. W. Chan. 2009. "Noninvasive monitoring of embryonic stem cells in vivo with MRI transgene reporter." *Tissue Eng Part C Methods* 15 (4):739-47. doi: 10.1089/ten.TEC.2008.0678.

Liu, Jun. 2009. "Ferritin as a Transgenic MRI Reporter in Mouse Embryonic Stem Cells." Ph.D., Biological and Biomedical Sciences Emory University.

Louie, A. Y., M. M. Huber, E. T. Ahrens, U. Rothbacher, R. Moats, R. E. Jacobs, S. E. Fraser, and T. J. Meade. 2000. "In vivo visualization of gene expression using magnetic resonance imaging." *Nat Biotechnol* 18 (3):321-5. doi: 10.1038/73780.

Ma, L., B. Hu, Y. Liu, S. C. Vermilyea, H. Liu, L. Gao, Y. Sun, X. Zhang, and S. C. Zhang. 2012. "Human embryonic stem cell-derived GABA neurons correct locomotion deficits in quinolinic acid-lesioned mice." *Cell Stem Cell* 10 (4):455-64. doi: 10.1016/j.stem.2012.01.021.

Ma, Y., A. Ramezani, R. Lewis, R. G. Hawley, and J. A. Thomson. 2003. "High-level sustained transgene expression in human embryonic stem cells using lentiviral vectors." *Stem Cells* 21 (1):111-7. doi: 10.1634/stemcells.21-1-111.

Marchler-Bauer, A., C. Zheng, F. Chitsaz, M. K. Derbyshire, L. Y. Geer, R. C. Geer, N. R. Gonzales, M. Gwadz, D. I. Hurwitz, C. J. Lanczycki, F. Lu, S. Lu, G. H. Marchler, J. S. Song, N. Thanki, R. A. Yamashita, D. Zhang, and S. H. Bryant. 2013. "CDD: conserved domains and protein three-dimensional structure." *Nucleic Acids Res* 41 (Database issue):D348-52. doi: 10.1093/nar/gks1243.

Martin, G. R. 1981. "Isolation of a pluripotent cell line from early mouse embryos cultured in medium conditioned by teratocarcinoma stem cells." *Proc Natl Acad Sci U S A* 78 (12):7634-8.

Matsunaga, T., C. Nakamura, J. G. Burgess, and K. Sode. 1992. "Gene transfer in magnetic bacteria: transposon mutagenesis and cloning of genomic DNA fragments required for magnetosome synthesis." *J Bacteriol* 174 (9):2748-53.

Mempel, T. R., M. J. Pittet, K. Khazaie, W. Weninger, R. Weissleder, H. von Boehmer, and U. H. von Andrian. 2006. "Regulatory T cells reversibly suppress cytotoxic T cell function independent of effector differentiation." *Immunity* 25 (1):129-41. doi: 10.1016/j.immuni.2006.04.015.

Moats, Rex A., Scott E. Fraser, and Thomas J. Meade. 1997. "A "Smart" Magnetic Resonance Imaging Agent That Reports on Specific Enzymatic Activity." *Angewandte Chemie International Edition in English* 36 (7):726-728. doi: 10.1002/anie.199707261.

Moore, A., J. P. Basilion, E. A. Chiocca, and R. Weissleder. 1998. "Measuring transferrin receptor gene expression by NMR imaging." *Biochim Biophys Acta* 1402 (3):239-49. doi: S0167-4889(98)00002-0 [pii].

Moroz, M. A., I. Serganova, P. Zanzonico, L. Ageyeva, T. Beresten, E. Dyomina, E. Burnazi, R. D. Finn, M. Doubrovin, and R. G. Blasberg. 2007. "Imaging hNET reporter gene expression with 124I-MIBG." *J Nucl Med* 48 (5):827-36. doi: 10.2967/jnumed.106.037812.

Murat, D., A. Quinlan, H. Vali, and A. Komeili. 2010. "Comprehensive genetic dissection of the magnetosome gene island reveals the step-wise assembly of a prokaryotic organelle." *Proc Natl Acad Sci U S A* 107 (12):5593-8. doi: 10.1073/pnas.0914439107.

Nakamura, C., J. G. Burgess, K. Sode, and T. Matsunaga. 1995. "An iron-regulated gene, magA, encoding an iron transport protein of Magnetospirillum sp. strain AMB-1." *J Biol Chem* 270 (47):28392-6.

Nakamura, C., T. Kikuchi, J. G. Burgess, and T. Matsunaga. 1995. "Iron-regulated expression and membrane localization of the magA protein in Magnetospirillum sp. strain AMB-1." *J Biochem* 118 (1):23-7.

Narsinh, K. H., J. Plews, and J. C. Wu. 2011. "Comparison of human induced pluripotent and embryonic stem cells: fraternal or identical twins?" *Mol Ther* 19 (4):635-8. doi: 10.1038/mt.2011.41.

Naumova, A. V., H. Reinecke, V. Yarnykh, J. Deem, C. Yuan, and C. E. Murry. 2010. "Ferritin overexpression for noninvasive magnetic resonance imaging-based tracking of stem cells transplanted into the heart." *Mol Imaging* 9 (4):201-10.

Neri, M., C. Maderna, C. Cavazzin, V. Deidda-Vigoriti, L. S. Politi, G. Scotti, P. Marzola, A. Sbarbati, A. L. Vescovi, and A. Gritti. 2008. "Efficient in vitro labeling of human neural precursor cells with superparamagnetic iron oxide particles: relevance for in vivo cell tracking." *Stem Cells* 26 (2):505-16. doi: 10.1634/stemcells.2007-0251.

Ntziachristos, V., C. Bremer, E. E. Graves, J. Ripoll, and R. Weissleder. 2002. "In vivo tomographic imaging of near-infrared fluorescent probes." *Mol Imaging* 1 (2):82-8.

Ntziachristos, V., C. Bremer, and R. Weissleder. 2003. "Fluorescence imaging with near-infrared light: new technological advances that enable in vivo molecular imaging." *Eur Radiol* 13 (1):195-208. doi: 10.1007/s00330-002-1524-x.

Oh, H. J., W. Hwang do, H. Youn, and D. S. Lee. 2013. "In vivo bioluminescence reporter gene imaging for the activation of neuronal differentiation induced by the neuronal activator neurogenin 1 (Ngn1) in neuronal precursor cells." *Eur J Nucl Med Mol Imaging* 40 (10):1607-17. doi: 10.1007/s00259-013-2457-0.

Park, S., E. Y. Kim, G. S. Ghil, W. S. Joo, K. C. Wang, Y. S. Kim, Y. J. Lee, and J. Lim. 2003. "Genetically modified human embryonic stem cells relieve symptomatic motor behavior in a rat model of Parkinson's disease." *Neurosci Lett* 353 (2):91-4. doi: S0304394003010826 [pii].

Patel, D., A. Kell, B. Simard, J. Deng, B. Xiang, H. Y. Lin, M. Gruwel, and G. Tian. 2010. "Cu2+-labeled, SPION loaded porous silica nanoparticles for cell labeling and multifunctional imaging probes." *Biomaterials* 31 (10):2866-73. doi: 10.1016/j.biomaterials.2009.12.025.

Pfeifer, A., M. Ikawa, Y. Dayn, and I. M. Verma. 2002. "Transgenesis by lentiviral vectors: lack of gene silencing in mammalian embryonic stem cells and preimplantation embryos." *Proc Natl Acad Sci U S A* 99 (4):2140-5. doi: 10.1073/pnas.251682798.

Picard, V., F. Renaudie, C. Porcher, M. W. Hentze, B. Grandchamp, and C. Beaumont. 1996. "Overexpression of the ferritin H subunit in cultured erythroid cells changes the intracellular iron distribution." *Blood* 87 (5):2057-64.

Ponomarev, V., M. Doubrovin, I. Serganova, J. Vider, A. Shavrin, T. Beresten, A. Ivanova, L. Ageyeva, V. Tourkova, J. Balatoni, W. Bornmann, R. Blasberg, and J. Gelovani Tjuvajev. 2004. "A novel triple-modality reporter gene for whole-body fluorescent, bioluminescent, and nuclear noninvasive imaging." *Eur J Nucl Med Mol Imaging* 31 (5):740-51. doi: 10.1007/s00259-003-1441-5.

Qin, C., K. Cheng, K. Chen, X. Hu, Y. Liu, X. Lan, Y. Zhang, H. Liu, Y. Xu, L. Bu, X. Su, X. Zhu, S. Meng, and Z. Cheng. 2013. "Tyrosinase as a multifunctional reporter gene for Photoacoustic/MRI/PET triple modality molecular imaging." *Sci Rep* 3:1490. doi: 10.1038/srep01490.

Qin, C., X. Lan, J. He, X. Xia, Y. Tian, Z. Pei, H. Yuan, and Y. Zhang. 2013. "An in vitro and in vivo evaluation of a reporter gene/probe system hERL/(18)F-FES." *PLoS One* 8 (4):e61911. doi: 10.1371/journal.pone.0061911.

Rahn-Lee, L., and A. Komeili. 2013. "The magnetosome model: insights into the mechanisms of bacterial biomineralization." *Front Microbiol* 4:352. doi: 10.3389/fmicb.2013.00352.

Raschdorf, O., F. D. Muller, M. Posfai, J. M. Plitzko, and D. Schuler. 2013. "The magnetosome proteins MamX, MamZ and MamH are involved in redox control of magnetite biomineralization in Magnetospirillum gryphiswaldense." *Mol Microbiol* 89 (5):872-86. doi: 10.1111/mmi.12317.

Ray, P., A. De, J. J. Min, R. Y. Tsien, and S. S. Gambhir. 2004. "Imaging tri-fusion multimodality reporter gene expression in living subjects." *Cancer Res* 64 (4):1323-30.

Remsen, L. G., C. I. McCormick, S. Roman-Goldstein, G. Nilaver, R. Weissleder, A. Bogdanov, I. Hellstrom, R. A. Kroll, and E. A. Neuwelt. 1996. "MR of

carcinoma-specific monoclonal antibody conjugated to monocrystalline iron oxide nanoparticles: the potential for noninvasive diagnosis." *AJNR Am J Neuroradiol* 17 (3):411-8.

Reubinoff, B. E., M. F. Pera, C. Y. Fong, A. Trounson, and A. Bongso. 2000. "Embryonic stem cell lines from human blastocysts: somatic differentiation in vitro." *Nat Biotechnol* 18 (4):399-404. doi: 10.1038/74447.

Rice, B. W., M. D. Cable, and M. B. Nelson. 2001. "In vivo imaging of light-emitting probes." *J Biomed Opt* 6 (4):432-40. doi: 10.1117/1.1413210.

Richter, M., M. Kube, D. A. Bazylinski, T. Lombardot, F. O. Glockner, R. Reinhardt, and D. Schuler. 2007. "Comparative genome analysis of four magnetotactic bacteria reveals a complex set of group-specific genes implicated in magnetosome biomineralization and function." *J Bacteriol* 189 (13):4899-910. doi: 10.1128/JB.00119-07.

Ritsma, L., S. I. Ellenbroek, A. Zomer, H. J. Snippert, F. J. de Sauvage, B. D. Simons, H. Clevers, and J. van Rheenen. 2014. "Intestinal crypt homeostasis revealed at single-stem-cell level by in vivo live imaging." *Nature* 507 (7492):362-5. doi: 10.1038/nature12972.

Rohani, R., R. Figueredo, Y. Bureau, J. Koropatnick, P. Foster, R. T. Thompson, F. S. Prato, and D. E. Goldhawk. 2013. "Imaging Tumor Growth Non-invasively Using Expression of MagA or Modified Ferritin Subunits to Augment Intracellular Contrast for Repetitive MRI." *Mol Imaging Biol*. doi: 10.1007/s11307-013-0661-8.

Rohani, R., R. Figueredo, Y. Bureau, J. Koropatnick, P. Foster, R. T. Thompson, F. S. Prato, and D. E. Goldhawk. 2014. "Imaging Tumor Growth Non-invasively Using Expression of MagA or Modified Ferritin Subunits to Augment Intracellular Contrast for Repetitive MRI." *Mol Imaging Biol* 16 (1):63-73. doi: 10.1007/s11307-013-0661-8.

Rosenberg, J. T., K. L. Sellgren, A. Sachi-Kocher, F. Calixto Bejarano, M. A. Baird, M. W. Davidson, T. Ma, and S. C. Grant. 2013. "Magnetic resonance contrast and biological effects of intracellular superparamagnetic iron oxides on human mesenchymal stem cells with long-term culture and hypoxic exposure." *Cytotherapy* 15 (3):307-22. doi: 10.1016/j.jcyt.2012.10.013.

Rueger, M. A., H. Backes, M. Walberer, B. Neumaier, R. Ullrich, M. L. Simard, B. Emig, G. R. Fink, M. Hoehn, R. Graf, and M. Schroeter. 2010. "Noninvasive imaging of endogenous neural stem cell mobilization in vivo using positron emission tomography." *J Neurosci* 30 (18):6454-60. doi: 10.1523/jneurosci.6092-09.2010.

Scheffel, A., A. Gardes, K. Grunberg, G. Wanner, and D. Schuler. 2008. "The major magnetosome proteins MamGFDC are not essential for magnetite biomineralization in Magnetospirillum gryphiswaldense but regulate the size of magnetosome crystals." *J Bacteriol* 190 (1):377-86. doi: 10.1128/JB.01371-07.

Schuldiner, M., O. Yanuka, J. Itskovitz-Eldor, D. A. Melton, and N. Benvenisty. 2000. "Effects of eight growth factors on the differentiation of cells derived from human embryonic stem cells." *Proc Natl Acad Sci U S A* 97 (21):11307-12. doi: 10.1073/pnas.97.21.11307.

Schwarz, S. C., and J. Schwarz. 2010. "Translation of stem cell therapy for neurological diseases." *Transl Res* 156 (3):155-60. doi: 10.1016/j.trsl.2010.07.002.

Segal, A. W., R. N. Arnot, M. L. Thakur, and J. P. Lavender. 1976. "Indium-111-labelled leucocytes for localisation of abscesses." *Lancet* 2 (7994):1056-8.

Selman, K., and F. C. Kafatos. 1974. "Transdifferentiation in the labial gland of silk moths: is DNA required for cellular metamorphosis?" *Cell Differ* 3 (2):81-94.

Sengupta, A., K. Quiaoit, R. T. Thompson, F. S. Prato, N. Gelman, and D. E. Goldhawk. 2014. "Biophysical features of MagA expression in mammalian cells: implications for MRI contrast." *Front Microbiol* 5:29. doi: 10.3389/fmicb.2014.00029.

Severance, S., S. Chakraborty, and D. J. Kosman. 2004. "The Ftr1p iron permease in the yeast plasma membrane: orientation, topology and structure-function relationships." *Biochem J* 380 (Pt 2):487-96. doi: 10.1042/bj20031921.

Sevick-Muraca, E. M., J. P. Houston, and M. Gurfinkel. 2002. "Fluorescence-enhanced, near infrared diagnostic imaging with contrast agents." *Curr Opin Chem Biol* 6 (5):642-50.

Shah, K., and R. Weissleder. 2005. "Molecular optical imaging: applications leading to the development of present day therapeutics." *NeuroRx* 2 (2):215-25. doi: 10.1602/neurorx.2.2.215.

Shapiro, E. M., L. N. Medford-Davis, T. M. Fahmy, C. E. Dunbar, and A. P. Koretsky. 2007. "Antibody-mediated cell labeling of peripheral T cells with micron-sized iron oxide particles (MPIOs) allows single cell detection by MRI." *Contrast Media Mol Imaging* 2 (3):147-53. doi: 10.1002/cmmi.134.

Sharma, A., N. Gokulchandran, G. Chopra, P. Kulkarni, M. Lohia, P. Badhe, and V. C. Jacob. 2012. "Administration of autologous bone marrow-derived mononuclear cells in children with incurable neurological disorders and injury is safe and improves their quality of life." *Cell Transplant* 21 Suppl 1:S79-90. doi: 10.3727/096368912x633798.

Sibov, T. T., L. F. Pavon, L. A. Miyaki, J. B. Mamani, L. P. Nucci, L. T. Alvarim, P. H. Silveira, L. C. Marti, and L. Gamarra. 2014. "Umbilical cord mesenchymal stem cells labeled with multimodal iron oxide nanoparticles with fluorescent and magnetic properties: application for in vivo cell tracking." *Int J Nanomedicine* 9:337-50. doi: 10.2147/ijn.s53299.

Siponen, M. I., G. Adryanczyk, N. Ginet, P. Arnoux, and D. Pignol. 2012. "Magnetochrome: a c-type cytochrome domain specific to magnetotatic bacteria." *Biochem Soc Trans* 40 (6):1319-23. doi: 10.1042/BST20120104.

Siqueira, R. C., A. Messias, J. C. Voltarelli, K. Messias, R. S. Arcieri, and R. Jorge. 2013. "Resolution of macular oedema associated with retinitis pigmentosa after intravitreal use of autologous BM-derived hematopoietic stem cell transplantation." *Bone Marrow Transplant* 48 (4):612-3. doi: 10.1038/bmt.2012.185.

Sterenczak, K. A., M. Meier, S. Glage, M. Meyer, S. Willenbrock, P. Wefstaedt, M. Dorsch, J. Bullerdiek, H. Murua Escobar, H. Hedrich, and I. Nolte. 2012. "Longitudinal MRI contrast enhanced monitoring of early tumour development with manganese chloride (MnCl2) and superparamagnetic iron oxide

nanoparticles (SPIOs) in a CT1258 based in vivo model of prostate cancer." *BMC Cancer* 12:284. doi: 10.1186/1471-2407-12-284.

Stuckey, D. J., C. A. Carr, E. Martin-Rendon, D. J. Tyler, C. Willmott, P. J. Cassidy, S. J. Hale, J. E. Schneider, L. Tatton, S. E. Harding, G. K. Radda, S. Watt, and K. Clarke. 2006. "Iron particles for noninvasive monitoring of bone marrow stromal cell engraftment into, and isolation of viable engrafted donor cells from, the heart." *Stem Cells* 24 (8):1968-75. doi: 10.1634/stemcells.2006-0074.

Sutton, E. J., T. D. Henning, B. J. Pichler, C. Bremer, and H. E. Daldrup-Link. 2008. "Cell tracking with optical imaging." *Eur Radiol* 18 (10):2021-32. doi: 10.1007/s00330-008-0984-z.

Takahashi, K., and S. Yamanaka. 2006. "Induction of pluripotent stem cells from mouse embryonic and adult fibroblast cultures by defined factors." *Cell* 126 (4):663-76. doi: 10.1016/j.cell.2006.07.024.

Tannous, B. A., J. Grimm, K. F. Perry, J. W. Chen, R. Weissleder, and X. O. Breakefield. 2006. "Metabolic biotinylation of cell surface receptors for in vivo imaging." *Nat Methods* 3 (5):391-6. doi: 10.1038/nmeth875.

Terrovitis, J., K. F. Kwok, R. Lautamaki, J. M. Engles, A. S. Barth, E. Kizana, J. Miake, M. K. Leppo, J. Fox, J. Seidel, M. Pomper, R. L. Wahl, B. Tsui, F. Bengel, E. Marban, and M. R. Abraham. 2008. "Ectopic expression of the sodium-iodide symporter enables imaging of transplanted cardiac stem cells in vivo by single-photon emission computed tomography or positron emission tomography." *J Am Coll Cardiol* 52 (20):1652-60. doi: 10.1016/j.jacc.2008.06.051.

Thomson, J. A., J. Itskovitz-Eldor, S. S. Shapiro, M. A. Waknitz, J. J. Swiergiel, V. S. Marshall, and J. M. Jones. 1998. "Embryonic stem cell lines derived from human blastocysts." *Science* 282 (5391):1145-7.

Till, J. E., and E.A. McCulloch. 1963. "Early repair processes in marrow cells irradiated and proliferating in vivo." *Radiat Res* 18:96-105.

Uebe, R., V. Henn, and D. Schuler. 2012. "The MagA protein of Magnetospirilla is not involved in bacterial magnetite biomineralization." *J Bacteriol* 194 (5):1018-23. doi: 10.1128/JB.06356-11.

Uebe, R., K. Junge, V. Henn, G. Poxleitner, E. Katzmann, J. M. Plitzko, R. Zarivach, T. Kasama, G. Wanner, M. Posfai, L. Bottger, B. Matzanke, and D. Schuler. 2011. "The cation diffusion facilitator proteins MamB and MamM of Magnetospirillum gryphiswaldense have distinct and complex functions, and are involved in magnetite biomineralization and magnetosome membrane assembly." *Mol Microbiol* 82 (4):818-35. doi: 10.1111/j.1365-2958.2011.07863.x.

Vande Velde, G., U. Himmelreich, and M. Neeman. 2013. "Reporter gene approaches for mapping cell fate decisions by MRI: promises and pitfalls." *Contrast Media Mol Imaging* 8 (6):424-31. doi: 10.1002/cmmi.1590.

Vande Velde, G., J. Raman Rangarajan, R. Vreys, C. Guglielmetti, T. Dresselaers, M. Verhoye, A. Van der Linden, Z. Debyser, V. Baekelandt, F. Maes, and U. Himmelreich. 2012. "Quantitative evaluation of MRI-based tracking of ferritin-labeled endogenous neural stem cell progeny in rodent brain." *Neuroimage* 62 (1):367-80. doi: 10.1016/j.neuroimage.2012.04.040.

Vande Velde, G., J. R. Rangarajan, J. Toelen, T. Dresselaers, A. Ibrahimi, O. Krylychkina, R. Vreys, A. Van der Linden, F. Maes, Z. Debyser, U. Himmelreich,

and V. Baekelandt. 2011. "Evaluation of the specificity and sensitivity of ferritin as an MRI reporter gene in the mouse brain using lentiviral and adeno-associated viral vectors." *Gene Ther* 18 (6):594-605. doi: 10.1038/gt.2011.2.

Vandsburger, M. H., M. Radoul, B. Cohen, and M. Neeman. 2013. "MRI reporter genes: applications for imaging of cell survival, proliferation, migration and differentiation." *NMR Biomed* 26 (7):872-84. doi: 10.1002/nbm.2869.

Venkataramana, N. K., S. K. Kumar, S. Balaraju, R. C. Radhakrishnan, A. Bansal, A. Dixit, D. K. Rao, M. Das, M. Jan, P. K. Gupta, and S. M. Totey. 2010. "Open-labeled study of unilateral autologous bone-marrow-derived mesenchymal stem cell transplantation in Parkinson's disease." *Transl Res* 155 (2):62-70. doi: 10.1016/j.trsl.2009.07.006.

von Andrian, U. H., and T. R. Mempel. 2003. "Homing and cellular traffic in lymph nodes." *Nat Rev Immunol* 3 (11):867-78. doi: 10.1038/nri1222.

Vymazal, J., R. A. Brooks, O. Zak, C. McRill, C. Shen, and G. Di Chiro. 1992. "T1 and T2 of ferritin at different field strengths: effect on MRI." *Magn Reson Med* 27 (2):368-74.

Walczak, P., D. A. Kedziorek, A. A. Gilad, B. P. Barnett, and J. W. M. Bulte. 2007. "Applicability and limitations of MR tracking of neural stem cells with asymmetric cell division and rapid turnover: The case of the Shiverer dysmyelinated mouse brain." *Magnetic Resonance in Medicine* 58 (2):261-269. doi: 10.1002/mrm.21280.

Walling, M. A., J. A. Novak, and J. R. Shepard. 2009. "Quantum dots for live cell and in vivo imaging." *Int J Mol Sci* 10 (2):441-91. doi: 10.3390/ijms10020441.

Wang, L., K. Tang, Q. Zhang, H. Li, Z. Wen, H. Zhang, and H. Zhang. 2013. "Somatostatin receptor-based molecular imaging and therapy for neuroendocrine tumors." *Biomed Res Int* 2013:102819. doi: 10.1155/2013/102819.

Wang, X., F. Wei, A. Liu, L. Wang, J. C. Wang, L. Ren, W. Liu, Q. Tu, L. Li, and J. Wang. 2012. "Cancer stem cell labeling using poly(L-lysine)-modified iron oxide nanoparticles." *Biomaterials* 33 (14):3719-32. doi: 10.1016/j.biomaterials.2012.01.058.

Ward, K. M., A. H. Aletras, and R. S. Balaban. 2000. "A new class of contrast agents for MRI based on proton chemical exchange dependent saturation transfer (CEST)." *J Magn Reson* 143 (1):79-87. doi: 10.1006/jmre.1999.1956.

Weissleder, R. 1991. "Target-specific superparamagnetic MR contrast agents." *Magn Reson Med* 22 (2):209-12; discussion 213-5.

Weissleder, R., A. Moore, U. Mahmood, R. Bhorade, H. Benveniste, E. A. Chiocca, and J. P. Basilion. 2000. "In vivo magnetic resonance imaging of transgene expression." *Nat Med* 6 (3):351-5. doi: 10.1038/73219.

Weissleder, R., M. Simonova, A. Bogdanova, S. Bredow, W. S. Enochs, and A. Bogdanov, Jr. 1997. "MR imaging and scintigraphy of gene expression through melanin induction." *Radiology* 204 (2):425-9. doi: 10.1148/radiology.204.2.9240530.

Welsh, D. K., and S. A. Kay. 2005. "Bioluminescence imaging in living organisms." *Curr Opin Biotechnol* 16 (1):73-8. doi: 10.1016/j.copbio.2004.12.006.

Wernig, M., J. P. Zhao, J. Pruszak, E. Hedlund, D. Fu, F. Soldner, V. Broccoli, M. Constantine-Paton, O. Isacson, and R. Jaenisch. 2008. "Neurons derived from

reprogrammed fibroblasts functionally integrate into the fetal brain and improve symptoms of rats with Parkinson's disease." *Proc Natl Acad Sci U S A* 105 (15):5856-61. doi: 10.1073/pnas.0801677105.

Westmeyer, G. G., Y. Durocher, and A. Jasanoff. 2010. "A secreted enzyme reporter system for MRI." *Angew Chem Int Ed Engl* 49 (23):3909-11. doi: 10.1002/anie.200906712.

Wolfs, E., B. Holvoet, R. Gijsbers, C. Casteels, S. J. Roberts, T. Struys, M. Maris, A. Ibrahimi, Z. Debyser, K. Van Laere, C. M. Verfaillie, and C. M. Deroose. 2014. "Optimization of Multimodal Imaging of Mesenchymal Stem Cells Using the Human Sodium Iodide Symporter for PET and Cerenkov Luminescence Imaging." *PLoS One* 9 (4):e94833. doi: 10.1371/journal.pone.0094833.

Wu, H., H. Shi, H. Zhang, X. Wang, Y. Yang, C. Yu, C. Hao, J. Du, H. Hu, and S. Yang. 2014. "Prostate stem cell antigen antibody-conjugated multiwalled carbon nanotubes for targeted ultrasound imaging and drug delivery." *Biomaterials* 35 (20):5369-80. doi: 10.1016/j.biomaterials.2014.03.038.

Youn, H., and J. K. Chung. 2013. "Reporter gene imaging." *AJR Am J Roentgenol* 201 (2):W206-14. doi: 10.2214/AJR.13.10555.

Youn, H., and K. J. Hong. 2012. "In vivo non invasive molecular imaging for immune cell tracking in small animals." *Immune Netw* 12 (6):223-9. doi: 10.4110/in.2012.12.6.223.

Zhang, X., B. Robledo, S. Harris, and Xiaoping Hu. 2010. "The magnetosome membrane protein Mms6 produces MR contrast in vitro." *19th Proc. Intl. Soc. Mag. Reson. Med*.

Zhou, R., P. D. Acton, and V. A. Ferrari. 2006. "Imaging stem cells implanted in infarcted myocardium." *J Am Coll Cardiol* 48 (10):2094-106. doi: 10.1016/j.jacc.2006.08.026.

Zhou, R., D. H. Thomas, H. Qiao, H. S. Bal, S. R. Choi, A. Alavi, V. A. Ferrari, H. F. Kung, and P. D. Acton. 2005. "In vivo detection of stem cells grafted in infarcted rat myocardium." *J Nucl Med* 46 (5):816-22.

Zurkiya, O., A. W. Chan, and X. Hu. 2008. "MagA is sufficient for producing magnetic nanoparticles in mammalian cells, making it an MRI reporter." *Magn Reson Med* 59 (6):1225-31. doi: 10.1002/mrm.21606.